TU Delft

Delft University of Technology

Power supply for degaussing systems with high temperature superconductors

Wikkerink, D.P.

DOI
10.4233/uuid:aefb1f75-2d92-4cb3-b4a9-64fe84f1cf66

Publication date
2024

Document Version
Final published version

Citation (APA)
Wikkerink, D. P. (2024). *Power supply for degaussing systems with high temperature superconductors*. [Dissertation (TU Delft), Delft University of Technology]. https://doi.org/10.4233/uuid:aefb1f75-2d92-4cb3-b4a9-64fe84f1cf66

Important note
To cite this publication, please use the final published version (if applicable).
Please check the document version above.

Copyright
Other than for strictly personal use, it is not permitted to download, forward or distribute the text or part of it, without the consent of the author(s) and/or copyright holder(s), unless the work is under an open content license such as Creative Commons.

Takedown policy
Please contact us and provide details if you believe this document breaches copyrights.
We will remove access to the work immediately and investigate your claim.

This work is downloaded from Delft University of Technology.
For technical reasons the number of authors shown on this cover page is limited to a maximum of 10.

POWER SUPPLY FOR DEGAUSSING SYSTEMS WITH HIGH TEMPERATURE SUPERCONDUCTORS

POWER SUPPLY FOR DEGAUSSING SYSTEMS WITH HIGH TEMPERATURE SUPERCONDUCTORS

Proefschrift

ter verkrijging van de graad van doctor
aan de Technische Universiteit Delft,
op gezag van de Rector Magnificus prof. dr. ir. T.H.J.J. van der Hagen,
voorzitter van het College voor Promoties,
in het openbaar te verdedigen op donderdag 3 oktober 2024 om 15:00 uur

door

Djurre Pier WIKKERINK

elektrotechnisch ingenieur,
Technische Universiteit Delft,
geboren te Smallingerland.

Dit proefschrift is goedgekeurd door de promotoren.

Samenstelling promotiecommissie:

Rector magnificus,	voorzitter
prof. dr. R. Ross,	Technische Universiteit Delft, promotor
dr. ir. H.P. Polinder,	Technische Universiteit Delft, promotor
dr. A. Rodrigo Mor,	Technische Universiteit Delft, Universitat Politècnica de València, Spanje, copromotor

Onafhankelijke leden:

prof. dr. T. Batista Soeiro,	Universiteit Twente
dr. M.M.J. Dhallé,	Universiteit Twente
dr. B.J. van Oers,	Ministerie van Defensie
prof. ir. P.T.M. Vaessen,	Technische Universiteit Delft
prof. dr. R.R. Negenborn,	Technische Universiteit Delft, reservelid

Front & Back: Rinske Wikkerink
Printed by: Ridderprint, Alblasserdam
ISBN: 978-94-6506-253-2

Copyright © 2024 by Djurre Wikkerink

What we do now echoes in eternity.

Marcus Aurelius

CONTENTS

SUMMARY

Ships with a ferromagnetic hull distort Earth's magnetic field in such a way that magnetic mines can detect them. On-board degaussing systems compensate for the magnetic signature, but the copper coils take up valuable space and cause losses. High-temperature superconductive (HTS) coils are a potential alternative because they don't have Ohmic losses. However, research is lacking on the application of HTS to degaussing. The objective of this thesis is to design an adequate HTS degaussing power supply.

A modelling framework is developed to quantify the magnetic signature and to estimate the degaussing parameters. Analytical and numerical modelling techniques are compared where the numerical provides the most accurate results but takes longer to calculate. Both are verified with an experimental test setup where the (reduced) magnetic signature was measured. A second test setup was built to demonstrate the performance and feasibility of HTS degaussing coils. The HTS coils are placed in a closed-loop vacuum-insulated cryostat filled with sub-cooled liquid nitrogen. The magnetic signature is measured in a static and dynamic case where the behaviour of the HTS coils is similar to that of the copper coils.

The high current-carrying capability of HTS has the advantage that fewer turns are required. However, a larger current density results in more power source and current lead losses. Both problems are solved using a cryo-cooled converter with low on-state resistance MOSFETs. A comparative study between four different topologies has been conducted, concluding that an H-bridge converter with cryo-cooled MOSFETs and a DC capacitor bank inside the cryostat can reduce the amount of losses by a factor 23 compared to a conventional converter. A cryogenic H-bridge converter with ten parallel MOSFETs per switching leg and an HTS load was built and tested. The converter produces a current of 50 A with an input voltage of 3.5 V and a duty cycle of only 0.025. The parasitic inductances cause unwanted effects regarding oscillations above a switching frequency of around 100 Hz because of the low PCB resistances.

A concern exists that a peak in the frequency spectrum can be detected in the magnetic signature around converter's switching frequency. Five switching frequency modulation schemes were tested to reduce this peak. A model of a full-sized frigate estimates the effect of the switching frequency on the magnetic signature. Of the tested schemes, random lead-lag shows the best results.

In this research, a framework is created where the magnetic signature and the degaussing parameters can be estimated. It was shown that HTS can be used to replace copper degaussing coils. Several converter topologies were compared, and it was shown that cryo-cooled MOSFETs can increase performance drastically. A cryogenic converter was built and tested successfully. A variety of switching frequency modulation schemes were tested, and it was found that random switching frequency modulation can be used to reduce the switching ripple in the magnetic signature.

SAMENVATTING

Schepen met een ferromagnetische romp vervormen het aardmagnetisch veld waardoor magnetische mijnen ze kunnen detecteren. Een demagnetiseringsinstallatie compenseert de magnetische signatuur, maar de koperen spoelen nemen veel ruimte in beslag en hebben verliezen. Hoge-temperatuur supergeleidende (HTS) spoelen zijn een mogelijk alternatief omdat ze geen Ohmse verliezen hebben. Er is echter meer onderzoek nodig voordat HTS kan worden toegepast. Het doel van dit proefschrift is om een adequate voeding voor een HTS demagnetiseringssysteem te ontwerpen.

Er is een model nodig om de magnetische signatuur te kwantificeren. Analytische en numerieke modelleringstechnieken zijn vergeleken waarbij de numerieke de meest nauwkeurige resultaten oplevert, maar langer duurt om uit te rekenen. Beide zijn geverifieerd met een testopstelling waarbij de (verminderde) magnetische signatuur is gemeten. Een tweede testopstelling is gebruikt om de haalbaarheid van HTS demagnetiseringsspoelen aan te tonen. Het gedrag van de HTS-spoelen is vergelijkbaar met dat van de koperen spoelen.

HTS heeft als voordeel dat het veel stroom kan geleiden en er dus minder windingen nodig zijn. Een hogere stroomdichtheid betekend echter ook meer stroombronen stroomleidingverliezen. Beide problemen kunnen worden opgelost door een cryogekoelde omvormer te gebruiken met MOSFET's met een lage weerstand. Er is een studie gedaan waarin vier topologieën met elkaar zijn vergeleken. Een H-brug omvormer met cryo-gekoelde MOSFET's en een DC-condensatorbank in de cryostaat verminderen de verliezen met een factor 23. Er is een cryogene H-brug omvormer gebouwd met tien parallelle MOSFET's per schakelarm en een HTS-belasting. De omvormer produceert een stroom van 50 A bij een ingangsspanning van 3.5 V en een arbeidsfactor van slechts 0.025. De parasitaire inductanties veroorzaken ongewenste effecten met betrekking tot oscillaties en prestaties boven een schakelfrequentie van ongeveer 100 Hz vanwege de lage PCB-weerstanden.

Er kan een piek in het frequentiespectrum van de magnetische signatuur worden gedetecteerd rond de schakelfrequentie van de omvormer. Vijf schakelfrequentiemodulatietechnieken zijn getest om deze piek te verminderen. Een model van een fregat schat het effect van de schakelfrequentie op de magnetische signatuur. Van de geteste technieken laat random lead-lag de beste resultaten zien.

In dit onderzoek is er een kader gecreëerd waarin de magnetische signatuur en de demagnetiseringsparameters kunnen worden ingeschat. Er is aangetoond dat HTS gebruikt kan worden als alternatief voor koper. Verschillende omvormers zijn met elkaar vergeleken en er is aangetoond dat het gebruik van cryo-gekoelde MOSFET's de prestaties van de omvormer drastisch kan verhogen. Er is een cryogene omvormer gebouwd en met succes getest. Er zijn verschillende schakelfrequentiemodulatietechnieken getest en er is aangetoond dat een willekeurige schakelfrequentie kan worden gebruikt om de schakelrimpel in de magnetische signatuur te verminderen.

1

INTRODUCTION

ON THE very same day that the British declared war on Nazi Germany, the Germans dropped naval mines into the North Sea. The most common mines in use at that time were contact mines, but some of the ships were hit by a new type of proximity mine; solely triggered by a ship's presence. Casualties quickly mounted, and since the mines were placed on essential shipping routes and at the entrance of harbours, the supply of goods was heavily impacted. It was impossible to counteract the mine because its trigger mechanism was unknown.

In November 1939, the Germans accidentally dropped one of their mystery mines onto a mud flat of the Thames. Luckily for the British, this mine was not only intact, but it was also dropped onto land belonging to an army base. At low tide, it could be carefully examined. They found that the trigger mechanism was magnetic. A sensor inside measures a deviation in Earth's magnetic field when a ship is near. Various methods of mine sweeping were developed as a result; dragging permanent magnets over the seabed, inducing currents in the seawater and even equipping ships and aeroplanes with coils to set off the mines. A picture of such an aeroplane is shown in figure 1.1.

Figure 1.1: Wellington bomber with coil to set off magnetic mines.

Figure 1.2: RMS Queen Mary with external degaussing coil to avoid detection by magnetic mines.

Meanwhile, engineers were working on making ships undetectable by demagnetising them. One of the methods was to place a coil around the bow and stern of the ship. A current through this coil provides an opposing magnetic field to the field induced by the ship's hull. Since the magnetic flux density in those days was measured in Gauss, this technique was soon named "degaussing". They quickly equipped every naval and even merchant vessels with a degaussing coil. Figure 1.2 shows the RMS Queen Mary with a degaussing coil as an example. Within a period of five months, degaussing systems were installed on approximately two thousand ships [1]–[3].

Nowadays, degaussing systems are still relevant. Old naval mines are still active, and new, more intelligent ones are being produced. Although it is impossible to say how many mines there are, some estimates suggest that up to 250 thousand potentially active mines remain from World War II. Currently, Iran has up to 20 thousand, North Korea up to 50 thousand, China up to 100 thousand and Russia has up to 250 thousand naval mines in their arsenals [4]. (However, there is a considerable degree of uncertainty With these numbers). Mines can be produced easily in secret and are relatively cheap. An example of the effectiveness of naval mines is the case of the USS Tripoli. This ship got hit by a mine in the Persian gulf in 1991. Although the mine was worth less than 1000 dollars, the costs to repair the ship were 3.5 million dollars [5]. For the above reasons, modern navy and merchant ships are still being equipped with degaussing coils.

1.1. SUPERCONDUCTORS AS AN ALTERNATIVE TO COPPER

Ships distort Earth's magnetic field because of their permeability. The characteristic of this distortion is called the magnetic signature [6]. To avoid detection, ships have to reduce their magnetic signature [7]. A degaussing system compensates for it by generating a similar magnetic field in the opposite direction [8]. Ideally, the magnetic signature is completely cancelled by the degaussing field, making the ship magnetically invisible. Degaussing systems consist of a set of on-board coils placed in three directions relative to the ship. The L-coils, placed in the longitudinal direction; the A-coils, placed in the athwartship direction and the M-coils, placed in the main or vertical direction. An example of the placement of the degaussing coils on a FREMM class naval ship can be seen in Figure 1.3. The degaussing currents are basically DC, but need to be adjusted for the ship's rolling, pitching and yawing. The DC current set-points depend on the ship's heading and its position in Earth's magnetic field.

To create the degaussing field, a considerable amount of magnetomotive force is needed. Degaussing coils are typically rated for 1000 A·t, requiring spacious and heavy cables [10]. Considering the current rating and the amount and length of the degaussing coils, the Ohmic losses in the coils are significant. One study estimates that the power dissipation of a degaussing system on a San Antonio class naval ship with a length of 208 m is around 207 kW of which more than 95 % are copper losses in the coils [11]. As a result, bulky and costly cables take up valuable on-board space and a significant amount of energy is lost. Fortunately, there is an alternative to copper degaussing coils.

High temperature superconductors (HTS) are materials that are perfect conductors in certain conditions. There are no Ohmic losses when a current flows through them because of the lack of electrical resistance. Moreover, the current density in HTS tape can be up to 500 times higher than in a copper wire because there is no heat dissipation.

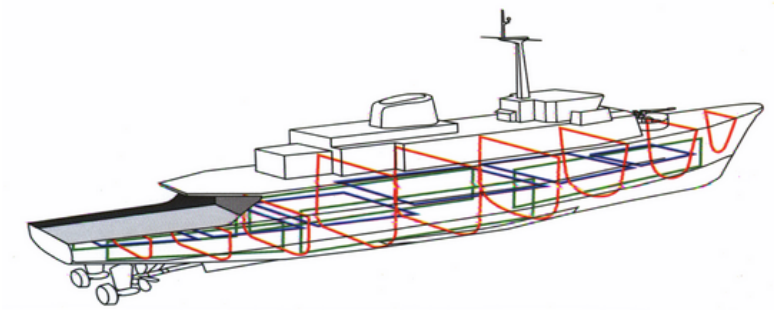

Figure 1.3: A schematic representation of a naval ship of the FREMM class. The longitudinal, athwartship and main coils are depicted in red, green and blue, respectively. Each direction has multiple coils for sufficient resolution of the degaussing field. [9]

The use of HTS instead of copper coils could therefore solve weight, volume and power dissipation issues in degaussing systems. There is a challenge, however.

Superconductors need to be cooled to below their critical temperature to be in superconductive state. For low temperature superconductors (LTS), this would require a complicated and expensive helium filled cryogenic system. However, HTS have their critical temperature above 77 K by definition, which is the boiling temperature of nitrogen. A cryogenic system based on liquid nitrogen is relatively cheap and energy efficient. Besides, the development of HTS has matured through the last decades and the material is now commercially available. This makes HTS a serious alternative for copper degaussing coils.

1.2. STATE OF THE ART

Degaussing is mostly a military application. The details regarding current set-points, inductances and coil placement are highly classified. However, the mathematical basics of the exploitation, reduction and modelling of magnetic signatures are well documented and available in a three-volume book series [6]–[8] and other publications [12]–[14]. Several magnetic signature modelling techniques are described. All have different accuracies and applications. For this thesis, the need exists for a framework to estimate degaussing currents, inductances and magnetic flux densities in a modelling environment for the specific cases of this research. Therefore, the first research objective is to create a framework in which the magnetic signature and the effect of degaussing can be visualised and quantified.

The first and only ship known to utilise an HTS degaussing coil is the USS Higgins. As a demonstration, the HTS coil was successfully in operation from June 2009 through February 2010 [15]. The current supply used in this demonstration is an off-the-shelf power supply. The cryogenic system uses helium as a coolant for the superconductor. The U.S. Navy also performed a study where they tested a gaseous helium flow in a 22-meter-long cryostat [16]. They also connected multiple cryostats to a single cryocooler to save costs [17]. The main challenge during this project was the heat leak into the cryostat. As part of the project related to the work in this thesis, it was desired to have an

explicit demonstration of the magnetic performance of an HTS degaussing system compared to a conventional copper installation. This leads to the second research objective, which is to demonstrate the equivalence of HTS and copper degaussing coils.

In addition to the research for the USS Higgins, several other studies have been performed in HTS for degaussing. One of them [10] concluded that the power supply for HTS degaussing coils needs further development to limit the power losses in the converter. When using HTS, the number of turns can be decreased, which saves conductor length. By doing so, the current needs to be increased to maintain the required Ampere-turn rating. An increased current rating causes more losses in the converter, which could even cancel out the benefits of using HTS in the first place. It is unknown what alternative to a continuous current source is the most suitable for an HTS deguassing system to reduce converter losses. Therefore, the third research objective is to identify a suitable converter topology to reduce converter losses when using HTS coils. For comparable applications, a potential candidate is a switched-mode power supply with cryocooled MOSFETs [18]. So, in addition, the fourth research objective is to design an H-bridge converter type with cryocooled MOSFETs.

The switching current ripple is expected to be more significant in an HTS degaussing system. The inductance of an HTS coil with fewer turns is smaller than for a copper degaussing system [10]. An alternative power supply could also require a lower switching frequency, resulting in less hull damping. A peak around the switching frequency might be detectable in the magnetic signature because of increased current ripple. A potential way to reduce the peak in the magnetic signature is to use random switching frequency modulation as used in other applications [19]. The effects of this have yet to be investigated for degaussing systems. The fifth and final research objective is therefore to achieve switching ripple reduction in the magnetic signature by means of switching frequency modulation.

In general, HTS degaussing coils have the potential to reduce the degaussing system's weight by a factor of 5-10 [8], [10], costs by more than a factor of 2 [8] and power dissipation up to 93 % [11]. No other HTS degaussing projects are known, either because they don't exist or because they are classified.

Besides degaussing, other potential superconductor applications for ships are HTS propulsion motors, HTS auxiliary or main generators, superconducting magnetic energy storage (SMES) and HTS power distribution for services, high energy weapons and radar [20]. The U.S. Navy has a long history in superconductivity research [21]. Using superconductors would not improve energy efficiency for distribution cables on board a destroyer class ship. The weight would be reduced, but not significantly [22]. The high power density and a reduced acoustic signature of HTS systems can benefit smaller non-cargo ships. Also, HTS power systems are suitable for vessels with a dynamic sailing profile [11]. For large ships that primarily sail at nominal load, it would be challenging to compete with a traditional power system in terms of energy efficiency [23].

Other topics than HTS are covered in recent degaussing research. The most prominent is closed loop degaussing (CLDG). The main challenge is to solve the inverse problem in real-time so that on-board measurements can estimate the magnetic field around the ship and feed it back into the control system [24]–[27]. Other topics are optimising the placement of degaussing coils [28], [29] and optimising the current set-points [30].

Also, detecting a faulty degaussing coil [31] and re-adjusting the current set-points after a fault [32] are under research. Mock-ups of various sizes with degaussing coils have been built where the magnetic signature and its reduction were measured [32]–[34].

1.3. RESEARCH GOALS

Currently, there is very little available research in HTS for degaussing. Moreover, the research that has been done, primarily focuses on the cryogenic system. However, it is clear that the power system surrounding an HTS degaussing system needs to be investigated in more detail. One of the challenges is the impact on the efficiency of the power source with higher current requirements. Also, the effect on the ripple in the magnetic signature because of lower switching frequencies needs to be analysed. Therefore, the primary objective of this thesis is

> *To design an adequate power supply for a degaussing system which uses HTS instead of copper degaussing coils.*

The main objective is further partitioned into the following five research objectives

1. To create a framework in which the magnetic signature and the effect of degaussing can be visualised and quantified.
2. To demonstrate the equivalence of HTS and copper degaussing coils.
3. To identify a suitable converter topology to reduce converter losses when using HTS coils.
4. To design an H-bridge converter type with cryocooled MOSFETs.
5. To achieve switching ripple reduction in the magnetic signature by means of switching frequency modulation.

1.4. RESEARCH APPROACH AND THESIS OUTLINE

In this thesis, each of the above research objectives is covered in a separate chapter.

Chapter 2 gives a brief review of magnetic signatures and their modelling. This is needed to be able to estimate the degaussing coil current set-points and the coil characteristics of a full-sized ship in a later stage of this thesis. Analytic and finite element modelling techniques are explored. A test set-up with three degaussing coils is built to measure the magnetic signature and its reduction by degaussing. The test set-up verifies the modelling techniques.

Chapter 3 explores the use of HTS for degaussing coils. A literature study is performed on the different HTS materials and the cooling system options. Its applications are reviewed with special attention to the power and control system of HTS coils. The use of the persistent mode, where an HTS coils is short-circuited so that the current doesn't damp out, is addressed as well. A demonstrator is built with both HTS and copper degaussing coils. This demonstrator intends to demonstrate that HTS coils can degauss a steel object in a similar manner as copper coils. The demonstrator shows degaussing in static and dynamic cases.

Chapter 4 investigates different converter topologies to minimize converter and current lead losses. By using HTS, we have to deal with higher currents and, therefore with higher power supply losses. Also, large current leads are needed, which introduces extra losses. Four H-bridge-based MOSFET topologies are presented that were designed to reduce the power supply and current lead losses. Measurements were done to determine the MOSFETs and capacitor performance in liquid nitrogen. The simulated losses of the four topologies are compared to determine the most energy-efficient option for supplying current to the HTS coils.

Chapter 5 tests a converter especially designed for an HTS degaussing application. The converter is an H-bridge with cryocooled MOSFETs. The converter is connected to an inductive HTS load. The measuring set-up is explained in detail. The performance of the converter is measured at different current set points and switching frequencies.

Chapter 6 aims to reduce the ripple in the magnetic field using a switching modulation scheme in the power supply. A model of a ship with degaussing coils is described. It is used to find the magnitude of the ripple in the magnetic signature. Also, the effect of reducing the current ripple by frequency modulation is investigated. Several modulation schemes are modelled.

Finally, chapter 7 draws a conclusion and gives recommendations for future work.

BIBLIOGRAPHY

[1] BBC, *The secret war: The deadly waves*, TV Series, 1977.

[2] N. B. Michel, "Shipboard Degaussing Installations for Protection Against Magnetic Mines", *Transactions of the American Institute of Electrical Engineers*, vol. 67, no. 2, pp. 1270–1277, Jan. 1948.

[3] H. Kelly, "Historical Introduction to Degaussing, Covering Pre-War Work and Development up to the Start of the Campaign Against the German Mine", *Journal of the Institution of Electrical Engineers - Part I: General*, vol. 93, no. 70, pp. 430–434, Oct. 1946.

[4] G. Evans, *Mine-hunters: are they still needed?*, https://www.naval-technology.com/analysis/featuremine-hunters-are-they-still-needed/, Feb. 2016.

[5] B. Szturomski, "The effect of an underwater explosion on a ship", *Zeszyty Naukowe Akademii Marynarki Wojennej*, vol. 201, no. 2, pp. 57–73, 2015.

[6] J. J. Holmes, "Exploitation of a Ship's Magnetic Field Signatures", *Synthesis Lectures on Computational Electromagnetics*, vol. 1, no. 1, pp. 1–78, Jan. 2006.

[7] J. J. Holmes, "Modelling a Ship's Ferromagnetic Signatures", *Synthesis Lectures on Computational Electromagnetics*, vol. 2, no. 1, pp. 1–75, Jan. 2007.

[8] J. J. Holmes, "Reduction of a Ship's Magnetic Field Signatures", *Synthesis Lectures on Computational Electromagnetics*, vol. 3, no. 1, pp. 1–68, Jan. 2008.

[9] di Marina Militare, *200716 degaussing.png*, https://www.difesaonline.it/sites/default/files/200716degaussing(1).png, Jul. 2016.

[10] R. Ross, C. G. Meijer, and R. J. van de Mheen, "Degaussing by Normal and Superconductive Windings", in *Conference Proceedings of 11th INEC Edinburgh*, May 2012.

[11] R. Ross, C. G. Meijer, and R. Hunik, "Maritime superconductivity perspectives", *IEEE Transactions on Applied Superconductivity*, vol. 23, no. 3, 2013.

[12] F. E. Baker and S. H. Brown, "Magnetic induction of ferromagnetic prolate spheroidal bodies and infinitesimally thin current bands", *Journal of Applied Physics*, vol. 53, pp. 3991–3996, 6 Jun. 1982.

[13] C. Aird, "Modelling the induced magnetic signature of naval vessels", PhD Dissertation, University of Glasgow, 2000.

[14] O. Chadebec, J. L. Coulomb, V. Leconte, J. P. Bongiraud, and G. Cauffet, "Modelling of static magnetic anomaly created by iron plates", *IEEE Transactions on Magnetics*, vol. 36, pp. 667–671, 4 PART 1 2000.

[15] B. K. Fitzpatrick, J. T. Kephart, and E. M. Golda, "High Temperature Superconducting Degaussing from Feasibility Study to Fleet Adoption", *IEEE Transactions on Applied Superconductivity*, vol. 21, no. 3, pp. 2229–2232, 2011.

[16] B. K. Fitzpatrick, J. T. Kephart, and E. Michael Golda, "Characterization of Gaseous Helium Flow Cryogen in a Flexible Cryostat for Naval Applications of High Temperature Superconductors", *IEEE Transactions on Applied Superconductivity*, vol. 17, no. 2, pp. 1752–1755, Jun. 2007.

[17] B. K. Fitzpatrick, E. M. Golda, J. T. Kephart, *et al.*, "High Temperature Superconducting Degaussing–Cooling Two HTS Coils with One Cryocooler for the Littoral Combat Ship", in *AIP Conference Proceedings*, vol. 985, AIP, 2008, pp. 277–283.

[18] M. Oomen, M. Leghissa, G. Ries, *et al.*, "HTS Flux Pump for Cryogen-Free HTS Magnets", *IEEE Transactions on Appiled Superconductivity*, vol. 15, no. 2, pp. 1465–1468, Jun. 2005.

[19] M. M. Bech, F. Blaabjerg, and J. K. Pedersen, "Random modulation techniques with fixed switching frequency for three-phase power converters", *IEEE Transactions on Power Electronics*, vol. 15, no. 4, pp. 753–761, 2000.

[20] J. Miller, D. Santosusso, M. Uva, K. Woods, and B. Fitzpatrick, "Naval Superconducting Integrated Power System", *Proceedings of the American Society of Naval Engineers: Intelligent Ships Symposium X*, vol. Intelligen, pp. 1–8, 2013.

[21] D. U. Gubser, "US Navy's Superconductivity Programs Scientific Curiosity to Fleet Utility", *IEEE Transactions on Applied Superconductivity*, vol. 21, no. 3, pp. 931–935, Jun. 2011.

[22] R. E. Hebner, A. L. Gattozzi, S. M. Strank, S. P. Pish, and J. D. Herbst, "Electrical and thermal system considerations for MVDC superconducting distribution on navy ships", *2017 IEEE Electric Ship Technologies Symposium, ESTS 2017*, pp. 592–597, 2017.

[23] R. Ross, J. J. Bosklopper, and K. H. Van Der Meij, "Operational merits of maritime superconductivity", *Physics Procedia*, vol. 36, pp. 985–988, Mar. 2012.

[24] A. R. P. J. Vijn, "Development of a Closed-loop Degaussing System: Towards Magnetic Unobservable Vessels", Ph.D. dissertation, Delft University of Technology, Delft, The Netherlands, Dec. 2021.

[25] Y. Vuillermet, O. Chadebec, J.-L. Coulomb, *et al.*, "Scalar Potential Formulation and Inverse Problem Applied to Thin Magnetic Sheets", *IEEE Transactions on Magnetics*, vol. 44, no. 6, pp. 1054–1057, Jun. 2008.

[26] C.-S. Yang, K. J. Lee, G. Jung, H.-J. Chung, J.-S. Park, and D.-H. Kim, "Efficient methodology for solving an inverse magnetostatic problem by utilizing material sensitivity", *Journal of Applied Physics*, vol. 103, no. 7, Apr. 2008.

[27] R. A. Wingo, J. J. Holmes, and M. H. Lackey, "Test of Closed-Loop Degaussing Algorithm on a Minesweeper Engine", *Naval Engineers Journal*, vol. 104, no. 3, pp. 219–227, 1992.

[28] M. M. Yang, D. M. Liu, and L. T. Lian, "Particle Swarm Optimization for Ship Degaussing Coils Calibration", *Applied Mechanics and Materials*, vol. 182-183, pp. 1446–1451, Jun. 2012.

[29] V. Modagekar, S. A. Karim, N. Singh, and F. Kazi, "Optimization in Tri-Axial Degaussing System Design and Estimation of Degaussing Coil Currents", *IEEE Transactions on Magnetics*, vol. 53, no. 4, pp. 1–12, Apr. 2017.

[30] Nak-Sun Choi, Giwoo Jeung, Chang-Seob Yang, Hyun-Ju Chung, and Dong-Hun Kim, "Optimization of Degaussing Coil Currents for Magnetic Silencing of a Ship Taking the Ferromagnetic Hull Effect Into Account", *IEEE Transactions on Applied Superconductivity*, vol. 22, no. 3, pp. 4 904 504–4 904 504, Jun. 2012.

[31] N.-S. Choi, D.-W. Kim, C.-S. Yang, H.-J. Chung, H.-G. Kim, and D.-H. Kim, "Efficient Fault Detection Method for a Degaussing Coil System Based on an Analytical Sensitivity Formula", *Journal of Magnetics*, vol. 18, no. 2, pp. 135–141, Jun. 2013.

[32] D.-W. Kim, S.-K. Lee, B. Kang, *et al.*, "Efficient Re-degaussing Technique for a Naval Ship Undergoing a Breakdown in Degaussing Coils", *Journal of Magnetics*, vol. 21, no. 2, pp. 197–203, Jun. 2016.

[33] L. Demilier, G. Cauffet, O. Chadebec, J.-L. Coulomb, and L.-L. Rouve, "Validation of Closed Loop Degaussing System for Double Hull Submarines", in *Conference Proceedings of MAST Rome*, MAST, 2010.

[34] R. R. Varma, "Design of Degaussing System and Demonstration of Signature Reduction on Ship Model through Laboratory Experiments", *Physics Procedia*, vol. 54, pp. 174–179, 2014.

2

MAGNETIC SIGNATURE

The magnetic signature of a ship can be reduced by means of degaussing. The magnetic signature needs to be modelled to make an estimation of the performance of the degaussing coils in a simulation environment. This chapter aims to create a framework in which the magnetic signature and the degaussing parameters can be estimated by means of a model. An analytical and numerical method are explored. The modelling approaches are verified with a test setup. The chapter also serves to achieve a better understanding in the definitions and the concept of the magnetic signature and degaussing.

The magnetic signature of a ship mainly exists because most hulls are made of ferromagnetic material, like steel. But there are more contributors to the magnetic signature. Generally, the magnetic signature can be split into the following components [1].

Induced magnetisation, $\vec{B}_{ind}$, which is caused by the low magnetic reluctance of the steel hull of the ship. The magnetic flux of Earth's magnetic field rather concentrates inside the hull of the ship than in the air and water around it. This causes a measurable distortion in the magnetic field around the ship.

Permanent magnetisation, $\vec{B}_{perm}$, which is caused by the magnetic flux that remains in the hull of the ship due to hysteresis. When a ship is exposed to a magnetic field for a period time, it becomes magnetised. This can happen during the construction of a ship, during sailing or when it is docked for a long time. Another cause can be a nearby explosion.

Corrosion currents, $\vec{B}_{corr}$, which are caused by voltage potential differences between the different metals used in the ship, like the steel of the hull and the bronze alloy of the propeller. Corrosion currents run through the hull or the conductive sea water and produce a magnetic field.

Parts of this chapter have been published as:
D. Wikkerink, A. Rodrigo Mor, H. Polinder, and R. Ross, "Design of a test setup to measure magnetic signature reduction", in *Conference Proceedings of ICMET Oman*, IMarEST, Nov. 2019.

Eddy currents, $\vec{B}_{eddy}$, which are induced when the ship changes position in Earth's magnetic field. These currents, in turn, cause a detectable magnetic field.

On-board equipment, $\vec{B}_{eq}$, which has a magnetic signature of their own. Transformer cores are made of iron and generally have a high permeability. Power electronics can cause common mode currents and the currents in electric motors, generators, breakers and distribution cables also add to the magnetic signature.

These individual components of the magnetic signature can be added as vector fields:

$$\vec{B}_{sig} = \vec{B}_{ind} + \vec{B}_{perm} + \vec{B}_{eddy} + \vec{B}_{corr} + \vec{B}_{eq} \tag{2.1}$$

2.1. MODELLING

In this chapter, the focus is on modelling the induced magnetisation. This can be done with an analytical or a finite element approach. Both are described in this section.

2.1.1. ANALYTIC MODELLING

The magnetic field in a ships hull changes slowly over time, so it can be considered static. The time dependence in the magnetic field can therefore be ignored and we can start with Maxwell's equations in *magnetostatic* form,

$$\nabla \times \vec{H} = \vec{J} \tag{2.2}$$

$$\nabla \cdot \vec{B} = 0 \tag{2.3}$$

where $\vec{H}$ is the magnetic field, $\vec{B}$ the magnetic flux density and $\vec{J}$ the electric current density. When the degaussing system is off, the space can be considered as current free so that $\vec{J} = 0$. For these regions the magnetic field $\vec{H}$ can be derived from a scalar potential,

$$\vec{H} = -\nabla\phi, \tag{2.4}$$

where ϕ is known as the magnetic scalar potential. Placing eq. (2.4) in eq. (2.3) with $\vec{B} = \mu\vec{H}$ results in Laplace's equation

$$\nabla^2 \mu\phi = 0, \tag{2.5}$$

with μ being the magnetic permeability of the modelled region. Applying the following boundary conditions between the regions provides a unique solution to eq. (2.5).

$$\left(\vec{H}_2 - \vec{H}_1\right) \times \hat{n} = \vec{J}_s \tag{2.6}$$

$$\left(\vec{B}_2 - \vec{B}_1\right) \cdot \hat{n} = 0 \tag{2.7}$$

As an example, figure 2.1 shows the solution of the above equations for two different shapes. It also shows how the shapes distort the uniform magnetic field around them.

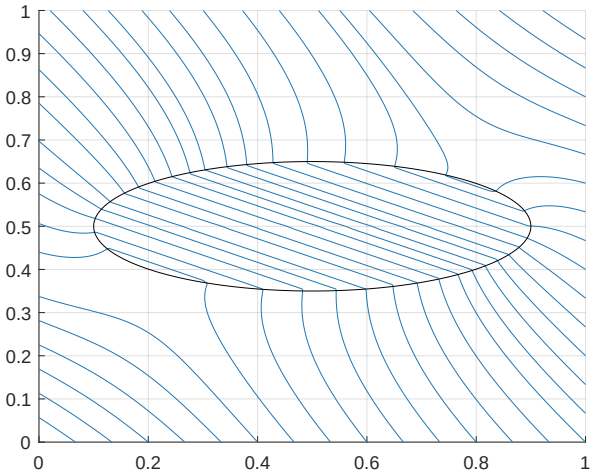

(a)

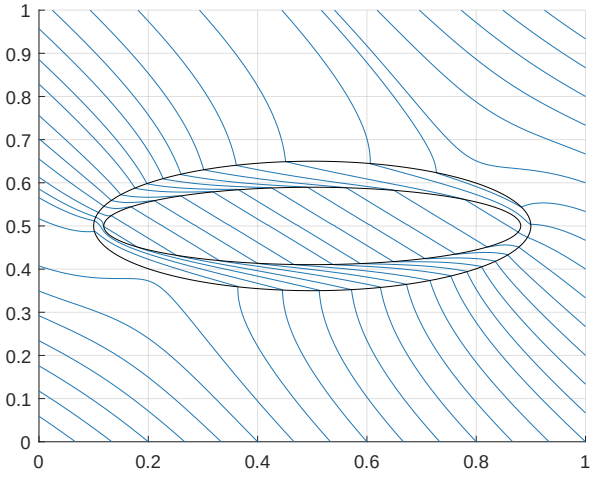

(b)

Figure 2.1: Maxwell's equations solved for shapes in the prolate spheroidal coordinate system to resemble the shape of a vessel. The shapes have a different magnetic permeability than the area around it. The first shape (a), consists of a solid region with a permeability which is a hundred times higher than its surroundings. The second shape (b), has an added inner region with the same permeability as the region around it.

In order to approximate the shape of a vessel, the equations can be solved in a different coordinate system than the Cartesian. In the case of figure 2.1, it is in the prolate spheroidal coordinate system. This is an elliptical coordinate system which can also be used in three dimensions [2]. An elliptical shape can approximate the shape of a vessel quite well and by removing the inner region, it resembles a ships hull.

Estimating the magnetic signature of a vessel can be done with the described method. An advantage is that the computing time is relatively fast. That means that an analytical model can be used in the feedback loop of a closed loop control system that is used to control the degaussing currents. However, it is not very accurate. The model uses an elliptical shape which is an approximation of the shape of the vessel. The accuracy is investigated in section 2.2.1.

2.1.2. FINITE ELEMENT MODELLING

A common way of modelling magnetic fields is the use of finite element modelling (FEM). FEM is a method that provides approximate solutions to boundary value problems. Any geometry can be created and is approximated by a mesh. The differential equations are then solved in between the nodes. The more nodes the mesh has, the higher the resolution of the model.

For a ship, the thickness of the hull is much smaller than its length. That means that if the ship needs to be modelled with a sufficient resolution, the mesh will get an unpractical amount of nodes [3]. A common solution to model thin iron plates like this is to use the reduced scalar potential [4]–[6]. FEM can be also used to model the magnetic signatures of the other devices on board of the ship [7].

FEM models generally take more time to compute than analytical models. The more accuracy is needed, the longer the computational time. However, they offer a better accuracy than an analytical approach. In this research, the computational time is not relevant. The model is only needed to estimate the requirements for a degaussing system.

2.2. EXPERIMENTAL VERIFICATION

The modelling methods described in this chapter are verified. A test setup is described that can measure the magnetic signature of a steel object. This section describes how the test setup was built.

2.2.1. SYSTEM DESCRIPTION

The table top demonstration consists of a steel hollow cylinder which is equipped with a set of three degaussing coils. The magnetic signature of the pipe and the effect of the degaussing coils can be measured with a movable sensor at a certain distance from the pipe along a line parallel to the longitudinal direction of the pipe. Earth's magnetic field is the external field.

Figure 2.2 shows a schematic representation of the test setup where, L is the length of the pipe, D is the diameter of the pipe, t is the thickness of the wall, d the vertical distance of the sensor from the pipe and μ_r is the relative permeability of the material. B_x, B_y and B_z are the Cartesian components of Earth's magnetic field, with respect to reference frame x, y and z. In this reference, z is pointing to the magnetic north pole

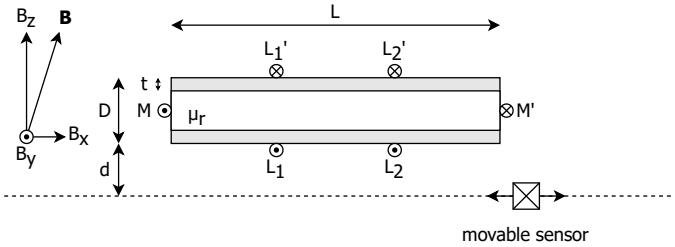

Figure 2.2: Schematic representation of the setup. The pipe has three degaussing coils; one main (M) coil and two longitudinal (L) coils. The pipe is placed in Earth's magnetic field and a magnetic sensor runs underneath.

and x is orthogonal to Earth's surface. L_1, L_2, and M represent the three degaussing coils. The sensor can move over a length of 3 m. Table 2.1 shows values for the parameters of the test setup.

Table 2.1: Properties of the test setup and conditions as described in figure 2.2.

Symbol	Description	Value	Unit
D	pipe diameter	200	mm
t	wall thickness	10	mm
μ_r	relative permeability	110	-
B_x	flux density in x direction	20.1	µT
B_y	flux density in y direction	0.7	µT
B_z	flux density in z direction	-35.4	µT

It should be noted that Earth's magnetic field was found not to be homogeneous at the measurement location. The values from table 2.1 are an average. Figure 2.3 shows a plot of the measured flux density of Earth's magnetic field over the measuring line.

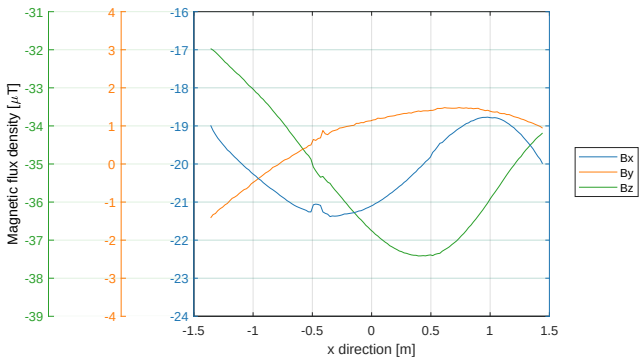

Figure 2.3: Measurement of Earth's magnetic field at the test location. The plot shows the vertical component, B_z, and the two horizontal components, B_x and B_y, of the magnetic flux density, $\vec{B}$, of Earth's magnetic field.

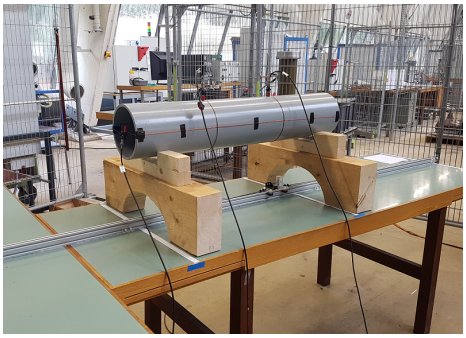

Figure 2.4: Metal pipe with three copper degaussing coils; one in the M and two in the L-direction.

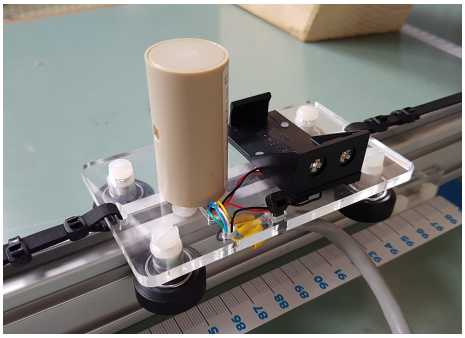

Figure 2.5: Movable magnetic flux gate sensor that travels underneath the pipe along a rail.

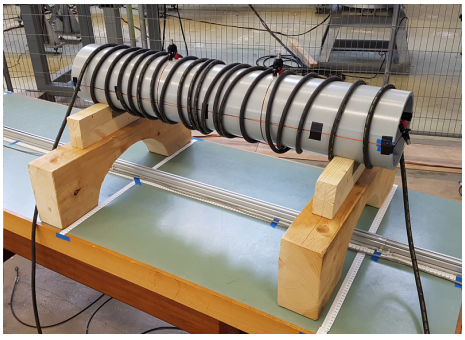

Figure 2.6: Metal pipe with a deperming coil. An alternating current with a decreasing amplitude is used to remove the permanent magnetic field .

Figure 2.4 shows a picture of the the test setup which was built according to the specifications shown in table 2.1. The degaussing coils are wound around the pipe with regular copper wire. Each coil has a number of two turns. The coils are individually supplied by direct current power sources. The connection from the power source to the degaussing coils is through co-axial cables in order to minimize the influence of the magnetic field of the supply current on the measurements.

The material of the pipe is S355J2H; a high tensile steel type which is used for the construction of ships. Underneath the pipe, a rail is placed which transports the sensor. At the end of the rail, an encoder measures the position of the sensor. Figure 2.5 shows the rail with the sensor cart.

The magnetic flux density underneath the pipe is measured with a fluxgate sensor (Stefan Mayer FLC3-70). Fluxgate sensors are known for their precision, however, the accuracy is relatively low. The fluxgate principle is based on magnetisation of a soft iron core inside the sensor. Due to a small permanent magnetisation of the core, an offset can occur. Therefore, all the measurements of the magnetic signature are calibrated to a reference measurement of the magnetic flux density in the room.

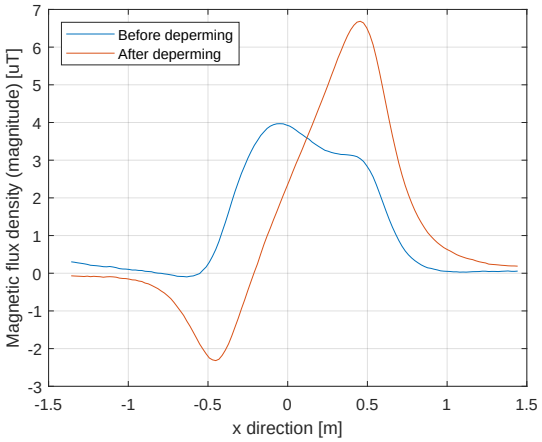

Figure 2.7: The measured magnitude of the magnetic flux density of the magnetic signature, $|\vec{B}_{sig}|$, before and after deperming on the trajectory of the sensor. The magnetic signature after the deperming process matches the simulated magnetic signature well. The simulated magnetic signature is shown in figure 2.8.

During the fabrication process of the steel or the construction of the pipe, it might have been permanently magnetised. In order to get rid of any permanent magnetisation within the pipe, it needs to be demagnetised. By applying a decreasing alternating magnetic field in the material induced by a external coil, the permanent magnetisation can be removed [8]. Figure 2.6 shows a picture of a deperming coil around the pipe.

With an AC current through the coil starting at 15 A, the residual flux was removed by slowly and constantly decreasing the amplitude of the current to zero. The frequency of the current was 50 Hz. Figure 2.7 shows the measured results of the magnetic signature of the pipe before and after the deperming procedure. It can be seen from this graph that there was a significant permanent magnetisation in the pipe. The measured magnetic signature after deperming shows a high similarity with the simulated magnetic signature which is shown in the next section. This implies the deperming procedure was successful.

2.2.2. MODEL AND OPTIMISATION

In order to find the optimal placement for the L-coils and the optimal amount of degaussing current, a model of the pipe is needed. This model should be usable in an optimisation loop to optimize the coil placement and currents values.

There are various ways to model the magnetic field around a steel object as described in section chapter 2. An analytic approach may be used when the object has a spherical or ellipsoidal geometry. This technique is based on solving Maxwell's equations in a ellipsoidal coordinate system as described in section 2.1. However, the use of finite element modelling (FEM) shows more accurate results when an object has a different kind of geometry [9].

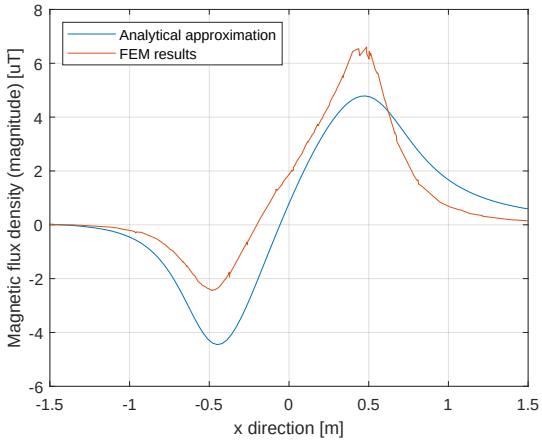

Figure 2.8: Modelled magnitude of the magnetic flux density of the magnetic signature, $|\vec{B}_{sig}|$ on the trajectory of the sensor. Analytical results compared to numerical (FEM) results. The analytical method uses an ellipsoidal shape instead of a cylinder, explaining the difference. The jumps in the plot of the FEM results are due to the courseness of the mesh.

Figure 2.8 shows a graph where the results of analytical modelling using the ellipsoidal coordinate system are compared to a FEM approach. In the analytical model, the pipe is modelled as an ellipsoid which has the same length and width as the pipe. In the FEM model a CAD drawing of the pipe is used. The FEM modelling is done in COMSOL [10].

Although the results do not completely match, the analytical results show some resemblance with the FEM results. The asymmetry in the plots is due to the incidence angle of the external field. The FEM results show a larger asymmetry than the analytic results which is due to the sharp edges of the pipe compared to the rounded edges of the ellipsoid.

In this case, analytical modelling is useful to approximate the geometry of an object with a similar shape as an ellipsoid and to make a first estimation of the flux densities. It might also be used in optimisation loops, because this technique requires less computing power than the use of FEM.

The goal of the optimisation loop is to find the ideal coil placement and degaussing currents. This is done by minimising the following optimisation criterion, c:

$$c = \int \left(\frac{|\vec{B}(I_{L1}, I_{L2}, I_{M1}, x_{L1}, x_{L2})|}{|\vec{B}_{des}|} - 1 \right)^2 dl \tag{2.8}$$

where l is placed on the measurement line, $\vec{B}$ is the magnetic flux density on the measurement line, which can be written as a function of optimisation variables. These are the degaussing currents I_{L1}, I_{L2} and I_{M1} and the L-coil positions x_{L1} and x_{L2}. $\vec{B}_{des}$ is the desired magnetic flux density on the measurement line.

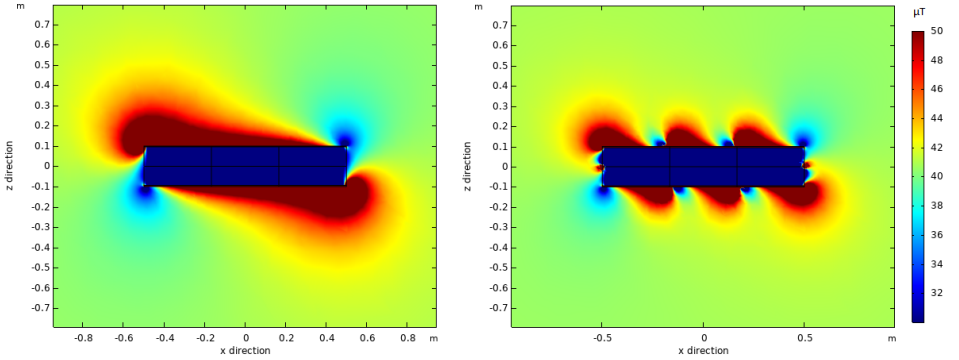

(a) (b)

Figure 2.9: 3D FEM modelling of the (a) magnetic signature and the (b) reduced magnetic signature of the pipe. It can be seen that the optimised degaussing currents are able to reduce the magnetic signature at some distance.

For an optimal degaussing effect, the desired magnetic flux density on the measurement line should be as close to the flux density which would have been there if the pipe was not there. This is the case when the optimisation criterion, c, is at a minimum. The solution for the optimal degaussing currents in Ampere-turns and the optimal placement of the L-coils are shown in table 2.2.

In figure 2.9a, the expected magnetic signature in the xz-plane is shown. For comparison, the effect of the degaussing coils in the xz-plane is shown in figure 2.9b. It can be seen that the magnetic signature is lowered by degaussing.

Table 2.2: Optimised degaussing current set-points.

Symbol	Description	Value	Unit
I_{L1}	current through first L-coil	3.64	A·t
I_{L2}	current through second L-coil	3.64	A·t
I_M	current through M coil	3.98	A·t
x_{L1}	position first L-coil	-167	mm
x_{L2}	position second L-coil	167	mm

The measurements where done according to the following procedure. First, a reference measurement was done by mapping the magnetic flux density in the room without the presence of the pipe. Secondly, the magnetic signature of the pipe was measured by placing the pipe in its location. And finally, with the pipe in the same location, the magnetic signature reduction was measured by running the calculated degaussing currents through the degaussing coils. The magnetic signature and magnetic signature reduction measurements were normalised by subtracting the reference measurement.

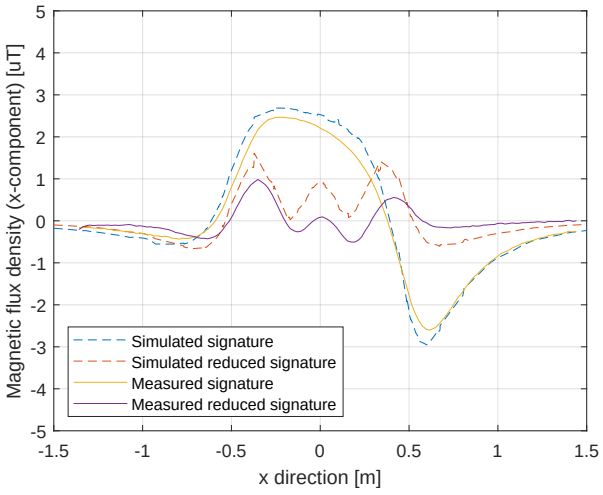

Figure 2.10: Results of the measurements compared to the simulations of the magnetic signature and the reduced magnetic signature. The plot shows the horizontal component, B_x, of the measured magnetic flux density. The measured background field is subtracted from the measured results to show the magnetic signature.

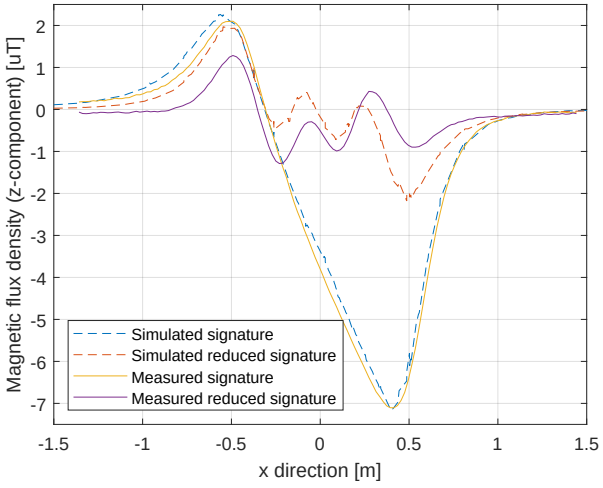

Figure 2.11: Results of the measurements compared to the simulations of the magnetic signature and the reduced magnetic signature. The plot shows the vertical component, B_z, of of the measured magnetic flux density. The measured background field is subtracted from the measured results to show the magnetic signature.

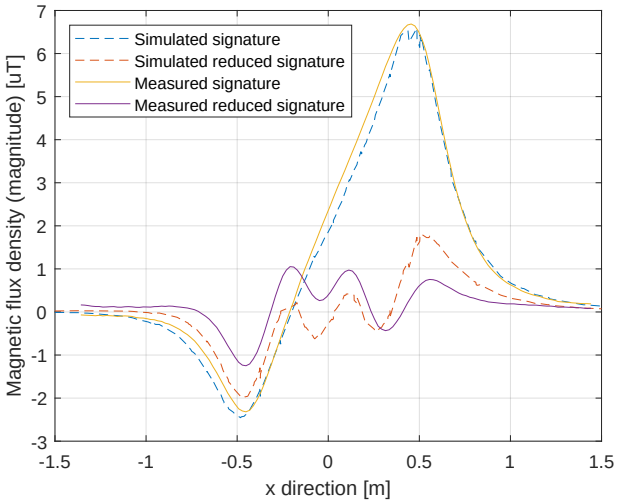

Figure 2.12: Results of the measurements compared to the simulations of the magnetic signature and the reduced magnetic signature. The plot shows the magnitude, $|\vec{B}|$ of the measured magnetic flux density. The measured background field is subtracted from the measured results to show the magnetic signature.

2.2.3. RESULTS

The magnetic flux density is measured in the x, y and z direction. The y direction is not shown here, because the external field only has an x and z component and the pipe is symmetrical in this plane.

In figure 2.10, the plots are shown of the measured and the simulated x-components (longitudinal) of the magnetic signature and the reduced magnetic signature. Figure 2.11 shows the plots of the z-component (vertical) of the measured and simulated magnetic flux density. Finally, the plots of the magnitude of the measured magnetic flux density is shown in figure 2.12. Again, the measured results are compared with the simulated results.

It can be seen from the results that the measured magnetic signature is quite similar to the modelled magnetic signature, but, there is a small difference. The results of the measured magnetic signature reduction show a larger deviation from the simulated results.

2.2.4. DISCUSSION

The results show a partial removal of the magnetic signature. A more effective degaussing is achieved when a finer mesh of deguassing coils is used. In the results, a difference is observed between the simulated and measured magnetic flux densities. One of the reasons is that the external magnetic flux density in the measuring room was not homogeneous, while in the simulations an average of this magnetic flux density was used. Another reason could be that after the deperming process still some permanent mag-

netisation remains in the pipe, which is not taken into account in the simulations.

The simulated degaussing shows a larger deviation from measurements than the simulated magnetic signature. This might be due to the use of edge current modelling and measurements and sensor errors. In chapter 3, a different table-top model is used with both copper and HTS coils. The goal is to not only compare static, but also dynamic behavior.

2.3. CONCLUSION

The magnetic signature consists of many components, but the one which is relevant for degaussing is the induced magnetisation. In order to measure the induced magnetisation properly however, one has to remove the permanent magnetisation first by means of deperming.

There are several ways to model the magnetic signature of a steel object. The analytical approach is accurate, but is limited to shapes which can be expressed analytically like ellipses and circles. If the shape that needs to be modelled can not be expressed analytically, it may still be approximated by another shape. The model then has a lower accuracy. Another advantage of analytical modelling is that it is fast to compute. This can be an advantage for applications like closed loop degaussing. A more practical and modern approach of modelling is the use of FEM. Any shape can be modelled accurately, but the simulation time is long in comparison.

A test setup consisting of an arbitrary metal object is used to show that the magnetic signature of the object can be modelled and measured. The measured magnetic signature corresponds to the modelled one. The influence of the surrounding near the setup can influence and distort Earth's magnetic field in the proximity of the setup, which is an important factor in these kind of measurements. Removing the permanent magnetisation of the test object is necessary, because its influence can be significant.

BIBLIOGRAPHY

[1] J. J. Holmes, "Exploitation of a Ship's Magnetic Field Signatures", *Synthesis Lectures on Computational Electromagnetics*, vol. 1, no. 1, pp. 1–78, Jan. 2006.

[2] F. E. Baker and S. H. Brown, "Magnetic induction of ferromagnetic prolate spheroidal bodies and infinitesimally thin current bands", *Journal of Applied Physics*, vol. 53, pp. 3991–3996, 6 Jun. 1982.

[3] P. Jankowski and M. Woloszyn, "Applying of thin plate boundary condition in analysis of ship's magnetic field", *COMPEL - The international journal for computation and mathematics in electrical and electronic engineering*, vol. 37, pp. 1609–1617, 5 Sep. 2018.

[4] X. Brunotte and G. Meunier, "Line element for efficient computation of the magnetic field created by thin iron plates", *IEEE Transactions on Magnetics*, vol. 26, pp. 2196–2198, 5 1990.

[5] X. Brunotte, G. Meunier, and J. P. Bongiraud, "Ship magnetizations modelling by the finite element method", *IEEE Transactions on Magnetics*, vol. 29, pp. 1970–1975, 2 1993.

[6] O. Chadebec, J. L. Coulomb, V. Leconte, J. P. Bongiraud, and G. Cauffet, "Modelling of static magnetic anomaly created by iron plates", *IEEE Transactions on Magnetics*, vol. 36, pp. 667–671, 4 PART 1 2000.

[7] P. Jankowski and M. Woloszyn, "Analysis of ship's magnetic field with consideration of inner ferromagnetic devices", IEEE, Sep. 2017, pp. 1–2.

[8] J. J. Holmes, "Reduction of a Ship's Magnetic Field Signatures", *Synthesis Lectures on Computational Electromagnetics*, vol. 3, no. 1, pp. 1–68, Jan. 2008.

[9] C. Aird, "Modelling the induced magnetic signature of naval vessels", PhD Dissertation, University of Glasgow, 2000.

[10] COMSOL AB, *Comsol multiphysics*, version 5.4, Oct. 3, 2018. [Online]. Available: `https://www.comsol.com/`.

3

HTS DEGAUSSING COILS

High temperature superconductors (HTS) are a fascinating material with many applications. Because of the lack of electrical resistance in DC, they can be used in high current density applications, to create strong magnetic fields or to eliminate conduction losses. Degaussing is such an application where a magnetic field is required but conduction losses are unwanted. This chapter provides some background on HTS. A literature review is conducted on the different types, applications and modes of operation of HTS. Furthermore, to show that HTS degaussing coils reduce a magnetic signature just as well as copper degaussing coils, an experimental demonstrator is build. This demonstrator includes a cryostat with liquid nitrogen and a measuring setup to map the magnetic flux density.

3.1. HIGH TEMPERATURE SUPERCONDUCTORS

Superconductivity was discovered in 1904, 35 years before the invention of degaussing. H. Kamerlingh-Onnes was studying the temperature dependence of the electrical resistivity of mercury when he noticed that around 4 K, the resistance suddenly dropped to zero [1]. As the temperature decreased, the resistance disappeared instantly and the material seemed to have transformed into a different state. This state was named superconductivity.

The temperature of the transition to the superconductive state is called the critical temperature, T_c. Soon after its discovery, it was found that the superconductive state can be destroyed by placing the material in a magnetic field. The magnetic field strength

Parts of this chapter have been published as:
D. Wikkerink, I. Hanse, A. Rodrigo Mor, H. Polinder, and R. Ross, “Demonstration of Degaussing by Copper and HTS Windings”, International Naval Engineering Conference and Exhibition (iNEC), 5-9 October, Delft, The Netherlands, 2020.
I. Hanse, D. Wikkerink, C. Vermeer, H. Holland. M. Dhallé and H.J.M. ter Brake. "Cryogenics for an HTS Degaussing System Demonstrator", International Naval Engineering Conference and Exhibition (iNEC), 5-9 October, Delft, The Netherlands, 2020.

to do so is called the critical field, H_c, of the material. The critical field is temperature dependent and described by the following empirical formula,

$$H_c(T) = H_c(0)\left[1 - \left(\frac{T}{T_c}\right)^2\right], \tag{3.1}$$

where $H_c(0)$ is the critical field extrapolated to absolute zero [2]. This formula shows that when the superconductor is exposed to a higher magnetic field, the temperature at which the state transition to superconductive state occurs is lower.

As the years went by, more and more materials were found that can be brought into superconductive state. In fact, many of the elements are superconductors, but their critical temperature is typically not higher than 12 K. Some compounds were discovered with a slightly higher critical temperature than elements, but a real breakthrough occurred in 1987, with the discovery of high temperature superconductors or HTS.

HTS are defined as superconductors with a critical temperate higher than the boiling point of liquid nitrogen, 77 K. Although this is still far below room temperature, they have a much higher critical temperature than previously found superconductors. This is important, because these superconductors can be cooled with liquid nitrogen instead of liquid helium. Cooling liquid nitrogen is much more energy efficient than cooling liquid helium because of the higher boiling temperature of nitrogen. Also, liquid nitrogen is relatively cheap and easy to handle compared to liquid helium. HTS generally have a high critical field, making them a good material for superconductive magnets. There exist several HTS materials. In this thesis, it was chosen to use YBaCuO, which is usually simply written as YBCO. The reason being that this material is the most common HTS at this time and it meets the requirements for a degaussing coil. Figure 3.1 shows the critical temperature of some of the superconductors and the year when they were discovered. A clear trend is visible that as time passes, superconductors with a higher critical temperature are discovered. If it keeps on this trend, we can expect superconductors with a critical temperature above room temperature any time soon.

The first claim for a room temperature superconductor was presented in the journal Nature in 2020 [4]. At a pressure of 270 GPa, H_3S shows zero resistance. However, this paper was revoked in 2022 because of questionable methods. In 2023, a team of Korean researchers claimed to have discovered the first superconductive material at room temperature and atmospheric pressure [5]. This material, LK-99, consists of abundant materials like lead, copper and phosphorous and is easy to synthesize [6]. At the time of writing however, these results couldn't be reproduced by other scientists yet. The scientific community remains very sceptical towards claims on room temperature superconductivity, which some consider the holy grail of physics.

3.1.1. HTS APPLICATIONS

The most prominent application for HTS are superconductive magnets. These can be found in MRI scanners, NMR scanners, particle accelerators and nuclear fusion reactors. For these applications however, LTS are still a popular choice as well since the needed amount is limited and money is usually not something that influences the design choices.

Another application for HTS is found in power systems and power components [7].

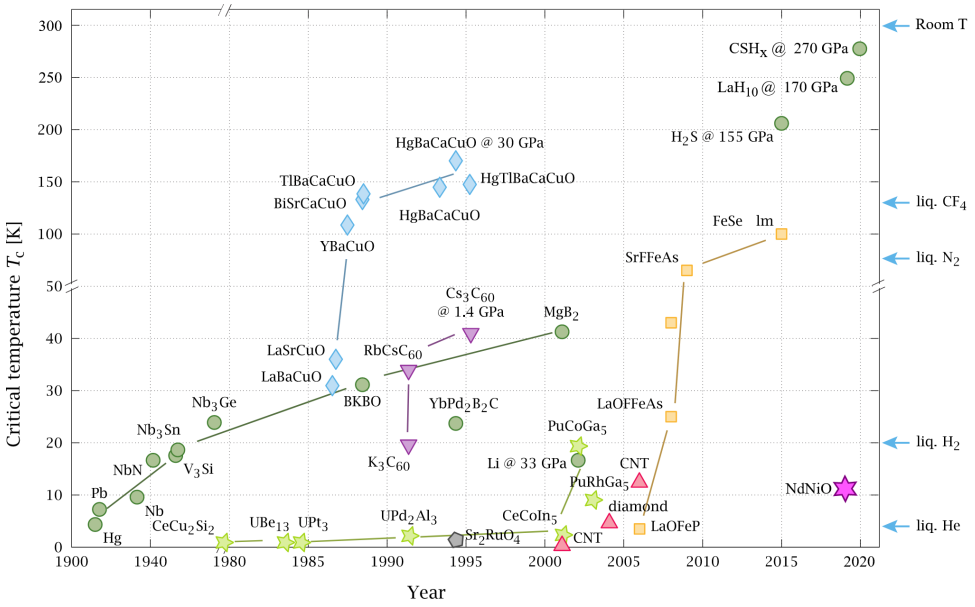

Figure 3.1: An overview of the most important superconductors discovered from 1900 until 2020. A breakthrough occurred when HTS was discovered in 1986 having a critical temperature higher than the temperature of LN_2. A clear trend is visible towards higher critical temperatures as time increases. If this trend continuous, room temperature superconductors are soon among us. [3]

Fault current limiters utilise saturated iron cores in superconductive coils or the unique quenching properties of HTS. Energy can be stored without losses in superconductive magnetic energy storage (SMES) system [8]. Transmission cables can be made more efficient by using a HTS as a conductor. Furthermore, the compact cables can be used in dense areas where there isn't much available space, but a high current is required. HTS based power components like transformers and electrical machines are energy efficient, compact and light [9]. This can be of great benefit for all kinds of applications, like wind turbines [10].

In the transport industry, HTS can have a big impact as well. The automotive industry can use superconductive coils to charge electric vehicles [11] wirelessly. Magnetic levitation trains can hover over magnetic fields created by HTS coils [12]. In the maritime industry, ships can use HTS for a more efficient propulsion, switchboards and machinery [13], [14]. And finally, it is expected that superconductors are a necessary part of large scale electric flying [15].

3.1.2. PERSISTENT MODE

Once a superconductive coil has been charged, it can be put into persistent mode by short-circuiting the superconductor. The windings are closed and the power supply can then be turned off. Because there is almost no damping, the current keeps on running. Like a permanent magnet, the magnetic field remains without adding additional energy

to the magnet. For the application of degaussing, this is exactly what's needed; a lossless DC magnetic field. Figure 3.2 shows a representation of the persistent mode.

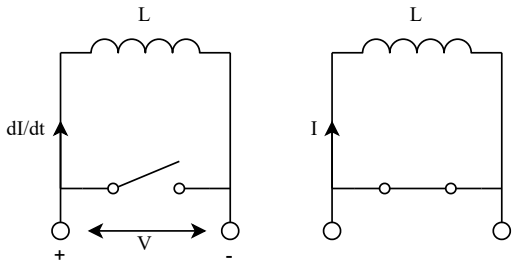

Figure 3.2: A DC current can run for a long time when it is in persistent mode. There is no resistance in the coil to dampen out the current. During the charging state, the current is increasing. When the coil is short-circuited the voltage is across the coil is zero, which means that the current is not changing.

A device that can bring a superconductive circuit in persistent mode is the persistent current switch (PCS). It works as follows: a small part of the closed superconductive coil is heated, so that this part of the loop is out of superconductive state. Now a voltage can be applied across the heated part so that a current can build up in the coil. When the current reaches the desired value, the heated part is cooled down and the current is "trapped" inside the superconductive loop [16]. Alternatively, instead of heating a part of the superconductor, one can also apply a magnetic field on this part of the superconductor. The superconductor then goes out of its superconductive state because of exceeding the critical magnetic field [17], [18]. One of the applications for a PCS is in MRI scanners [19]. The switching of PCSs is in the range of seconds, which is too slow for the application of degaussing.

A problem occurs when bringing HTS into persistent mode. Unlike for LTS, the resistance of the soldered joint of HTS is never zero. Some reports of an almost superconductive weld have been made [20], but they are very complicated to achieve which make them impractical for a degaussing application. A closed loop HTS coil with a small weld resistance is therefore said to be in quasi persistent mode. The current still remains to flow, but it slowly decays. To compensate for these losses, another device can be used to slowly add magnetic flux to the coil. A flux pump.

Several types of flux pumps exist [21]. Most of them are based on the phenomenon that a small voltage can be induced in a HTS by applying a traveling wave inside the HTS by using a varying magnetic field. A large solenoid is needed where the HTS tape is placed in a small air gap so that a magnetic field can be created on in the tape. The solenoid needs to be placed inside a cryostat in order to ensure the small air gap. Another type, which supplies an asymmetric AC current to the HTS, makes use of the quenching of the PCS of the superconductor during one half of the cycle. This make the PCS behave as a rectifier [22]. However, this topology still needs a transformer inside a cryostat to supply the current to the superconductive coil.

In conclusion, persistent mode is a potential technique that can be used for HTS degaussing systems to improve their efficiency. Unfortunately, the known flux pump techniques to compensate for the losses in the weld would be impractical to implement

in an HTS degaussing system. The introduction of the losses of the magnetic core and copper inside the cryostat will undo the advantages of using persistent mode in the first place. Besides, a PCS is very slow, but the degaussing current needs to be controllable to anticipate the roll and heading changes of the ship. For these reasons, this thesis takes a different approach of supplying the degaussing currents. A solution inspired by persistent mode. The superconductive coil is charged by switching transistors, but the serial resistance in path with the superconductor is kept to a minimum so that the decay time is long. This solution is further explained in chapter 4.

3.1.3. BENEFITS AND ISSUES USING HTS FOR DEGAUSSING

The use of HTS degaussing coils eliminates most of the Ohmic losses in the coils. However, two extra sources of power loss are introduced. Firstly, HTS can only function when it is cooled down to a temperature where it is in a superconductive state. This causes cooling losses. Besides, heat leak into the cryostat needs to be cooled away causing even more losses. Secondly, HTS can handle a high current density, so it might be useful to design the degaussing coils with fewer turns and higher current than with the copper degaussing coil. This will save material and is easier to install, but will also cause an increase in the energy dissipation in the power supply source because of the higher current. From an efficiency point of view, HTS is only beneficial when these two loss sources are smaller than the initial Ohmic losses from a copper degaussing system. This is a trade-off of which the outcome also depends on the size of the system.

With the small resistance in HTS degaussing systems, the time constant might become too big to control the current through the coil. Equation (3.2) shows how the time constant, τ, of a coil depends on its inductance, L, and series resistance R.

$$\tau = \frac{L}{R} \tag{3.2}$$

With the resistance approaching zero, the time constant becomes very large. This is problematic when the system needs to react fast. In a practical case however, the power source has an internal series resistance. Also the leads from the power source to the superconductor are made of copper, so there will be a source of damping in the system. Moreover, if fewer number of turns are used in the HTS system, the inductance of the degaussing coils, and therefore the time constant, will decrease as well.

For a system of degaussing coils, the coupling of the coils might play a role because of the lack of damping. The following equation describes the coupling of a degaussing coil, i, with the rest of the coils in a system of degaussing coils.

$$v_i = R_i i_i + L_i \frac{\mathrm{d}i_{L_i}}{\mathrm{d}t} \pm \sum_{\substack{j=1 \\ j \neq i}}^{N} M_{ij} \frac{\mathrm{d}i_{L_j}}{\mathrm{d}t}, \tag{3.3}$$

where v_i is the voltage, i_i is the current, L_i is the inductance and R_i is the resistance of degaussing coil i. M_{ij} is the mutual inductance between coil i and j. In an HTS system, the term with the series resistance might become so small that the mutual inductance, M, becomes significant. This means that the degaussing coil is more responsive

to the current running through the coupled coils. Again, the series resistance does not go to zero because of the power source and the current leads.

3.2. HTS DEGAUSSING DEMONSTRATOR

To compare the functionalities of an HTS degaussing system with a copper degaussing system, a table-top demonstrator was equipped with both copper and HTS degaussing coils. The two degaussing topologies are compared by measuring the corresponding reduced magnetic signatures. A preliminary study was done where the magnetic signature reduction with only copper coils was measured [23].

3.2.1. SYSTEM DESCRIPTION

The table top demonstrator consists of a hollow steel pipe with caps welded on the ends to simulate a ship. The pipe is equipped with degaussing coils in two directions, one in the M, i.e., vertical direction and two in the L, i.e., longitudinal direction. For each degaussing coil there is a copper and HTS variant which are placed as close to each other as possible, so almost in the same position.

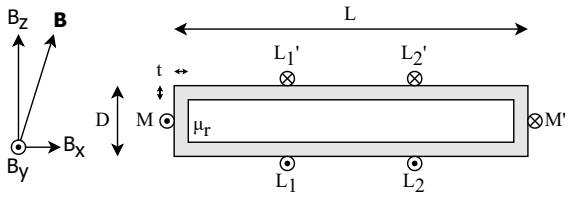

Figure 3.3: Schematic representation of the test setup. A metal pipe with welded caps is placed in the magnetic field of the Earth. The pipe has three copper and three HTS degaussing coils.

The demonstrator is placed parallel to the magnetic meridian, so the magnetic distortion is expected to take place in two dimensions. The degaussing can then also be done in two dimensions which makes a coil in the athwart ship direction unnecessary. A schematic representation of the demonstrator is depicted in figure 3.3, where L is the length of the pipe, D is the diameter of the pipe, t is the thickness of the pipe and μ_r the relative permeability of the pipe. B_x, B_y and B_z are the Cartesian components of the magnetic flux density of Earth's magnetic field with respect to reference frame x, y and z. M, L1, and L2 represent the three degaussing coil positions for which each position has a copper and HTS degaussing coil. The values of the parameters are listed in table 3.1.

The values of B_x, B_y and B_z are the average of the measured magnetic flux density over the distance of the measuring line without the pipe in place, this is further explained in section 3.2.3. Since the pipe is placed parallel to the magnetic north-south line, the y component of the measured zero field is close to zero. The relative permeability is found by fitting the measurement of the magnetic signature to the simulated magnetic signature.

Table 3.1: Demonstrator parameters. The background magnetic flux density is measured and averaged over the length of the sensor rail.

Symbol	Description	Value	Unit
L	pipe length	1500	mm
D	pipe diameter	320	mm
t	wall thickness	5	mm
μ_r	relative permeability	320	-
B_x	flux density in x direction	18.02	µT
B_y	flux density in y direction	0.07	µT
B_z	flux density in z direction	-42.45	µT

3.2.2. DEFINITION OF THE TESTS

Two tests were conducted in order to demonstrate that HTS and copper degaussing are similar. The static test is a set of measurements where the demonstrator is in a fixed position in the magnetic field of the Earth. First, the magnetic signature of the pipe is mapped by moving a magnetic sensor underneath the demonstrator over a distance of 4 m. This is defined as the measuring length. Then the reduced magnetic signature is measured with the copper degaussing coils on and then the reduced magnetic signature is measured also with the HTS degaussing coils on.

The dynamic test involves a pitching motion of the demonstrator. When the pipe is pitched within Earth's magnetic field, the magnetic signature changes. During the test, the pitching angle of the pipe is measured. The degaussing current set points are set accordingly with a control loop. First, the magnetic signature is measured on the five points as a function of pitching angle. Then the reduced magnetic signature by means of copper degaussing is measured and finally the reduced magnetic signature by means of HTS degaussing is also measured.

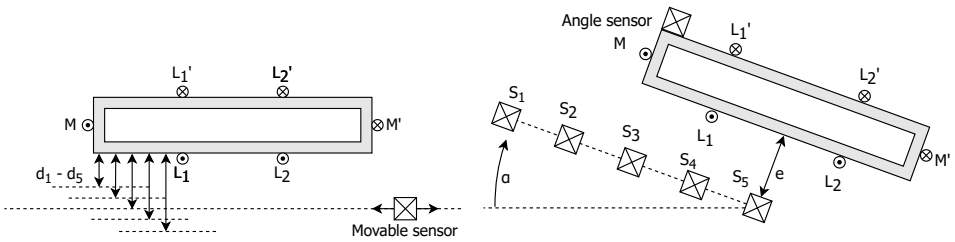

(a) (b)

Figure 3.4: Schematic representation of the static (a) and the dynamic (b) test. In the static test, the magnetic signature is reduced and measured at different distances from the pipe while the pipe is not moving. In the dynamic test, the magnetic signature is reduced and measured at different points while the pipe is moving.

Figure 3.4 shows a schematic representation of the two tests, where d_1 to d_5 are the measuring distances from the outside of the pipe to the movable sensor, e is the measuring distance from sensors S_1 to S_5 to the outside of the pipe and α is the pitching angle

of the pipe. The parameters of the two tests are listed in table 3.2.

Table 3.2: The different locations of the sensors for the static and dynamic test.

Symbol	Description	Value	Unit
e	measuring distance in the dynamic test	445	mm
d_1, d_2, d_3, d_4, d_5	measuring distances of the sensor to the pipe wall in the static test	439, 389, 339, 289, 239	mm
S_1, S_2, S_3, S_4, S_5	sensor 1, 2, 3, 4 and 5 with distance from the center of the pipe	0, 300, 600, 900, 1200	mm
α	pitching angle range	0 - 25	degree

3.2.3. BACKGROUND FIELD

The test setup was built in a wooden building where Earth's magnetic field was expected to be uniform and stronger than within a steel construction. Before the test were done, the magnetic field in the room needed to be mapped. Figure 3.5 shows the flux density of the three components of Earth's magnetic field over a distance of 4 m where the magnetic sensor is able to move.

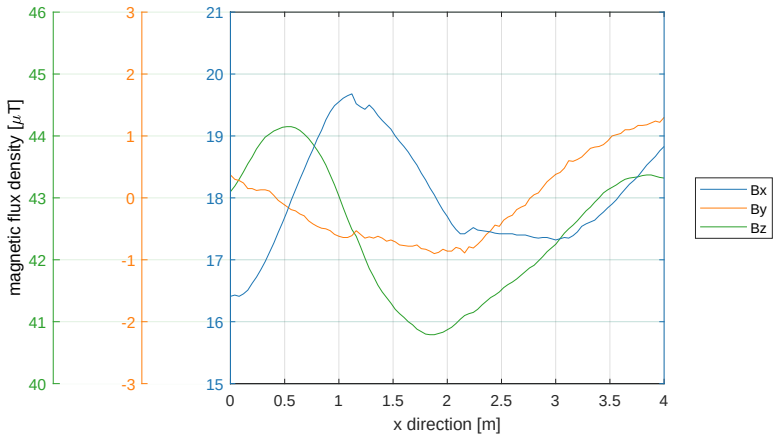

Figure 3.5: x, y and z component of the magnetic flux density of the background field where the magnetic sensor is. The bump in the x-component of the magnetic flux density at 1.25 m is caused by irregularities in the sensor rail, but is consistent throughout the measurements.

Although the background magnetic flux density was expected to be homogeneous, the measurements show a deviation of almost 4 µT in the x and z component of the measured field. This is probably due to the magnetic signature of the construction of the building where the test setup was placed. The values for B_x, B_y and B_z in Table 3.2 are the averages of the data in Figure 3.5. The magnitude of Earth's magnetic field is mapped at several measuring heights. The results are shown in Figure 3.6.

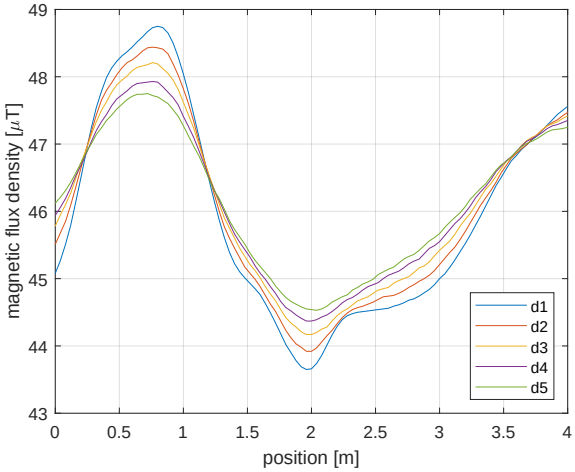

Figure 3.6: Measurement of the magnitude of the magnetic flux density of the background field at different sensor heights.

It can be observed that Earth's magnetic field gets more uniform as the sensor moves away from the floor. An explanation for this could be a steel reinforced floor which interferes with the measurements. The measurements from figure 3.6 are used as a reference measurement for the following measurements. The measurements of the background field will be subtracted from the magnetic signature measurements, so that only the magnetic signature remains. By doing this, also the unwanted offset in the magnetic sensors is removed.

3.3. REALISATION

There are several ways to model the magnetic field around a steel object. An analytical approach may be used when the geometry of the object resembles a spherical or ellipsoidal geometry [24] as described in section 2.1. In this method, Maxwell's equations are solved in a spheroidal or ellipsoidal coordinate system. The cylinder in this test setup can be approximated by a hollow ellipsoid. The results of the analytical approach for this test setup are shown in figure 3.9. An analytical model is useful for fast calculations in feedback loops, fast approximations or optimisation loops. When the geometry gets more complicated and more accurate results are needed, finite element modelling (FEM) gives a better result [25]. The simulated magnetic signature and the reduced magnetic signature are shown in figure 3.7.

The colour map in figure 3.7a shows the magnetic signature of the pipe when it is placed in Earth's magnetic field. The values for the external field are taken from table 3.1. Figure 3.7b shows the colour map of the pipe when there is a current in the degaussing coils. It is clear that the degaussing system reduces the magnetic signature of the pipe.

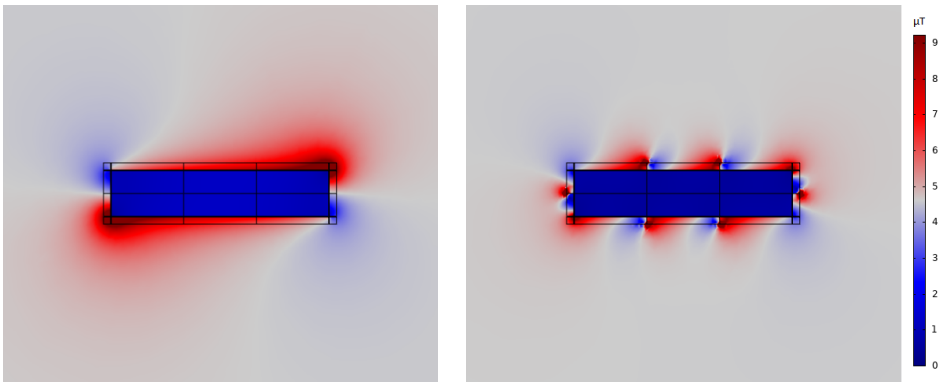

(a) (b)

Figure 3.7: Simulation of the (a) magnetic signature and the (b) reduced magnetic signature. The degaussing coils do not remove the magnetic signature fully. This is only possible when a higher resolution (more coils) is used.

The coupling factors between the main coil, M, and the longitudinal coils, $L1$ and $L2$, are simulated using the same FEM model. The results are shown in table 3.3. The coupling factors are also computed for the case that the degaussing coils are mounted on the inside of the pipe. These are shown in table 3.4.

Table 3.3: Coupling factors (external coils).

	M	L1	L2
M	1	0.102	0.102
L1	0.102	1	0.150
L2	0.102	0.150	1

Table 3.4: Coupling factors (internal coils).

	M	L1	L2
M	1	10e-6	10e-6
L1	10e-6	1	4e-3
L2	10e-6	4e-3	1

From these tables it can be seen that the degaussing coils in the demonstrator might be responsive to the current in other degaussing coils because of the high coupling factors. However, in the case where the coils are mounted on the inside of the pipe, the coupling of the coils is very low. The flux paths are not enclosed by the other coils, because most of the flux is going through the hull. This will be closer to the reality because, on a ship, the degaussing coils will also be mounted on the inside.

3.4. MAGNETIC SIGNATURE

A photo of the test setup is shown in figure 3.8.Figure 3.8a shows the metal pipe with end caps welded on the sides. The material of the pipe is S355J2H, a high tensile steel which is used for the construction of ships. The HTS degaussing coils are placed inside cryostats for insulation and cooling.

The copper degaussing coils are simple insulated copper wires which are wound around the pipe. The measurement rail is placed underneath the pipe. The pipe is placed in a wooden construction which makes it possible to place it under different angles with

respect to Earth's magnetic field. This is used in the dynamic test to simulate a pitching motion. The angle is measured with an acceleration sensor. The acceleration is integrated twice to obtain the angle. The angle sensor and the five magnetic sensors are fixed to the wooden construction. The cryostats of the HTS degaussing coils are connected to a closed liquid nitrogen system to ensure that the coils maintain their superconductive state. The sensor cart for the static measurements is shown in figure 3.8b. The height of the sensor is changed by adjusting the nuts on the non-magnetisable threads.

The magnetic flux density is measured by flux gate sensors. These sensors are very sensitive, but have a relatively low accuracy. Therefore, all the measurements are normalised with a reference measurement. This eliminates most of the offset in the sensors. In order to avoid disturbances in the measurements, all the materials in the test setup are chosen to have a relative permeability of close to one. The magnetic signature of the pipe is determined by subtracting the measurement of the pipe first measuring the magnetic field without the pipe.

The measured magnetic signatures are shown in figure 3.9 and figure 3.10. Figure 3.9 shows a comparison with the different modelling approaches. It can be seen that the results of the FEM model are very similar to the measurements. The ellipsoidal analytical model does not match the measurements that well. The horizontal position of the peaks of the magnetic signature is different than the measurements. This is because the analytical model uses an ellipsoidal geometry to approximate the cylindrical shape of the demonstrator. Still, it can be used for an estimation of the order of magnitude of the magnetic signature. The exact horizontal position of the peaks in the context of this experiment is not relevant, because the position of the peaks also depends on the location

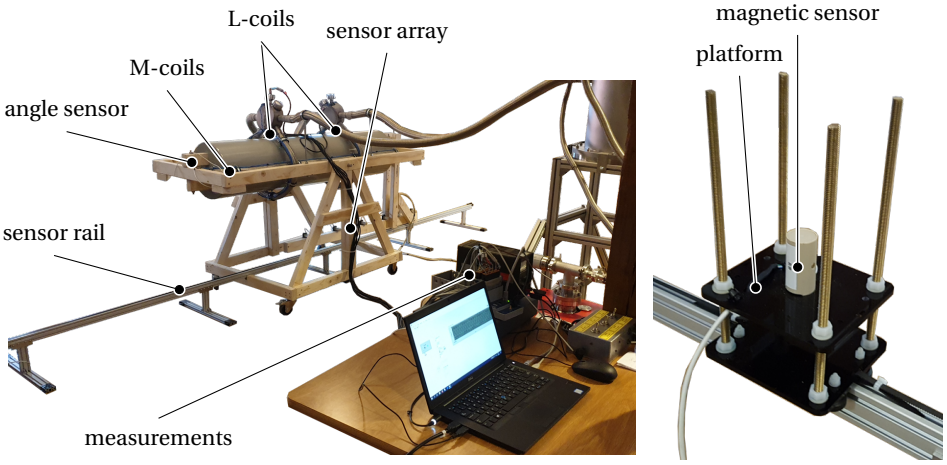

Figure 3.8: Photos of the magnetic measurements of the demonstrator. (a) The steel pipe is placed in a tiltable wooden frame with sensors attached to it. Underneath is a rail which can carry a movable sensor cart (b). The pipe has three copper and three HTS degaussing coils. The HTS degaussing coils are placed inside a cryostat. The signals of the sensors are processed through a digital acquisition card from National Instruments.

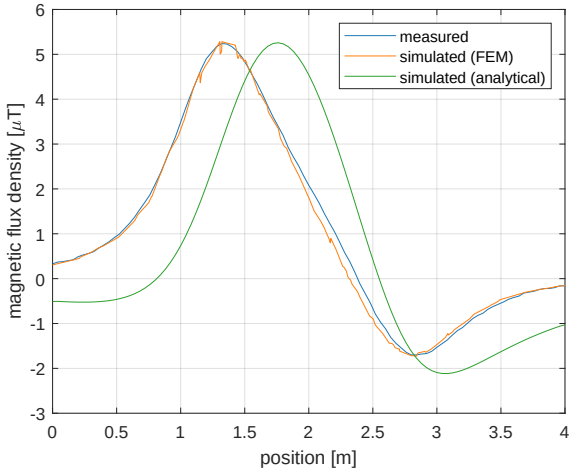

Figure 3.9: Plots of the magnetic signature of the pipe. The plot shows the measured, the simulated FEM, and the analytically simulated magnetic signature.

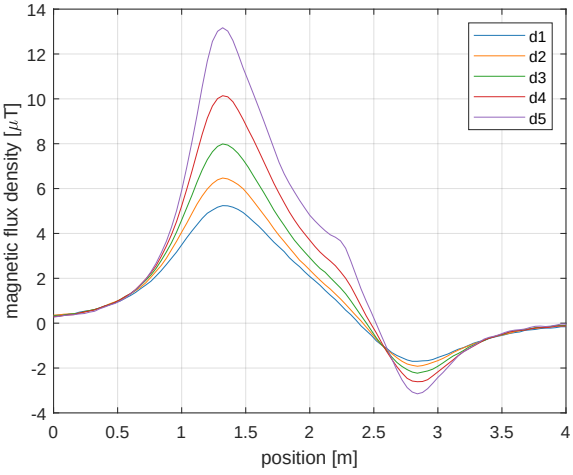

Figure 3.10: Plots of the measured magnetic signatures of the pipe at different sensor heights which are defined in table 3.2.

of the vessel. Ultimately, it's the variation in the magnetic field which triggers the sensor in a magnetic mine.

Figure 3.10 shows the measured magnetic signature with the sensor positioned at several measuring heights. The values for these measuring heights are given in table 3.2.

3.5. DEPERMING

To ensure that the measured magnetic signature corresponds to the simulated magnetic signature, the permanent magnetisation has to be removed from the pipe as much as possible. Due to the magnetic hysteresis of the pipe, a residual magnetic flux remains when the pipe gets magnetised. This remanent flux can be removed by cyclic magnetising and demagnetising of the pipe. Every cycle, some residual flux will remain. However, if the amplitude of the magnetising field is reduced every cycle, the residual flux will reduce and eventually disappear. [26]. The pipe in this setup is depermed by a deperming coil.

In this case, the magnetising current has a frequency of 2 Hz and an amplitude of 1540 A t at the start of the deperming session. The amplitude was decreased to zero over a period of 180 s. It is important to ensure that the deperming process is done while the background field is zero [27]. A DC current was maintained in both the L deperming coil and the M degaussing coils so the horizontal and vertical components of Earth's magnetic field were compensated for. The graph in figure 3.11 shows the results of the deperming process.

The magnetic signature changed significantly due to the deperming. The magnetic signature after the deperming shows a good resemblance with the simulated magnetic signature figure 3.11. This implies that the deperming process was successful.

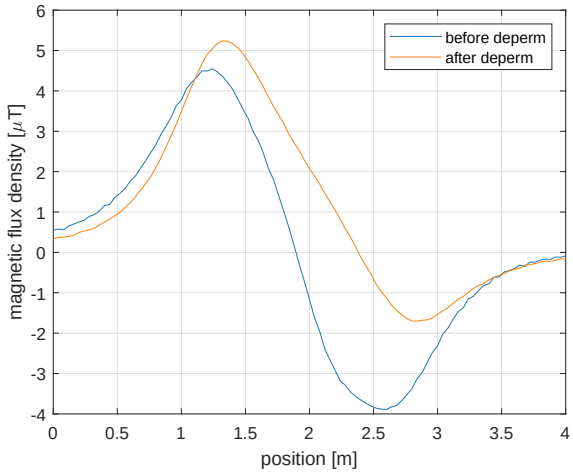

Figure 3.11: Magnetic signature before and after the deperming process. The magnetic signature after deperming process matches the FEM modelled magnetic signature.

3.6. CRYOSTAT

The HTS degaussing coils consist of YBCO tape which is wound around a flexible core. The critical temperature of YBCO is 93 K. A cryostat is used to cool the tape well below

the critical temperature to ensure some thermal margin. Section 3.6 shows a photo of the cryogenic system.

The superconductive tape is cooled by direct cooling, which means that the tape is in direct contact with the cryogen. The temperature of the cryogen should be low enough to ensure sufficiently large currents in the HTS. However, the lower the aimed temperature by cooling, the higher will be the expected power consumption. Sub-cooled liquid nitrogen was chosen as a cryogen for the demonstrator. Liquid nitrogen has a large heat capacity and a wide temperature range in which it can be used (65 K - 77 K) compared to liquid air. The temperature of liquid helium is too low for an efficient system because it requires more cooling power. By using sub-cooled nitrogen instead of boiling nitrogen, any bubbles in the system are eliminated that can cause local heat spots.

A closed system is used for nitrogen flow so that there is no need to fill the system during operation. The nitrogen flows through a heat exchanger where it is sub-cooled by a cooler. A nitrogen pump then pumps the nitrogen to the degaussing coils and back to the cooler. In front of the cooler, a degasser is placed to remove any nitrogen gas from

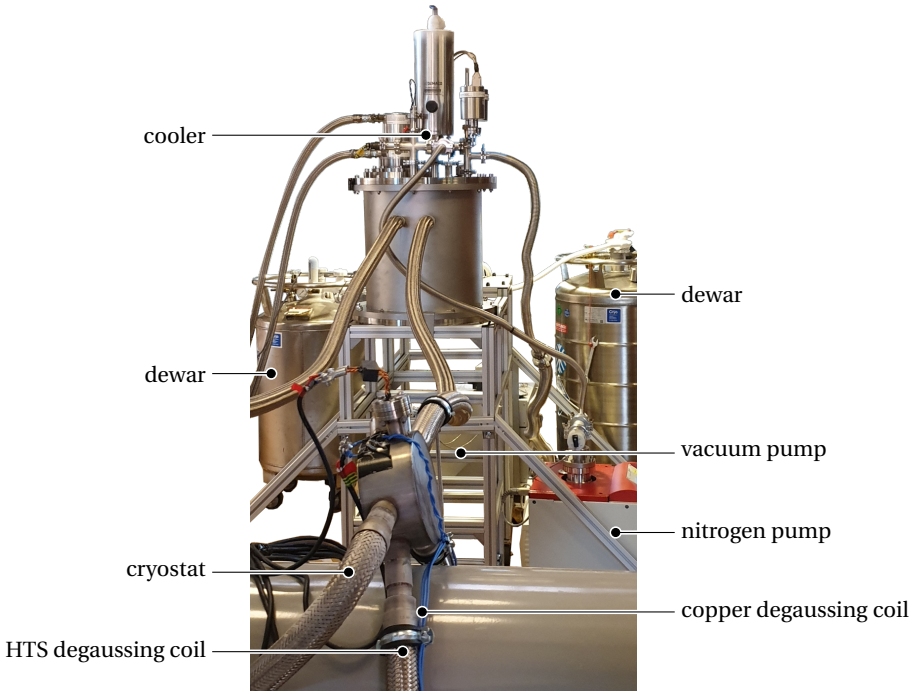

Figure 3.12: Photo of the cryogenic system. A nitrogen pump is used to pump the nitrogen through the system. The nitrogen is cooled by a cooler to compensate for heat leaks. A vacuum pump is used to keep the insulating vacuum around the cryostat.

the system. Vacuum insulated flexible cryostats are used around the degaussing coils and to transport the liquid nitrogen. A vacuum pump is used to maintain the vacuum in the cryostat.

3.7. RESULTS

3.7.1. SEPERATE COILS

The difference between the behaviour of HTS and copper degaussing coils is investigated by measuring the effect of each coil independently. The effect of one degaussing coil can be measured by running a current through this coil and measuring the magnetic signature of the whole setup. Then, the magnetic signature of the setup with zero current through the coil is subtracted. Now only the effect of the coil remains. A measurement was done where each coil was powered with 15 A·t. Figure 3.13 shows the results.

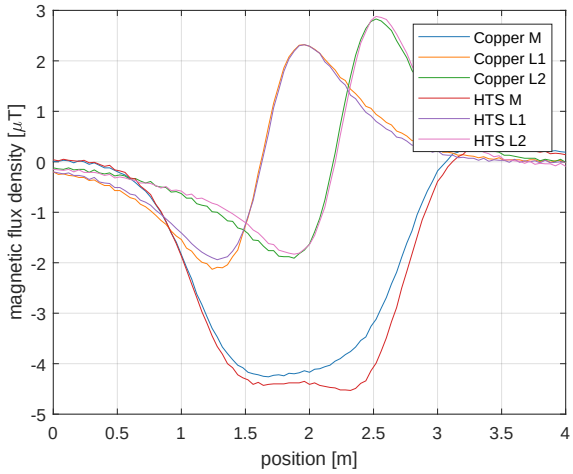

Figure 3.13: The effect of each separate degaussing coil on the magnetic field measured by the sensor rail. The measurement distance, d, is 439 mm in this test.

The HTS degaussing coils show very similar behaviour to the copper degaussing coils. There are some small differences visible. This is most likely because the copper and HTS degaussing coils could not be placed on the exact same location.

3.7.2. STATIC TEST

In the static test, the magnetic signature of the demonstrator is measured while the demonstrator is in a fixed position in Earth's magnetic field. First, a reference measurement was done without the pipe in place. This measurement is subtracted from the following measurements to get the in-homogeneity of the background field out of the results. Then the magnetic signature is measured with the pipe in place following by the reduced magnetic signatures of both the copper as the HTS degaussing coils.

Figure 3.14a shows the absolute values of the measurements, where the reference measurement is not subtracted from the final measurements in this graph. Figure 3.14b shows the corrected results. It can be seen that the copper and HTS degaussing coils behave very similar. A small difference is observed between both cases which most likely has to do with the placement of the coils.

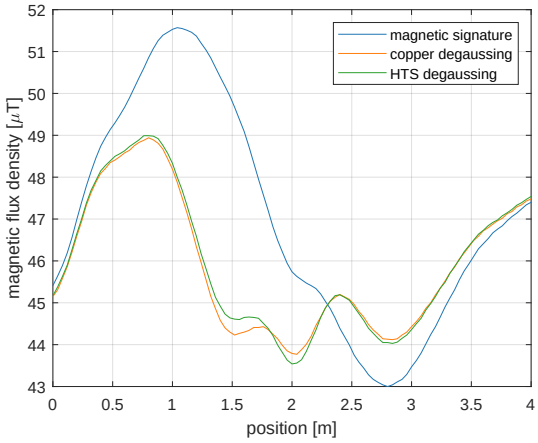

(a)

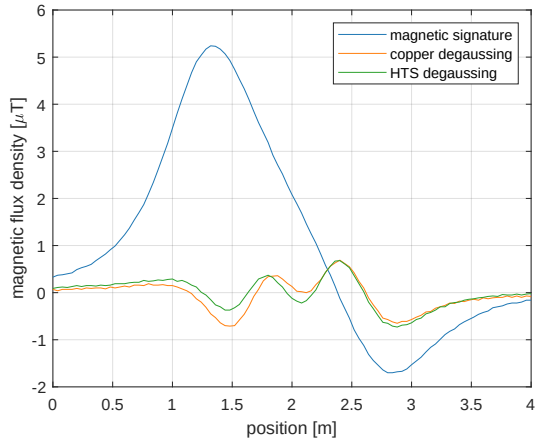

(b)

Figure 3.14: Plots of the measured and reduced magnetic signature. The plots show the (a) absolute values of the measurements and the (b) corrected values of the measurements. The measurement distance, d, is 439 mm in this test.

3.7.3. DYNAMIC TEST

In the second test, the dynamic behaviour of the setup was tested. The pipe was pitched at an angle ranging from zero to twenty-five degrees. As with the static test, the background field was measured without the pipe in the vicinity. This measurement was later on subtracted from the magnetic signature measurements. Then, the pipe was introduced and pitched over twenty-five degrees. After measuring the magnetic signature, the actual dynamic degaussing performance was measured. First, the copper coils were tested where the current set-points were adjusted according to the pitching angle. Finally, the HTS degaussing performance was tested. The results are shown in figure 3.15.

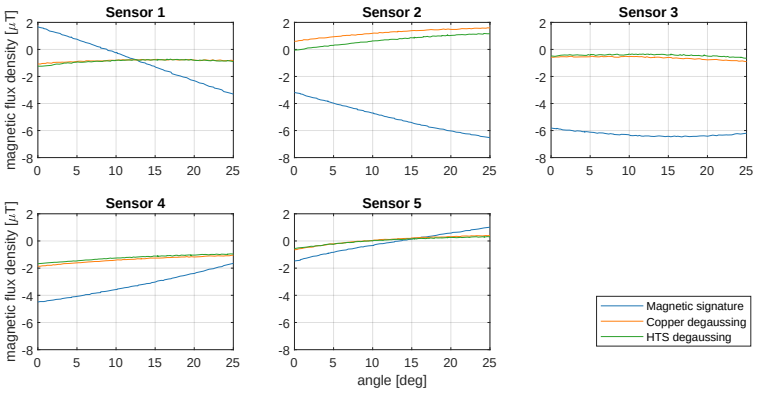

Figure 3.15: The results of the dynamic test. Each plot shows the magnetic flux density measured per separate sensor as a function of tilting angle of the pipe. The measurements from the background field are subtracted from the results. The measurement distance, e, is 445 mm in this test.

3.8. CONCLUSION

The main goal of the demonstrator tests was to demonstrate the equivalent behaviour of HTS degaussing coils compared to copper degaussing coils, and that HTS coils can thus be qualified as degaussing coils on ships. The magnetic behaviour of both copper and HTS degaussing coils is presented in this chapter. Overall, both in the static and the dynamic experiments, the copper and HTS coils show a similar behaviour. The difference in magnetic field between the both sets of coils is small and can be explained by small differences in the positions of the coils. The degaussing performance of both sets of coils is the same. The differences between the HTS and copper L1 and L2 coils is smaller than the difference between the M coils. This can be explained by the difference in the position of these coils. Also, the construction around the pipe might have an influence on the magnetic signature.

The static test is a good way to visualize and compare the differences between copper and HTS degaussing. These tests gave an insight in the possibilities of using HTS for a degaussing system. The dynamic test is used to test the control system and the dynamics of the degaussing currents. In this test setup, the effect on the dynamics is not notable be-

cause the resistance of the degaussing coils is only a small portion of the total resistance in the system. The cables connecting the power supplies to the degaussing coils and the power supplies themselves are also resistive. There was not a notable difference between the time constant of the copper and HTS coils. To further investigate the dynamic effects of HTS coils in a degaussing system, a larger setup is needed so the large time constant of the superconductive coil without damping becomes more present, which would be the case in a full sized ship. In such a setup, the energy efficiencies of both systems will be comparable as well.

The power consumption of an optimised cryostat would be relatively low so a fair comparison can be made with the Ohmic losses in a copper degaussing system. The coupling factors of the degaussing coils in a ship are so small that they are negligible as shown in this chapter. For the experiments conducted, the permeability of the pipe was determined by fitting the measurements of the magnetic signature to simulated magnetic signature. In the future, the permeability of the pipe could be measured directly with an independent measurement. The deperming of the pipe only took place in the longitudinal direction. The magnetising field from the deperming coil might not have affected the end caps of the pipe. A deperming coil in the vertical direction could be employed for this.

BIBLIOGRAPHY

[1] H. K. Onnes, "The resistance of pure mercury at helium temperatures.", *Journal of Applied Physics*, vol. 1, pp. 3991–3996, 6 Jun. 1911.

[2] V. Schmidt, *The Physics of Superconductors*. Moskau: Nauka Publishers, 1982.

[3] PJRay, *Timeline of Superconductivity from 1900 to 2020.png*, https://commons.wikimedia.org/wiki/File:Timeline_of_Superconductivity_from_1900_to_2015.svg, Nov. 2015.

[4] E. Snider, N. Dasenbrock-Gammon, R. McBride, *et al.*, "RETRACTED ARTICLE: Room-temperature superconductivity in a carbonaceous sulfur hydride", *Nature*, vol. 586, no. 7829, pp. 373–377, Oct. 2020.

[5] S. Lee, J.-H. Kim, and Y.-W. Kwon, *The first room-temperature ambient-pressure superconductor*, 2023. arXiv: 2307.12008 [cond-mat.supr-con].

[6] S. Lee, J. Kim, H.-T. Kim, S. Im, S. An, and K. H. Auh, *Superconductor* $pb_{10-x}cu_x(po_4)_6o$ *showing levitation at room temperature and atmospheric pressure and mechanism*, 2023. arXiv: 2307.12037 [cond-mat.supr-con].

[7] J. X. Jin, Y. J. Tang, X. Y. Xiao, *et al.*, "Hts power devices and systems: Principles, characteristics, performance, and efficiency", *IEEE Transactions on Applied Superconductivity*, vol. 26, no. 7, pp. 1–26, 2016.

[8] M. H. Ali, B. Wu, and R. A. Dougal, "An overview of smes applications in power and energy systems", *IEEE Transactions on Sustainable Energy*, vol. 1, pp. 38–47, 2010.

[9] S. Kalsi, K. Weeber, H. Takesue, C. Lewis, H.-W. Neumueller, and R. Blaugher, "Development status of rotating machines employing superconducting field windings", *Proceedings of the IEEE*, vol. 92, no. 10, pp. 1688–1704, 2004.

[10] X. Song, C. Bührer, A. Mølgaard, *et al.*, "Commissioning of the world's first full-scale mw-class superconducting generator on a direct drive wind turbine", *IEEE Transactions on Energy Conversion*, vol. 35, no. 3, pp. 1697–1704, 2020.

[11] Z. H. Shi, X. Y. Chen, and Z. C. Qiu, "Modelling of mutual inductance between superconducting pancake coils used in wireless power transfer (wpt) systems", *IEEE Transactions on Applied Superconductivity*, vol. 29, no. 2, pp. 1–4, 2019.

[12] S. Miura, S. Oki, T. Furukawa, and M. Iwakuma, "Experimental validation of theoretical expressions on additional ac loss of two-strand parallel conductors composed of reba2cu3oy tapes via pick-up-coil method", *IEEE Transactions on Applied Superconductivity*, vol. 29, no. 5, pp. 1–4, 2019.

[13] D. U. Gubser, "US Navy's Superconductivity Programs Scientific Curiosity to Fleet Utility", *IEEE Transactions on Applied Superconductivity*, vol. 21, no. 3, pp. 931–935, Jun. 2011.

[14] R. Ross, C. G. Meijer, and R. Hunik, "Maritime superconductivity perspectives", *IEEE Transactions on Applied Superconductivity*, vol. 23, no. 3, 2013.

[15] C. A. Luongo, P. J. Masson, T. Nam, *et al.*, "Next generation more-electric aircraft: A potential application for hts superconductors", *IEEE Transactions on Applied Superconductivity*, vol. 19, no. 3, pp. 1055–1068, 2009.

[16] S. Ohtsuka, H. Ohtsubo, T. Nakamura, J. Suehiro, and M. Hara, "Characteristics of nbti mechanical persistent current switch and mechanism of superconducting connection at contact", *Cryogenics*, vol. 38, pp. 893–902, 9 Sep. 1998.

[17] J. Geng, K. Matsuda, B. Shen, *et al.*, "Hts persistent current switch controlled by ac magnetic field", *IEEE Transactions on Applied Superconductivity*, vol. 26, pp. 2–5, 3 2016.

[18] J. Liu, R. Mansour, and M. Salama, "A new low-loading hts current switch triggered by rf signals", *IEEE Transactions on Appiled Superconductivity*, vol. 15, pp. 1994–1997, 2 Jun. 2005.

[19] Y. Choi, Y. Li, D. Park, *et al.*, "A tabletop persistent-mode, liquid helium-free 1.5-t mgb2 "finger" mri magnet: Construction and operation of a prototype magnet", *IEEE Transactions on Applied Superconductivity*, vol. 29, no. 5, pp. 1–5, 2019.

[20] S. Mukoyama, A. Nakai, H. Sakamoto, *et al.*, "Superconducting joint of rebco wires for mri magnet", *Journal of Physics: Conference Series*, vol. 1054, p. 012 038, Jul. 2018.

[21] T. A. Coombs, J. Geng, L. Fu, and K. Matsuda, "An overview of flux pumps for hts coils", *IEEE Transactions on Applied Superconductivity*, vol. 27, 4 2017.

[22] Y. Zhai, P. Zhou, J. Li, *et al.*, "Performance investigation of contactless self-regulating hts flux pump", *IEEE Transactions on Applied Superconductivity*, vol. 31, 5 2021.

[23] D. Wikkerink, A. Rodrigo Mor, H. Polinder, and R. Ross, "Design of a test setup to measure magnetic signature reduction", in *Conference Proceedings of ICMET Oman*, IMarEST, Nov. 2019.

[24] F. E. Baker and S. H. Brown, "Magnetic induction of ferromagnetic prolate spheroidal bodies and infinitesimally thin current bands", *Journal of Applied Physics*, vol. 53, pp. 3991–3996, 6 Jun. 1982.

[25] C. Aird, "Modelling the induced magnetic signature of naval vessels", PhD Dissertation, University of Glasgow, 2000.

[26] T. Baynes, G. Russell, and A. Bailey, "Comparison of stepwise demagnetization techniques", *IEEE Transactions on Magnetics*, vol. 38, no. 4, pp. 1753–1758, 2002.

[27] J. J. Holmes, "Reduction of a Ship's Magnetic Field Signatures", *Synthesis Lectures on Computational Electromagnetics*, vol. 3, no. 1, pp. 1–68, Jan. 2008.

4

CONVERTER TOPOLOGIES FOR HTS COILS

A feature of HTS is that it can facilitate a current density of over a hundred times more than copper. When a higher current is used, the number of turns can be reduced while still maintaining the needed magnetomotive force. This is useful, because HTS tape is expensive and the large degaussing coils on a ship demand long lengths of wire. Besides, installing multiple windings on the ship is labour intensive. If the current exceeds the critical current of the tape, the superconductor goes out of its superconductive state. This should be avoided. Two problems arise when utilising fewer turns with a higher current.

Firstly, the power supply for the HTS coils needs to deliver more current than for the copper coils. Current supplies typically dissipate more energy at higher current levels. This would make the HTS system less efficient than the copper system for the same magnetomotive force rating [1].

Secondly, current leads are needed to connect the power source at room temperature to the HTS at cryogenic temperature. Through the current leads, heat leaks into the cryostat. The losses are expected to be significant [2]. The current leads need to be able to handle the large current as well. In order to minimize Ohmic losses, they have to be designed with a sufficient cross-section. This causes more heat to leak into the cryostat which needs to be cooled away.

A solution to reduce the energy dissipation in the current source is to connect the HTS coil through an H-bridge topology with low on-state resistance MOSFETs. The idea is to avoid a forward voltage drop in series with the current path. By using MOSFETs with a low on-state resistance, the degaussing current will decay slowly during the discharge state because of the low resistance in the current path and the large inductance of the HTS degaussing coil [3]. Because of the low resistance, a small duty cycle can be used.

Parts of this chapter have been published as:
D. Wikkerink, A. Rodrigo Mor, H. Polinder, and R. Ross, "Converter Design for High Temperature Superconductive Degaussing Coils", in IEEE Access, vol. 10, pp. 128656-128663, 2022.

During the short charging state of the coil, there will be a temporary and relatively high energy dissipation in the source. However, during the relatively long discharge state, almost no energy is dissipated.

A possible way to reduce the size of the current leads is to move part of the electronics inside the cryostat. This will reduce the rated current of the current leads, but it will introduce extra losses inside the cryostat. Also, a transformer can be used to transfer the energy to the degaussing coils through the cryostat wall by magnetic coupling. A rectifier then needs to be placed inside the cryostat. This would eliminate the need of current leads at all, but introduce even more losses inside the cryostat because of the forward voltage of the rectifier. When the MOSFETs are placed inside the cryostat, their losses are decreased as a side effect because the on-state resistance and switching losses are lower at cryogenic temperatures [4]–[7]. The extra heat that is introduced inside the cryostat needs to be lifted sby the cooler. This is known to be very inefficient [8], [9].

The objective of this chapter is to investigate different possible current supply designs for an HTS degaussing coil. The previously presented ideas are tested in order to answer the following research questions:

- Is it more energy efficient to move part of the electronics into the cryostat?
- Is it more energy efficient to use a transformer in order to eliminate current leads?

To answer these questions, the efficiencies of several converter topologies are estimated and compared to one another. This is done by identifying and quantifying the sources of loss in the power supply topologies. In addition to the the electrical losses, also the cryostat losses are taken into account. Only the loss sources which differ from topology to topology are taken into consideration. The performance of the MOSFETs and capacitors in liquid nitrogen are found by measurements.

Section 4.1 defines the requirements for the power supply and presents the different converter topologies. In section 4.2, all the sources of loss of the topologies are identified and modelled. Section 4.3 presents and discusses the results. Finally, section 4.4 draws a conclusion.

4.1. CONVERTER DESIGN

The most obvious configuration to power an HTS degaussing coil is to directly connect the degaussing coil to a current source as shown in figure 4.1. In this case, the HTS degaussing coil is placed inside a cryostat in order to ensure that the HTS material is in superconductive state. Two current leads are needed which connect the HTS coil, L, at cryogenic temperature to the current source at room temperature. The current leads cause heat to enter the cryostat which needs to be cooled away. The current source, V_s, constantly needs to deliver the required current which causes internal source losses caused by the internal resistance, R_s. As a reference, this configuration is considered as topology 0 and will be compared to four alternative, and supposedly more efficient topologies.

In section 4.1.1, the requirements and assumptions of the system are defined. In section 4.1.2, the alternative topologies are presented which are expected to be more efficient.

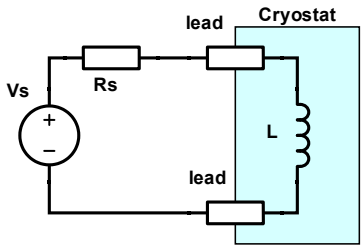

Figure 4.1: Topology 0. The DC current source is directly connected to the HTS degaussing coil. The coil is placed inside a cryostat and is connected through current leads.

4.1.1. REQUIREMENTS

To compare different current source topologies, the specifications for the degaussing coils are specified first. For now if suffices to understand that the specifications are determined and taken from a magnetic signature model. This model is a FEM model of a full-sized ship with 15 degaussing coils which is used to find the rated current, I_r, and inductance, L, of the degaussing coils. The model will be discussed in more detail in section 6.1. In this research, the degaussing coil with the highest current rating is chosen to be the load for which the current source needs to be designed. The specifications for this coil are given in table 4.1. The current source shall be bi-directional, because the degaussing field needs to be both negative and positive.

Table 4.1: Requirements of the load extracted from a FEM model of a full sized ship.

Symbol	Quantity	Value	Unit
I_r	Rated current	100	A
ΔI_r	Current ripple	0.5	%
L	Inductance	15	mH

In the model it is assumed that:

- the degaussing coils have linear inductance,
- the mutual inductances between the degaussing coils is neglegible,
- the cryostat uses liquid nitrogen and operates at a temperature of 77 K and
- there are no blocking losses in the MOSFETs.

4.1.2. TOPOLOGIES

A MOSFET-based H-Bride topology is considered as the basic design for the converter. As required, an H-bridge is able to provide the current in both directions. The rated degaussing current is 100 A, so a device like an IGBT with a fixed voltage drop would have more losses than MOSFETs. For example, an IGBT with a forward voltage of 0.7 V that conducts 100 A will dissipate a power of 70 W. A MOSFET with an on-state resistance of 500 µΩ only dissipates 5 W for the same case. The on-state losses can even be lowered by placing multiple MOSFETs in parallel. Figure 4.2 shows the waveform of the current in the HTS coil.

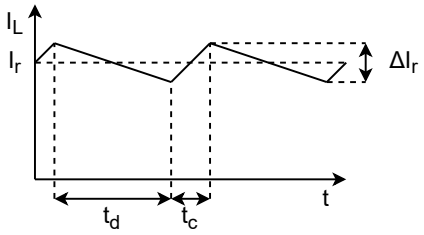

Figure 4.2: HTS coil current waveform. The duty cycle is small so the discharge state is much longer than the charging state.

The low resistance in combination with the high inductance and no resistance of the HTS degaussing coil will cause the current to decay very slowly during discharge state, t_d. Most of the losses occur during the relatively short charging state, t_c. During this state, the current needs to flow from the source the the H-Bridge. But during the much longer discharge state, the current is "trapped" in the H-bridge where almost no energy is dissipated.

TOPOLOGY 1

The HTS coil is placed inside a cryostat and is connected to the output of the H-Bridge through current leads as shown in figure 4.3. The degaussing coil is charged by closing Q_1 and Q_4. During the discharging state, Q_3 and Q_4 are closed. The source only has to deliver current during the charging state, which is expected to be very short compared to the discharging state because of the large time constant of the HTS coil in combination with the MOSFETs. The current leads have to be designed for the rated current, I_R.

TOPOLOGY 2

The HTS coil is placed inside the cryostat together with the H-Bridge as shown in figure 4.4. The current leads can be made smaller because they only have to be sized for the RMS current during the cycle. The on-state resistance of the MOSFETs drops because they are placed inside the liquid nitrogen. This will reduce the duty cycle even further. However, the conduction and switching losses of the MOSFETs are dissipated inside the cryostat which adds to the cryostat losses.

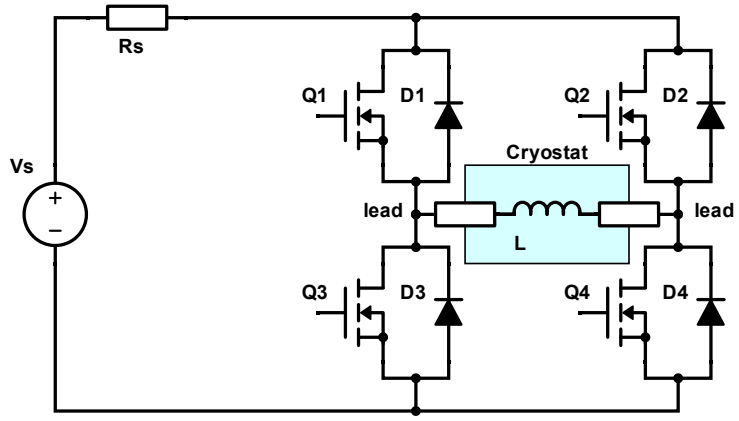

Figure 4.3: Converter topology 1: only the degaussing coil is inside the cryostat, large current leads are needed because they have the same current rating as the coil. The current decays fast during the discharge state because part of the circuit is at room temperature

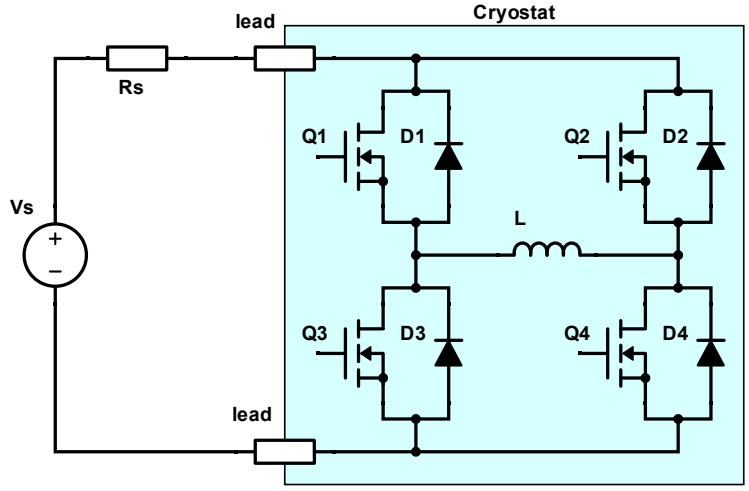

Figure 4.4: Converter topology 2: the H-bridge is placed inside the cryostat. More energy is dissipated inside the cryostat, but smaller current leads are needed. The current only flows through the current leads during the charging state. The inductor current decays slower because there is less resistance in its serial path

TOPOLOGY 3

A smoothing capacitor is added inside the cryostat as shown in figure 4.5. This capacitor causes the current that flows through the current leads to change from short high current pulses, to a steady DC current. Now the source doesn't have to be able to deliver the rated current, I_r, anymore. It will also decrease the Ohmic losses in the current leads. However, the capacitor will add extra Ohmic losses inside the cryostat.

TOPOLOGY 4

A transformer is added where the secondary side is inside the cryostat as shown in figure 4.6. This eliminates the need of current leads at all. Because of the low duty cycle, the current that flows in the smoothing capacitor is expected to be low. A diode is needed to rectify the current, but the power dissipation shouldn't be too high because of the low secondary current.

4.2. METHODOLOGY

In order to compare the topologies to one another, the efficiencies are analysed. For this, the sources of losses that differ per topology are quantified. The sources are then added and the total power loss, P_{tot}, is found as follows:

$$P_{tot} = P_s + P_{circ(room)} + COP^{-1}\left(P_{cl} + P_{circ(cryo)} + P_{sw}\right) \tag{4.1}$$

where P_s are current source losses, $P_{circ(room)}$ the circuit losses outside the cryostat, $P_{circ(cryo)}$ the circuit losses inside the cryostat, P_{cl} the current lead losses, P_{sw} the switching losses and COP is the coefficient of operation of the cooler. Depending on the topology, some of the circuit losses are dissipated inside the cryostat. The current lead losses are dissipated inside the cryostat as well. These losses need to be cooled away by the cooler and therefore divided by COP.

To find the amount of energy loss, the waveforms of the currents in the circuit are needed. A model was created in the circuit software PLECS to test the topologies and retrieve the waveforms of the currents. As an example, table 4.2 shows the values for the duty cycle D, the minimum switching frequency f_s, and the RMS values for the source current I_s, capacitor current I_C and the diode current I_D for the case where there are no parallel MOSFETs. These values have been obtained for a 100 A current with 0.5 % ripple as stated in table 4.1. The source voltage, V_s, is set at 10 V.

Table 4.2: Relevant values from the model in the case of no parallel MOSFETs.

Symbol	T_1	T_2	T_3	T_4	Unit
D	3.6	1.3	0.6	0.5	%
f_s	16.98	5.35	5.38	5.38	Hz
$I_{s(RMS)}$	18.9	11.4	0.77	3.2	A
$I_{C(RMS)}$	-	-	7.7	7.1	A
$I_{D(RMS)}$	-	-	-	2.26	A

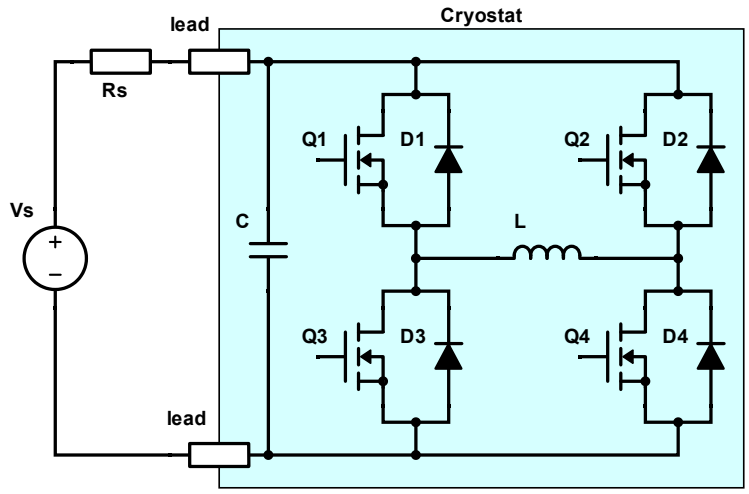

Figure 4.5: Converter topology 3: a smoothing capacitor is added inside the cryostat. By adding the capacitor, the source can continuously charge the capacitor with small current during the complete cycle. A much smaller current source is needed.

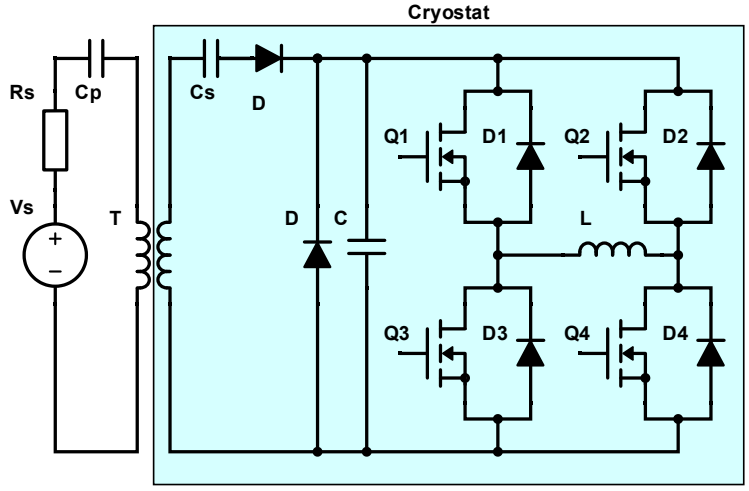

Figure 4.6: Converter topology 4: a transformer added so that the energy can be transferred wirelessly. A rectifier inside the cryostat converts the current from AC to DC. This eliminates the need of current leads at all, but the rectifier and transformer introduce extra losses in the cryostat.

The on-state resistance of the MOSFETs and the performance of the capacitors are determined by measurements. Each of the sources of loss identified in eq. (4.1) are further examined in the following subsections.

4.2.1. SWITCHING LOSSES

The switching losses are estimated according to the following equation:

$$P_{sw} = f_s N_p (E_{on} + E_{off} + E_{onD} + E_{dead}) \tag{4.2}$$

where f_s is the switching frequency, N_p the number of parallel MOSFETs, E_{on} is the MOSFET switch-on energy, E_{off} is the MOSFET switch-off energy and E_{onD} is the diode energy during MOSFET switch-on transient. The switch off losses in the diode, E_{offD}, are assumed to be zero. The dissipated energy components are estimated according to the following equations:

$$E_{on} = \int_0^{t_{ri}+t_{fu}} u_{DS}(t)\, i_D(t)\, \mathrm{d}t \tag{4.3}$$

$$E_{onD} = \int_0^{t_{ri}+t_{fu}} u_D(t)\, i_F(t)\, \mathrm{d}t \tag{4.4}$$

$$E_{off} = \int_0^{t_{ru}+t_{fi}} u_{DS}(t)\, i_D(t)\, \mathrm{d}t \tag{4.5}$$

where t_{ri} is the current rise time, t_{fi} the current fall time, t_{ru} the voltage rise time and t_{fu} the voltage fall time. The rise times, fall times, currents and voltages are calculated using the datasheet parameters [10].

During the dead-time, the degaussing current needs to flow through a diode. The power which is dissipated in the diode can be expressed as follows:

$$E_{dead} = T_d (V_f I + R_D I^2) \tag{4.6}$$

where T_d is the dead time, V_f is the forward diode voltage drop, R_D is the diode resistance and I is the diode current. The voltage drop over the diode is much higher than the on-state voltage drop over the MOSFETs. In combination with the high degaussing current, the losses are much higher during the dead time than during the rest of the switching cycle. This causes extra losses inside the cryostat when the MOSFETs are inside the cryostat. This also causes the current to decay faster during the discharge state. The dead time should therefore be kept to a minimum.

4.2.2. CIRCUIT LOSSES

The circuit losses are divided into the following components:

$$P_{circ} = P_{DSon} + P_{PCB} + P_{trans} \tag{4.7}$$

where P_{DSon} are the on state losses in the MOSFETs, P_{PCB} the copper losses on the PCB and P_{trans} the transformer losses. The copper losses on the PCB are estimated by the size of the trace and the resistivity at the temperature. The transformer losses are

estimated with by using the length and surface area of the copper wire from the transformer described in section 4.2.4. The on-state losses are estimated as follows:

$$P_{DSon} = \frac{1}{N_p} I_{DS}^2 R_{DSon}(T) \tag{4.8}$$

where N_p is the number of parallel MOSFETs, I_{DS} the MOSFET current and $R_{DSon}(T)$ the on-state resistance as a function of temperature, T.

4.2.3. COMPONENT CHARACTERISTICS AT CRYOGENIC TEMPERATURE

It is essential that the MOSFETs have an as low as possible on-state resistance. With this in mind, the SiR178DP by Vishay was chosen. While it is known that MOSFETs are generally able to perform in a cryogenic environment [4], it is still necessary to verify that this is also the case for this particular type of MOSFET. Besides, the on-state resistance at 77 K needs to be known in order to estimate the performance of the topologies.

The on-state resistance of the MOSFET was measured by injecting a known current from the drain through the source while applying a voltage to the gate. The voltage across the drain and the source of the MOSFETs was measured using a Keithley Nanovoltmeter Model 2182A. The measurements were done at room temperature and in liquid nitrogen in a cryostat. 6 samples were tested. Figure 4.7 shows a photo of the test setup used to measure the on-state resistance of the MOSFETs.

Table 4.3 shows the mean, $\bar{x}$, and the standard deviation, s_N, of these measurements. It can be seen from the measurement results that the on-state resistance of the selected MOSFETs is about 34 % lower when submerged in liquid nitrogen. The measured on-state resistance values are a bit higher than the datasheet values. This is probably due to

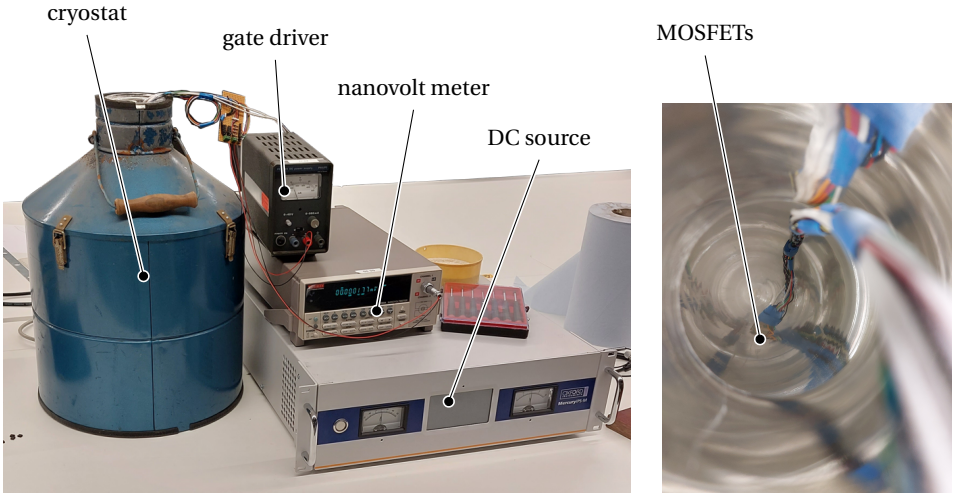

(a) (b)

Figure 4.7: (a) Photo of the test setup used to measure the parameters of the components in liquid nitrogen. (b) A photo inside of the cryostat with the 6 MOSFETs placed inside.

Table 4.3: Measured values of the on-state resistance and capacitance in liquid nitrogen.

Symbol	Quantity	$\bar{x}$	s_N	Unit
R_{DSon}(293 K)	On-state resistance	611	30.1	μΩ
R_{DSon}(77 K)	On-state resistance	404	8.2	μΩ
C (293 K)	Capacitance	216	0.32	μF
C (77 K)	Capacitance	161	0.45	μF

measuring some resistance at the leads of the MOSFETs.

Regarding the capacitors, not every capacitor can operate at cryogenic temperatures [11]. Electrolytic capacitors, for example, freeze and lose their capacitive abilities. For the smoothing capacitor in topologies 3 and 4 however, a large capacitance is needed. For this, the best option is to use tantalum solid capacitors. The capacity of six samples of 220 μF tantalum solid capacitors was measured at room temperature and at 77 K. Table 4.3 shows the mean value and the standard deviation of these measurements. Though the capacitors lose about 20 % of their capacitance, they still work at cryogenic temperatures. The capacitances were measured using an Agilent U1731C LCR Meter.

4.2.4. TRANSFORMER

The transformer is chosen to be of a flat air-cored helix type. The use of a core is not possible, because this would be a bad thermal insulator for the cryostat. A COMSOL simulation was done where the primary inductance, L_p, is equal to the secondary inductance, L_s. The coupling factor of the transformer was found to be 0.2. In order the improve the efficiency of the power transfer, resonant inductive coupling is used as can be seen in figure 4.6. Capacitors C_p and C_s are placed in series with the inductors at the primary and secondary side with transformer frequency f so that:

$$C_p = C_s = \frac{1}{L_s(2\pi f)^2} \tag{4.9}$$

4.2.5. CURRENT LEAD LOSSES

The losses in the current leads consist of two parts; the heat flow through the current lead into the cryostat and the heat generated inside the current lead because of Ohmic losses. These can be modelled as follows [12]:

$$dT = -\frac{dl}{kA}\dot{Q} \qquad\qquad d\dot{Q} = I^2\frac{dl}{\sigma A} \tag{4.10}$$

where dT is the temperature difference, l the length, k the thermal conductivity, A the cross-section, $\dot{Q}$ the heat flow, $d\dot{Q}$ the generated heat, I the current and σ the electrical conductivity of the current lead. The heat flow due to the current leads has to be minimised, so the diameter of the current leads should be as low as possible. On the other hand, by decreasing the diameter, the generated heat increases due to Ohmic losses. There is a trade-off. The solution for the minimum heat flow through the current lead $\dot{Q}_{min}$ can be found by combining Equation (4.10):

$$\dot{Q}_{min} = I\sqrt{\frac{2k}{\sigma}(T_H - T_L)} \tag{4.11}$$

where T_H is the temperature outside the cryostat and T_L is the temperature inside the cryostat. From the minimum heat flow, the optimal wire length to surface area ratio follows. In our case we choose the current lead to be 10 cm and the optimal surface area is calculated. It should be noted that eq. (4.11) assumes a constant current. However, for topology 2, the current through the leads differs during the switching cycle. In this case, we will model the generated heat as follows:

$$d\dot{Q} = \frac{dl}{\sigma A}\frac{1}{T_s}\int_0^{T_s} I(t)^2\, dt = D\left(\frac{I}{D}\right)^2 \frac{dl}{\sigma A} \tag{4.12}$$

where T_s is the length of the switching cycle and D is the duty cycle. The calculated dimensions of the current leads are presented in table 4.4 for the case that there are no parallel MOSFETs.

Table 4.4: Current lead parameters for topologies T_1, T_2, T_3, and T_4 when there are no parallel MOSFETs.

Symbol	Quantity	T_1	T_2	T_3	T_4	unit
I_{peak}	peak current	I_r	I_r	DI_r	-	A
I_{avg}	average current	I_r	$\sqrt{D}I_r$	DI_r	-	A
l	length	10	10	10	-	cm
A	cross-section	5.13	0.59	0.037	-	mm^2
R	resistance	0.46	3.98	63.1	-	mΩ
$\dot{Q}$	heat influx	9144	1051	66	0	mW

4.2.6. COOLING EFFICIENCY

To check the merits of putting electronics inside the cryostat, the efficiency of the cooling process must be known. If, by placing an element inside the cryostat, the losses decrease more than it costs to cool them away, it is considered a good choice. The efficiency of the cooling process is limited by the efficiency of the Carnot cycle and the efficiency of the cooler itself. The coefficient of operation, COP, can then be expressed as follows:

$$COP = \frac{\dot{Q}}{P} = \eta\epsilon_c = \eta\frac{T_L}{T_H - T_L} \tag{4.13}$$

where $\dot{Q}$ is the heat which is lifted from the cooler, P the power used by the cooler, η the efficiency of the cooler, ϵ_c the efficiency of the Carnot cycle, T_H the temperature outside the cryostat and T_L the temperature inside the cryostat. Since the cryostat operates at a temperature of 77 K, the efficiency of the Carnot cycle is 0.36. The efficiency of coolers for the power rating for degaussing systems can be assumed to be 0.2 [8], [9]. That means that for every Watt that is dissipated inside the cryostat, the cooler consumes 14 Watts of power. This is an efficiency of 7.14 %.

4.3. RESULTS

This section discusses the results of the simulations. Section 4.3.1 shows the power losses for each loss component for the four topologies. Section 4.3.2 shows the effects of using a higher switching frequency and the use of more parallel MOSFETs on the power dissipation for each topology.

4.3.1. POWER BALANCE

With all the loss sources known, the balance can be made of the total loss of the topologies. The losses per component per topology are shown in figure 4.8 and figure 4.9. The topologies from figures 4.3 to 4.6 are compared with topology 0 from figure 4.1.

The power balance is shown for the case with no parallel MOSFETs in figure 4.8. It can be seen that for topology 0, the main contributor is the loss in the current source. This part is so big, because the rated current constantly has to flow through the source. Also, the current leads are sized for the rated current. This makes the current lead losses high as well.

For topology 1, the source losses are considerably lower when compared to topology 0. This is because the rated current only flows from the source during the charging state. During the discharging state, the source current is zero. The current lead losses are still high, because the leads are still rated for the rated current. The circuit losses caused

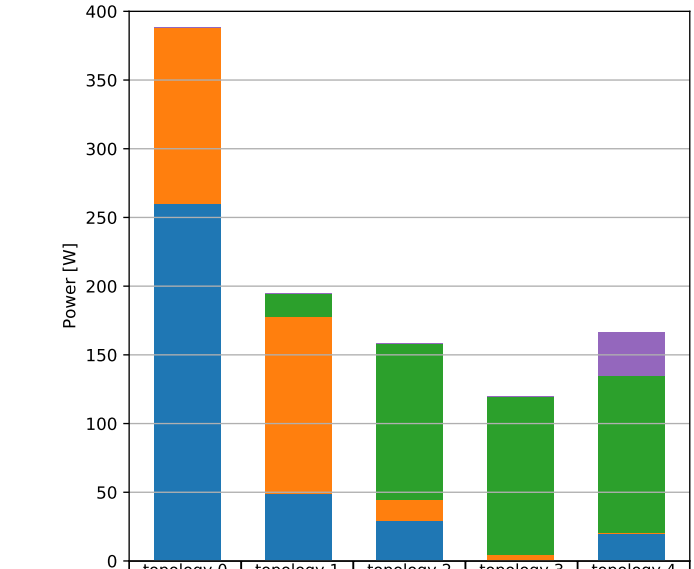

	topology 0	topology 1	topology 2	topology 3	topology 4
transformer					3.2e+01
switching		3.1e-02	1.4e-01	1.4e-01	1.4e-01
circuit		1.7e+01	1.1e+02	1.1e+02	1.1e+02
current leads	1.3e+02	1.3e+02	1.5e+01	4.7e+00	
source	2.6e+02	4.9e+01	3.0e+01	1.5e-02	2.0e+01

Figure 4.8: The sum of the power losses for each source of loss in each topology for one MOSFETs per switch.

by the MOSFETs and the PCB are small, but present as well. The switching losses are insignificant, which is explained by the low switching frequency which is possible in this configuration.

For topology 2, the current leads can be made much smaller. This has a large effect on the power loss in the current leads. However, the circuit losses become much larger. This is because the components are now inside the cryostat, so a lot more cooling power is needed. Also, the switching losses happen inside the cryostat, but they are still very small compared to the other losses. It should be noted that the source losses are a bit lower than for topology 1. This is because the resistance of the MOSFETs is lower in liquid nitrogen and therefore the duty cycle is lower as well.

For topology 3, the source and current lead losses are decreased even further. This is because the source current waveform is smoother which causes the RMS value of the source current to be lower than in the previous cases. The capacitor adds extra losses inside the cryostat, but these are insignificant.

For topology 4, a transformer is added to remove the current lead losses completely. However, the current lead losses were already very small in topology 3, so it does not have a large effect. There are extra transformer and rectifier losses inside the cryostat however. Also, the source losses are increased more. The total added losses are higher than in the previous case.

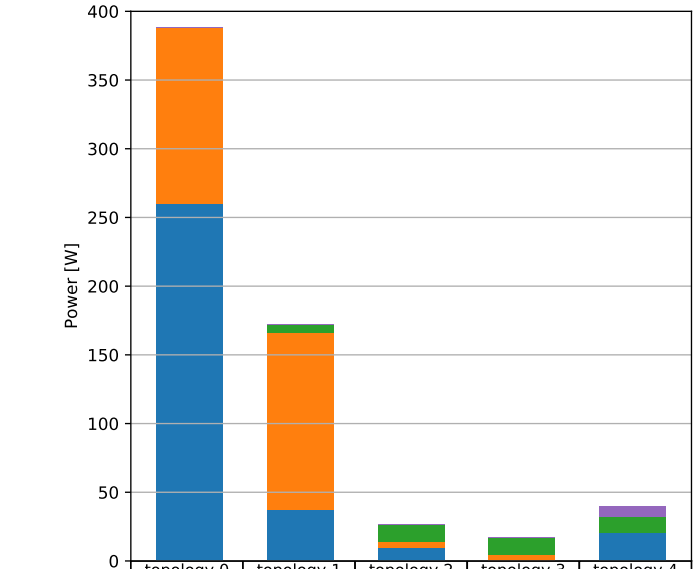

	topology 0	topology 1	topology 2	topology 3	topology 4
transformer					7.3e+00
switching		1.3e-01	1.0e-01	1.0e-01	1.0e-01
circuit		6.3e+00	1.2e+01	1.2e+01	1.2e+01
current leads	1.3e+02	1.3e+02	4.7e+00	4.7e+00	
source	2.6e+02	3.8e+01	9.6e+00	1.6e-03	2.1e+01

Figure 4.9: The sum of the power losses for each source of loss in each topology for ten MOSFETs per switch.

For the topologies in which the components are placed inside the cryostat, it seems that circuit losses, which include the on-state losses, become dominant because of the coefficient of performance of the cooler. A way to lower these losses is to place multiple MOSFETs in parallel so that the resistance is lower. Figure 4.9 shows the power balance of the topologies again, but now with ten parallel MOSFETs per switch. Now the circuit losses become much smaller. Also, the current lead losses and the source losses become smaller. This is because the lower resistance enables a lower duty cycle. Figure 4.10 shows the total power dissipation as a function of parallel MOSFETs. It can be seen that even by placing one extra MOSFET in parallel, the power can be decreased drastically. Placing more than ten MOSFETs in parallel does not seem to have a large impact on the final power use.

From figure 4.8 and figure 4.9 it can be concluded that the most energy efficient solution is topology 3. Besides energy-efficiency, this solution is also a practical one. The source does not have to be able to deliver the rated current so it can be made much smaller. The capacitor can be slowly charged during relatively long discharge time. Topology 4, which uses a transformer, does not add more advantages. Also, it adds more complexity to the circuit so it is not useful to use a transformer.

4.3.2. SWITCHING FREQUENCY

In the analysis until now, the topologies use the lowest switching frequency as possible while still meeting the current ripple requirement of 0.5 %. It can be argued that it is useful to use a higher switching frequency so that the current ripple can be lowered. Also a higher switching frequency causes the ripple in the magnetic signature to be damped more [13]. However, a higher switching frequency also causes more switching losses. For the topologies where the MOSFETs are placed inside the cryostat, the switching losses are even higher because of the coefficient of performance of the cooler. Figure 4.11 shows the percentage that the switching losses are of the total amount of losses. For topology 1, where the MOSFETs are not placed inside the cryostat, it can be seen that the converter can operate above 1 kHz without any problems. For the topologies where the MOSFETs are placed inside the cryostat, the switching losses become too high in this range. It should also be noted that a higher switching frequency in combination with the low duty cycle that is used in this topologies can cause problems. The on-state of the MOSFETs is very short compared to the off-state. If the frequency is also high, the on time of the MOSFET might be too short to switch.

4.4. CONCLUSION

Several converter topologies were investigated to be applied for HTS degaussing coils in this chapter. Measurements were done to validate the performance of the electronic components in liquid nitrogen. It was shown that it is more energy efficient to place the MOSFETs inside the cryostat. By doing this, the rated current for the current leads is drastically decreased and therefore the losses as well. However, by placing the MOSFETs inside the cryostat, the cooler needs to lift more heat. This is an inefficient process which can be counteracted by placing multiple MOSFETs in parallel so that the conduction losses inside the cryostat are limited.

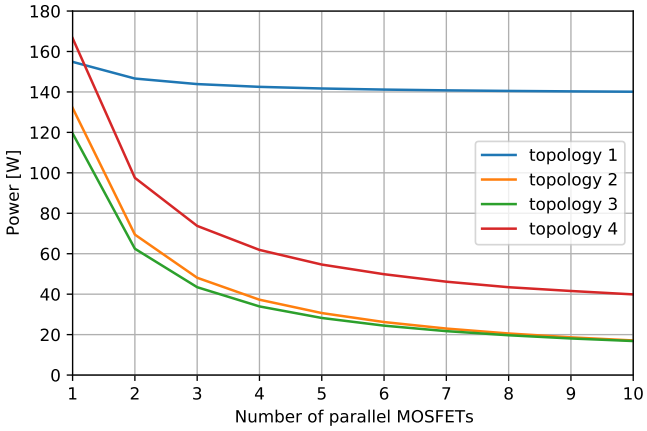

Figure 4.10: Added power of the loss sources as a function of parallel MOSFETs.

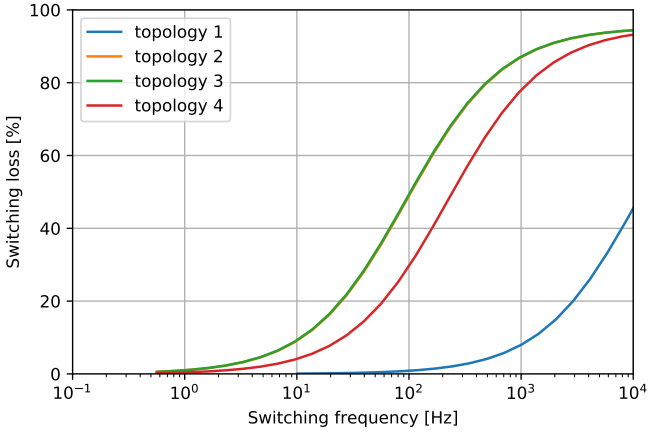

Figure 4.11: Switching losses in percentage of the total losses as a function of switching frequency. Note that the graphs of topology 2 and 3 are overlapped in the figure.

As a side effect of cooling and paralleling the MOSFETs, the time constant of the load increases. This is beneficial for the energy efficiency of the converter. By adding a smoothing capacitor inside the cryostat, the current leads can be made even smaller. This also limits the need for large peak currents from the current source. It appeared not useful to use a transformer to completely remove the current leads. The secondary coil and the rectifier inside the cryostat introduce more losses than that the elimination of the current leads yield. Besides, placing more components increases the risk of failure which affects the reliability of the system.

BIBLIOGRAPHY

[1] R. Ross, C. G. Meijer, and R. Hunik, "Maritime superconductivity perspectives", *IEEE Transactions on Applied Superconductivity*, vol. 23, no. 3, 2013.

[2] I. Hanse, D. Wikkerink, C. Vermeer, H. J. Holland, M. M. J. Dhallé, and H. J. M. ter Brake, "Crygenics for an HTS Degaussing System Demonstrator", in *Conference Proceedings of iNEC Delft*, IMarEST, Oct. 2020.

[3] M. Oomen, M. Leghissa, G. Ries, *et al.*, "HTS Flux Pump for Cryogen-Free HTS Magnets", *IEEE Transactions on Appiled Superconductivity*, vol. 15, no. 2, pp. 1465–1468, Jun. 2005.

[4] O. Mueller, "On-resistance, thermal resistance and reverse recovery time of power MOSFETs at 77 K", *Cryogenics*, vol. 29, no. 10, pp. 1006–1014, Oct. 1989.

[5] O. Mueller, "Switching losses of the cryogenic mosfet and sit", *Cryogenics*, vol. 30, no. 12, pp. 1094–1100, 1990.

[6] L. J. Woodend, P. M. Gammon, V. A. Shah, *et al.*, "Cryogenic characterisation and modelling of commercial sic mosfets", *Materials Science Forum*, vol. 897 MSF, pp. 557–560, 2017.

[7] S. Chen, C. Cai, T. Wang, Q. Guo, and K. Sheng, "Cryogenic and high temperature performance of 4h-sic power mosfets", in *2013 Twenty-Eighth Annual IEEE Applied Power Electronics Conference and Exposition (APEC)*, 2013, pp. 207–210.

[8] H. J. Ter Brake and G. F. Wiegerinck, "Low-power cryocooler survey", *Cryogenics*, vol. 42, no. 11, pp. 705–718, 2002.

[9] P. Kittel, "Cryocooler Performance Estimator", *Cryocoolers*, vol. 14, pp. 563–572, 2007.

[10] D. Graovac, M. Purschel, and A. Kiep, "Mosfet power losses calculation using the data-sheet parameters", in *Infineon: Application Note 2006-07 V1.1.*, Infineon Technologies AG, 2006, pp. 1–23.

[11] R. Patterson, A. Hammond, and S. Gerber, "Evaluation of capacitors at cryogenic temperatures for space applications", in *Conference Record of the 1998 IEEE International Symposium on Electrical Insulation (Cat. No.98CH36239)*, vol. 2, 1998, 468–471 vol.2.

[12] R. McFee, "Optimum input leads for cryogenic apparatus", *Review of Scientific Instruments*, vol. 30, no. 2, pp. 98–102, 1959.

[13] D. Wikkerink, A. R. Mor, H. Polinder, and R. Ross, "Magnetic signature reduction by converter switching frequency modulation in degaussing systems", *IEEE Access*, vol. 10, pp. 74 103–74 110, 2022.

5

CRYOGENIC CONVERTER

5.1. INTRODUCTION

When using HTS, a higher current can be utilised than when using copper. The number of turns can therefore be limited, and less HTS material is needed. However, the power supply needs to supply a higher current than in the conventional case. This is expected to cause more losses in the current supply [1]. Also, with a higher current, larger current leads are needed [2]. Through the current leads, heat leaks into the cryostat which needs to be cooled away. Cooling is an energy inefficient process [3]. It was estimated that for every watt of dissipated power inside the cryostat, the cooler consumes 14 watts of power. Dissipating heat in the cryostat should be avoided as much as possible.

A solution for reducing the extra losses in the current sources and the cryostat, has been suggested in chapter 4. By using a converter with MOSFETs with a low on-state resistance, the duty cycle can be minimised [4]–[6]. Because the HTS coils have no resistance at DC but the inductance is in the range of tens of milli Henries, the time constant of the system is large. During the relatively long freewheeling state, almost no energy is dissipated. Moreover, by placing the MOSFETs inside the cryostat, the RMS current through the current leads is decreased and the heat leak into the cryostat minimised. The cross-section of the current leads can be made more than a hundred times smaller if a sufficiently large smoothing capacitor is used in the cryostat [4]. As a side effect, the on-state resistance of the MOSFETs will be decreased by cooling them down. The MOSFETs themselves do dissipate energy directly in the cryostat however. For this reason, the switching frequency should be kept low to reduce the switching losses inside the cryostat. By placing multiple MOSFETs in parallel, the on-state losses can be reduced even further which, in turn, also reduces the duty cycle.

In this chapter, the results from chapter 4 will be experimentally tested. The aim is to investigate a cryo-cooled H-bridge converter with multiple MOSFETs in parallel

Parts of this chapter have been published as:
D. Wikkerink, M. Gagić, A. Rodrigo Mor, H. Polinder, and R. Ross, "Cryogenic H-Bridge Converter for HTS Degaussing Application", in IEEE Transactions on Applied Superconductivity, vol. 34, no. 1, pp. 1-7, Jan. 2024.

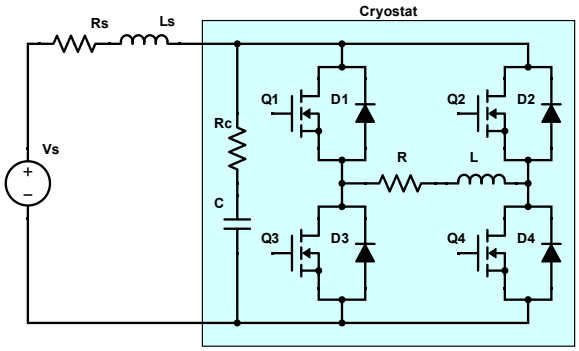

Figure 5.1: Simplified schematic of the converter. During the short charge state, losses occur in the source equivalent resistance. During the much longer discharge state, there are almost no losses because of the low series resistance.

that delivers a DC current to an inductive HTS load. The focus is to obtain the lowest duty cycle and switching frequency while still meeting the requirements for a maximum current ripple of 0.5 % and a current of 50 A. Also, different switching frequencies will be tested to investigate the effects of low switching frequencies on the behaviour of the converter. The measured results are then compared to simulations.

For the experiments, a converter is needed which is able to operate at cryogenic temperatures. The series resistance in the HTS coil current path and the dead-time should be minimised so that the lowest possible duty cycle can be obtained.

Section 5.2 describes the experimental test setup and provides the design requirements of the converter. This section also describes the parallel MOSFET gate driver circuit and the HTS coil design. Section 5.3 analyses the results of the system model simulation and laboratory prototype experiment. Section 5.4 discusses the results and future work. Finally, section 5.5 concludes this chapter.

5.2. DESCRIPTION OF THE SETUP

This section describes the different components of the test setup. The test setup consists of a DC current source which interfaces the DC voltage bus of the full-bridge cryogenic power electronic converter. An HTS load connects between the two mid points of the H-bridge. Independent gate drivers drive the MOSFET switches, while the measurements setup collects the input and output currents and voltage values.

5.2.1. CONVERTER

The system consists of a full-bridge topology that enables bi-directional DC load current flow. The degaussing coils need to be able to create a magnetic field in two directions which is why the current has to be able to be both positive and negative. A simplified schematic of the design is shown in figure 5.1.

The DC current through the load is controlled by either alternately opening and clos-

ing Q_1 and Q_3 and keeping Q_4 closed or by alternately opening and closing Q_2 and Q_4 and keeping Q_3 closed. The discharge time is long compared to the charge time because of the high time-constant of the load and low series resistance on the PCB. For this reason, the only losses during the discharge state are in the MOSFETs and the copper traces of the PCB. The power source experiences almost no conduction losses during the discharge period, which makes this design very energy efficient.

The reason that the MOSFETs are placed inside the cryostat, is that the current-leads do not have to be dimensioned for the full rated load current. The current-leads only have to be able to handle the RMS source current over the whole cycle, which significantly limits the heat leak into the cryostat [4].

The power input to the cryogenic converter connects to an external HP 6269A 60 A DC voltage source by means of a cable. Table 5.1 contains the parameters of the system obtained from the measurements of the experimental setup. These are also the parameters which are used in the simulations.

Table 5.1: Converter parameters.

Symbol	Description	Value	Unit
I_r	Rated coil current	50	A
V_s	Supply voltage	3.5	V
R_s	Cable and supply resistance	29.3	mΩ
L_s	Cable and supply inductance	3.9	μH
R	Total resistance on PCB	102	μΩ
L	HTS coil inductance	1.46	mH
C	DC bus capacitance	21.7	μF
R_C	Capacitor ESR	14.9	mΩ
R_{DSon}	Parallel MOSFET on-state resistance	45	μΩ
N_{mos}	Number of parallel MOSFETs per switching arm	10	

Each switching arm consists of ten parallel connected SiR178DP MOSFETs from Vishay. In chapter 4, it was shown that it is not useful to place more than ten MOSFETs in parallel. The individual MOSFET on-state resistance was measured to be 611 μΩ at room temperature and 404 μΩ at 77 K. Parallel operation minimizes the losses and enables an even lower duty cycle. However, caution must be taken as these high-current MOSFETs have a relatively low blocking voltage, in this case, a datasheat listed value of only 20 V.

The total resistance through the PCB and the MOSFETs between the connection points of the HTS coils was measured by injecting a known DC current and measuring the voltage with a Keithley Nanovoltmeter Model 2182A. This measured resistance represents the sum-total resistance of the system discharge state and determines the limitations on the duty-cycle.

Due to a lack of adequate damping, high-frequency current transients across parasitic inductances increased the risk of drain-source voltage overshoot. To prevent the damage or destruction of the low-voltage switches, an RC snubber was later incorporated. However, this was still not sufficient to protect the MOSFETs. The voltage oscilla-

tions were found to be a factor four higher than the input voltage, so the input voltage needed to be kept below 5 V.

Figure 5.2a shows a photo of the converter. The parallel MOSFETs are placed as close as possible to the HTS connection points. The MOSFETs are placed in such a way that the distances from the each MOSFET to the HTS coil connection point are symmetrical and equal. This ensures an optimal load-current sharing in the MOSFETs. The HTS coil is clamped between two copper bars over a distance to minimize the contact resistance.

5.2.2. GATE DRIVER

Each switching arm is driven by a separate cryogenic rated gate driver board. The gate driver boards are connected to the converter board through headers ensuring an equal distance from the gate driver chips to the MOSFETs. Each gate driver boards consist of:

- a common isolated and several step-down linear power supply regulators,
- a common input signal port,
- ten gate driver ICs and
- ten identical gate driving circuits.

In this way, the driver is able to deliver sufficient gate current to switch the MOSFET as quickly as possible so that the dead-time can be kept as short as possible. Figure 5.2b shows a photo of the gate drivers. Just as the MOSFETs, the gate drivers are placed in a circular manner on the PCB. This is done to ensure and equal propagation delays and gate-driving circuit impedance amongst all ten parallel MOSFETs.

The input signals for the gate drivers are provided by a function generator which has an adjustable switching frequency, duty cycle and dead time between the two signals. The control of the switching is open loop.

5.2.3. HTS LOAD

For the superconductive coil, ReBCO HTS tape with a critical current of 105 A is used. The HTS tape is wound around an iron core to maximise the inductance and to simulate the ferromagnetic hull of a ship. Iron doesn't perform well under cryogenic temperatures because it loses some of it's permeability. However, at 77 K it should still have at least 80 % of the permeability at room temperature [7].

An amount of thirty meter of HTS tape is used. With all the tape used, the inductor has eighty eight turns. In order for the iron core not to saturate, an air gap is installed that increases the reluctance of the core. The inductance of the coil which is stated in table 3.1, is measured with an LCR meter.

The current in the superconductive coil can not be measured with a shunt because the series resistance of the coil needs to be kept as low as possible. Therefore, the current is measured indirectly by measuring the magnetic flux density due to the current in the HTS coil. Hall sensors of different types are installed in the air gap of the iron core. Figure 5.3 shows a photo of the HTS load.

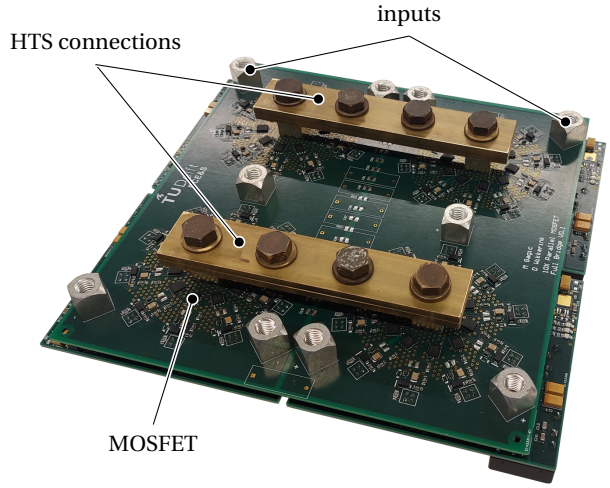

(a)

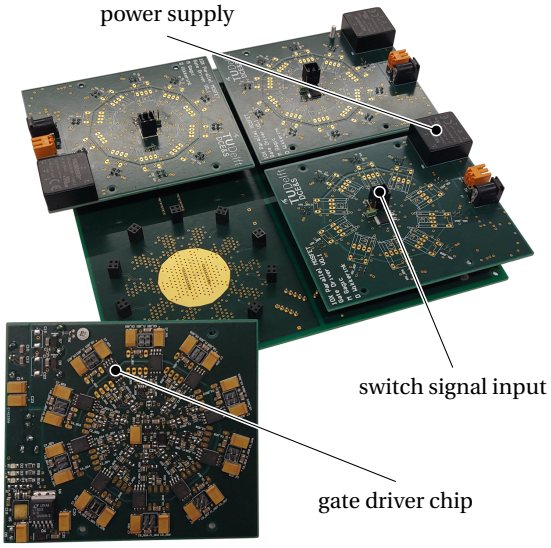

(b)

Figure 5.2: Photos of the PCB which was designed to operate in cryogenic temperatures. (a) Top-view of the PCB. The ends of the HTS coil are clamped between two copper bars. The ten parallel MOSFETs per switch of the H-bridge configuration are placed as close as possible to the HTS connection points. (b) Bottom-view of the PCB. The gate-drivers are connected through headers, with each MOSFET having its own gate-driver circuit.

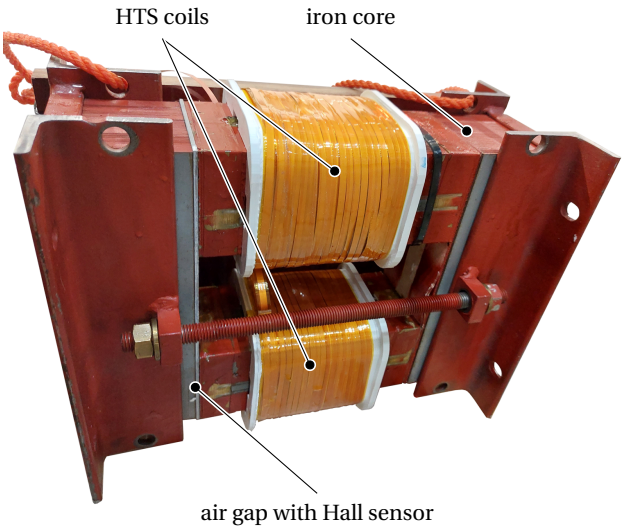

Figure 5.3: HTS tape wound around an iron core. An air gap in the core prevents the core from saturating. Magnetic flux sensors are placed inside the air gap.

5.2.4. MEASUREMENT SETUP

Since measuring current with an Ohmic shunt significantly influences the measurement, Hall sensors of the type HE244 by ASensor Technology AB are placed in the iron core of the load to measure the current in the coil indirectly. These sensors have a bandwidth of DC - 100 kHz. However, there is always a conducting MOSFET in series with the current path. By measuring the voltage across this MOSFET as a shunt, the current can be measured directly as well. The voltage across the MOSFET was probed by soldering thin copper shielded wires as close the MOSFET drain and source as possible. This voltage was connected to a differential amplifier and then to an oscilloscope. The sensitivity of the on-state resistance of the MOSFETs at different currents and at 77 K was investigated in previous work and showed consistent results [4]. The Hall sensors and the shunt measurements both show an accurate reading of the current in the coil. Finally, the shunt measurements are used in the graphs of this chapter.

The current measurements were calibrated by injecting a range of known currents into the HTS coil and measuring the corresponding steady-state voltages from the current sensors. Linear amplification circuits then condition these voltage measurements who are then logged. In order to measure the ripple at every switching frequency, a special amplifier was developed to be able to have AC-coupling for the whole frequency range. The current ripple is obtained by post-processing of the measured current wave forms.

During the measurements, the PCB and the HTS load are entirely submerged in liquid nitrogen. A photo of the test-setup under operation is shown in figure 5.4.

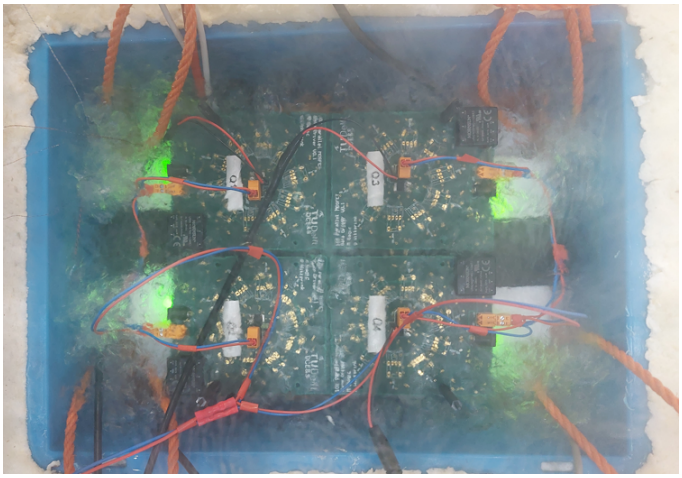

Figure 5.4: The PCB connected to the HTS coil. The setup is operating while submerged in liquid nitrogen.

5.3. RESULTS

Figures 5.5 and 5.6 shows the coil current of the HTS coil for different cases. The measured results are compared to simulations with the modelling software LTSpice XVII from Analog Devices. The output current was measured for all the combinations within a range of frequencies and duty cycles. Figure 5.5 shows the output current as a function of frequency at two of the measured duty cycles. Figure 5.6 shows the output current as a function of duty cycle at two of the measured switching frequencies.

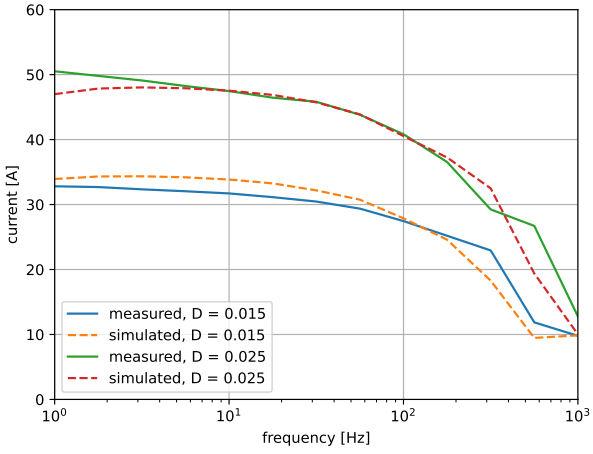

Figure 5.5: Simulated and measured output current of the converter as a function of frequency for two different duty cycles.

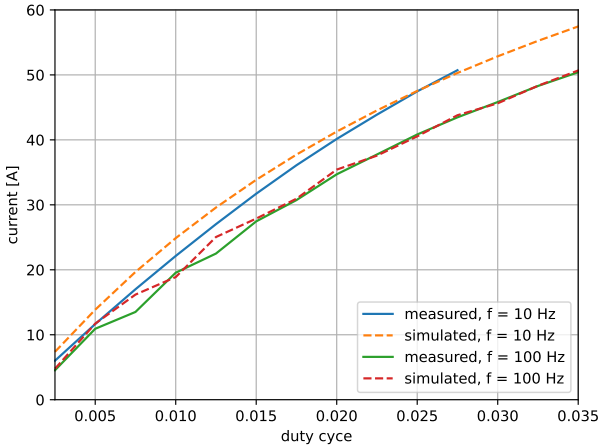

Figure 5.6: Simulated and measured output current of the converter as a function of duty cycle for two frequencies.

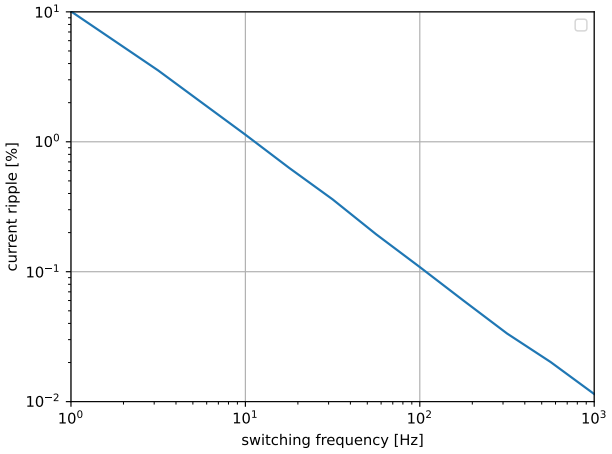

Figure 5.7: The measured current ripple in the output current as a function of frequency for a duty cycle of 0.025.

Figure 5.7 shows the ripple in the coil current as a function of frequency for a duty cycle of 0.025. The requirement of a minimum ripple of 0.5 % is met when the switching frequency is at least 21 Hz. The ripple was found not to be dependent on the duty cycle.

Figure 5.8 shows the oscillations in the drain-source voltage across the MOSFETs. The voltage is very close to the blocking voltage of the MOSFETs with a supply voltage of only 4.5 V.

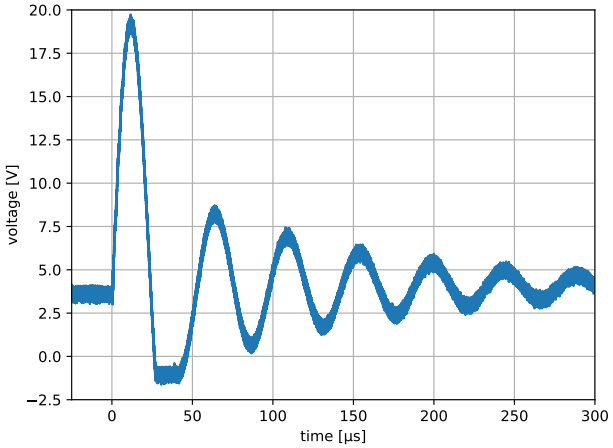

Figure 5.8: Switching MOSFET drain-source voltage oscillations as a results of parasitic inductances for a supply voltage of 4.5 V.

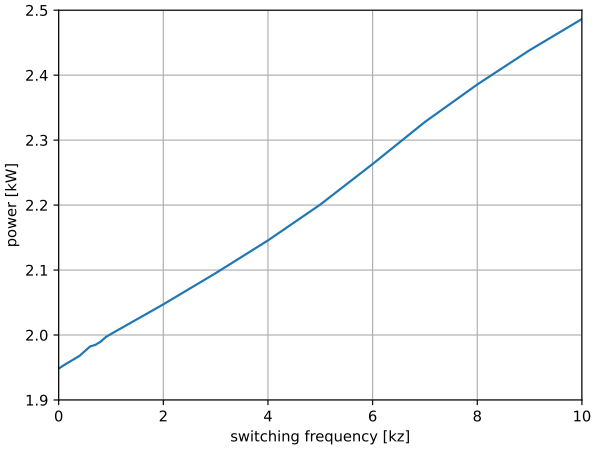

Figure 5.9: The measured gate driver losses for one gate driver as a function of switching frequency.

Figure 5.9 shows the measured power losses of one gate driver as a function of switching frequency. During operation, two gate drivers are switching. One gate driver produces a DC signal to ensure that one leg is continually conducting, consuming 1.5 W.

The effect of different dead times was investigated as well. A range of dead times from 100 ns to 1 µs was tested. However, the losses in the parasitic diodes of the MOSFETs during the dead time were not so significant that a difference could be observed in the coil current.

5.4. DISCUSSION

While the source voltage is only 3.5 V, the required current of 50 A can be achieved with a duty cycle of just 0.025. In a regular converter, the low duty cycle would be a problem because the on-time might become too short for the switches. However, since the switching frequency in this converter can be kept very low compared to a regular converter, the low duty cycle is not a problem. The on-time of the MOSFETs is still long enough.

As the switching frequency increases, the performance of the converter is drops. The inductance in the cable that connects the power source to the converter in combination with the capacitance on the PCB acts as a low-pass filter. The effect is so significant because of the lack of damping in the circuit. However, for a cryo-cooled converter, a low switching frequency is wanted anyway. A lower switching frequency reduces switching losses which otherwise would have been dissipated inside the cryostat. The current ripple requirements should be met to reduce the ripple in the magnetic signature though. The current ripple can be reduced by using an interleaved forward converter topology [6], but this will increase the losses because there are more components inside the cryostat [4]. Another solution to reduce the current ripple is to use a switching frequency modulation scheme [8].

A low input voltage is necessary because MOSFETs with a low on-state resistance usually also have a low blocking voltage. Oscillations should be taken into consideration carefully. This problem probably occurs because of the lack of damping in the system. With almost no resistance, the oscillations can reach high amplitudes. Even when using a snubber circuit, the oscillations in this particular circuit are four times higher than the input voltage. Besides, the snubber circuit introduces extra losses inside the cryostat which makes the system less efficient. In future designs, the oscillations should be controlled by using a soft switching scheme. The extra losses and reduction of oscillations with a soft switching scheme need to be quantified in future work. However, the losses are expected not to have such a large impact that the output current is affected. This is because in this chapter, it has been shown that also with longer dead times, the output current is not affected. Another solution is by decreasing the parasitic inductances on the PCB by using short traces.

By placing the MOSFETs inside the cryostat, the size of the current leads can be limited and therefore also the heat leak into the cryostat. However, the gate signal still has to be delivered to the MOSFETs by means of a galvanic connection. A potential solution for this problem is to use an optic fiber connection for the gate signal. Optic fiber cable has a much lower heat transfer coefficient than copper. The gate signal can be transported wirelessly by means of a transformer as well. In this case, no physical connection is needed at all. However, in both cases, some kind of active secondary circuit is needed inside the cryostat.

By placing multiple MOSFETs in parallel, the resistance in the conduction path of the HTS coils can be reduced and therefore, the time-constant increases. At some point, adding more switches in parallel doesn't decrease the on-state resistance significantly because the resistance of the PCB is dominant. However, the switching losses increase by adding more parallel MOSFETs. An optimum amount of parallel MOSFFETs must be found.

The dead time doesn't have a big influence on the performance of the converter. This might be because of the low switching frequency. The period time is much longer than the dead time. The gate drivers are designed in such a way that the MOSFETS can switch as fast as possible to reduce the dead time losses. Because of this, the gate drivers have a large power consumption which is dissipated in the cryostat. Since the dead time don't influence the performance of the converter significantly and soft switching can reduce the switching oscillations, the gate drivers can be less powerful in a future design which reduces the losses.

In future designs, the series resistance of the PCB should be decreased even further. This can be done by using a thicker copper layer on the PCB. Or, since the PCB is inside the cryostat anyway, by using a superconductive layer on the PCB. Also, the distance between the switches can be made shorter.

5.5. CONCLUSION

When a cryo-cooled MOSFET based H-Bridge converter is used to power an HTS degaussing coil, losses can be decreased significantly. A condition for this converter is that it should operate with a very low duty cycle and switching frequency. A prototype with an HTS load was build successfully. It was found that a load current of 50 A can be achieved with a duty cycle of 0.025 and an input voltage of 3.5 V while still meeting the requirement of a maximum current ripple of 0.5 %.

At switching frequencies higher than 100 Hz, the output current decreases. This is a consequence in the inductance in the cables and the lack of damping in the superconductor. This research shows that a cryogenic H-Bridge converter for an HTS degaussing application is a feasible option to improve the performance of an HTS degaussing system.

MOSFETs with a low on-state resistance usually have a low blocking voltage. The oscillations in this converter are high because of the lack of resistive damping. The oscillation voltage should be taken into consideration carefully when designing a converter like this.

The conducted experiments show that a cryogenic H-Bridge converter for an HTS degaussing application is a viable approach to power energy efficient HTS Degaussing systems.

BIBLIOGRAPHY

[1] R. Ross, C. G. Meijer, and R. J. van de Mheen, "Degaussing by Normal and Superconductive Windings", in *Conference Proceedings of 11th INEC Edinburgh*, May 2012.

[2] R. McFee, "Optimum input leads for cryogenic apparatus", *Review of Scientific Instruments*, vol. 30, no. 2, pp. 98–102, 1959.

[3] P. Kittel, "Cryocooler Performance Estimator", *Cryocoolers*, vol. 14, pp. 563–572, 2007.

[4] D. Wikkerink, A. R. Mor, H. Polinder, and R. Ross, "Converter design for high temperature superconductive degaussing coils", *IEEE Access*, vol. 10, pp. 128 656–128 663, 2022.

[5] M. Oomen, M. Leghissa, G. Ries, *et al.*, "HTS Flux Pump for Cryogen-Free HTS Magnets", *IEEE Transactions on Appiled Superconductivity*, vol. 15, no. 2, pp. 1465–1468, Jun. 2005.

[6] A. Elwakeel, N. McNeill, R. Pena-Alzola, M. Zhang, and W. Yuan, "Cryogenic dc/dc converter for superconducting magnet application", *IEEE Transactions on Applied Superconductivity*, vol. 32, 6 Sep. 2022.

[7] X. Pei, A. C. Smith, L. Vandenbossche, and J. Rens, "Magnetic characterization of soft magnetic cores at cryogenic temperatures", *IEEE Transactions on Applied Superconductivity*, vol. 29, no. 5, pp. 1–6, 2019.

[8] D. Wikkerink, A. R. Mor, H. Polinder, and R. Ross, "Magnetic signature reduction by converter switching frequency modulation in degaussing systems", *IEEE Access*, vol. 10, pp. 74 103–74 110, 2022.

6

MAGNETIC SIGNATURE RIPPLE REDUCTION

In the past, degaussing coils were powered with a low voltage motor-generator set, where the motor was connected to the AC bus of the ship. In case of a DC ship, the degaussing coils could be powered from the DC bus and the currents were controlled by rheostats [1]. Nowadays, degaussing coils are powered by switched-mode power supplies. This is done for energy efficiency and system compactness. However, switched-mode power supplies inherently impose a current ripple on top of the degaussing current. A concern is that the degaussing current ripple will be seen in the magnetic signature of the ship as well. A Fast Fourier Transform of the magnetic signature will then show clear peaks at the converter switching frequency and its harmonics. Moreover, with the use of ultra-sensitive SQUID magnetic sensors, the detection of very low magnetic fields with a large bandwidth is already possible [2].

It is known that there are several other relevant AC components in the magnetic signature [3]. The impressed current cathodic protection (ICCP), for example, is a system which actively pumps an electric current through the sea water to prevent corrosion of the hull. This current is provided by switch mode power supplies as well [4]. Also the use of HTS for degaussing systems can add to the ripple.

A potential way to reduce the ripple in the magnetic signature caused by the switching power supplies is to use a frequency modulation switching scheme in the converters. With such a scheme the switching frequency changes over time. Instead that all the power is concentrated in one switching frequency, the power of the ripple is spread over a frequency band. This technique is already used to reduce EMI in microchips and power converters [5]. It is also used to reduce acoustic noise in electrical machines [6], [7]. It has not been seen in degaussing systems yet.

Parts of this chapter have been published as:
D. Wikkerink, A. Rodrigo Mor, H. Polinder, and R. Ross, "Magnetic Signature Reduction by Converter Switching Frequency Modulation in Degaussing Systems", in IEEE Access, vol. 10, pp. 74103–74110, 2022.

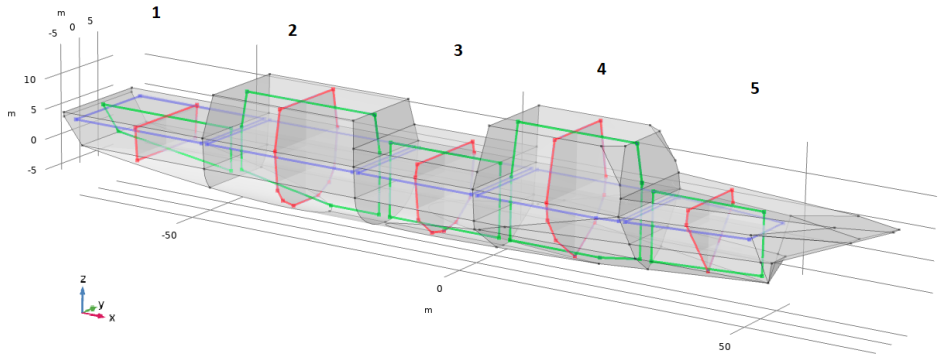

Figure 6.1: Ship geometry of a frigate with 5 M (main), 5 L (longitudinal) and 5 A (athwart ship) degaussing coils depicted in blue, red and green respectively.

In order to evaluate the need for the use of switching frequency modulation, the amount of ripple in the magnetic signature needs to be determined. The first aim of this chapter is to estimate the contribution of the ripple to the magnetic signature due to the degaussing system. After that, the possibility to reduce the ripple in the magnetic signature by means of frequency modulation is explored. The second aim of this chapter is to estimate by how much the ripple can be reduced by means of switching frequency modulation.

The organisation of this chapter is as follows. Section 6.1 describes the model to find the magnetic signature of a ship with degaussing coils supplied by switched-mode power supplies. This model is validated by experiments and the results of the model are discussed. Section 6.2 presents an overview of the switching modulation schemes which can be implemented in the converter. The modulation schemes are modelled and applied to a degaussing case. The results are discussed. Finally, in section 6.3 a conclusion is drawn.

6.1. MODEL DESCRIPTION

In order to find the influence of the degaussing current ripple on the magnetic signature, a model is developed. The model is split into two parts, the static and the dynamic model. The first one is used to calculate the static magnetic signature. From this model, the nominal degaussing currents, coil inductances and coil resistances are determined. The degaussing currents are optimised in such a way so that the magnetic signature is minimised. The dynamic model determines the waveform and magnitude of the current ripple on top of the degaussing currents. This is incorporated in the magnetic model to determine how the current ripple translates to the magnetic signature. Finally, the models calculate the magnetic signature at any point in space as a function of current, switching frequency and externally applied magnetic flux density.

Table 6.1: Magnetic model parameters of a frigate with a steel hull.

Symbol	Description	Value	Unit
l	ship length	150	m
w	ship width	12	m
h	ship height	20	m
t	hull thickness	25	mm
μ_r	relative permeability hull	320	
$\hat{B}_{\text{Earth}}$	Earth's magnetic field	46.1	μT

6.1.1. STATIC MODEL

A simplified geometry of a modern sized frigate has been created. Degaussing coils are usually placed in such a way that the magnetic field can be altered in three dimensions. In this model, the ship is divided into five compartments, each having a coil positioned perpendicular to the longitudinal (L), athwart ship (A) and main (M) direction, highlighted in red, green and blue respectively in figure 6.1. The parameters used for the modelling of the ship are shown in table 6.1. It is assumed that the magnetic permeability is linear and frequency independent.

The simulations are set out using the commercial finite element modelling software COMSOL [8]. The thickness of the hull is relatively small compared to the size of the ship which makes it difficult to generate a mesh. The model could be made by creating an extremely fine mesh, but then the simulations would take a long time to finish. A better way is to model the hull using the magnetic shielding node in COMSOL. This node describes a thin layer of permeable material with an adjustable thickness and permeability. The degaussing currents are modelled as edge currents along a 2D plane. This way of simulating the magnetic signature of a steel object with degaussing coils has been experimentally verified in chapter 2.

The total vector field of the magnetic flux density around the ship, $\vec{B}$, can then be found by adding the magnetic signature of the hull to the magnetic signature from each degaussing coil as follows:

$$\vec{B} = \vec{B}_{\text{sig}}(\vec{B}_{\text{Earth}}) + \sum_{i=1}^{N} \frac{I_i}{I_0} \vec{B}_i(I_0) + \vec{B}_{\text{Earth}}, \tag{6.1}$$

where $\vec{B}_{\text{sig}}$ is the magnetic signature of the ship due to Earth's magnetic field $\vec{B}_{\text{Earth}}$, N is the number of degaussing coils, I_i is the current through degaussing coil i and $\vec{B}_i$ is the magnetic field due to current I_0 through degaussing coil i.

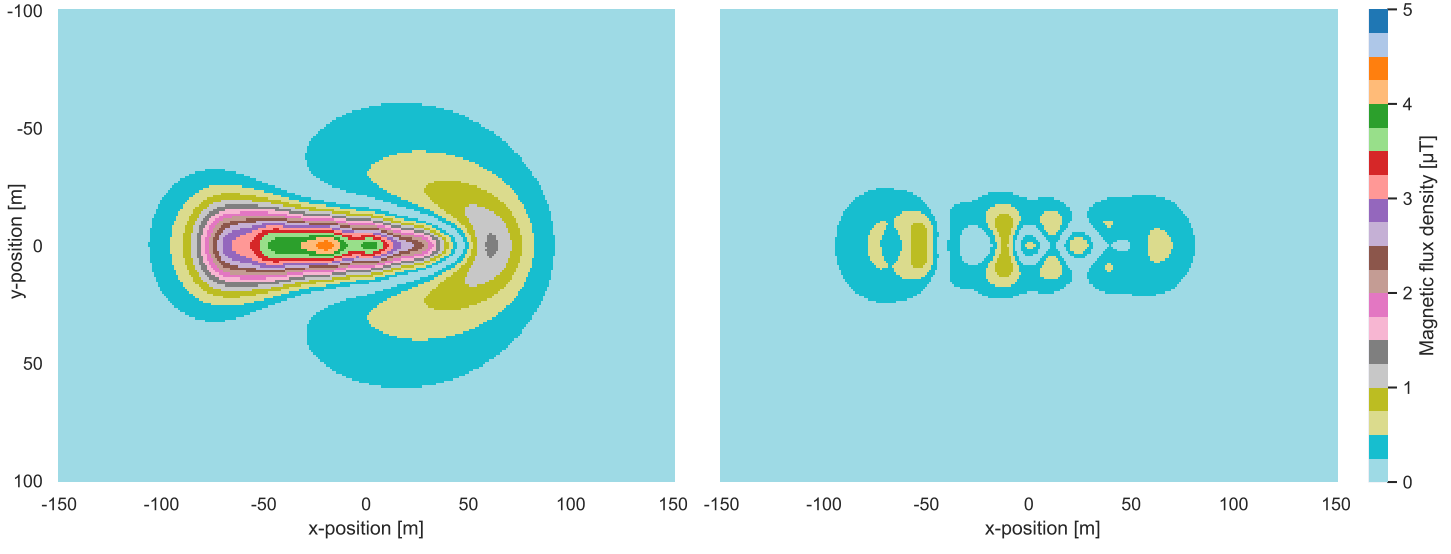

(a) (b)

Figure 6.2: The magnetic signature of the ship in a horizontal plane 15 m beneath sea level. The plots show the magnitude of the magnetic flux density. (a) The magnetic signature of the modelled ship without the degaussing coils active. (b) The reduced magnetic signature of the ship with the optimised currents through the degaussing coils.

By adjusting the degaussing currents, I_i, in equation 6.1, the difference between the magnetic flux density around the ship, $\vec{B}$, and Earth's magnetic field, $\vec{B}_{\text{Earth}}$, can be minimised. An optimisation loop is used to minimise the highest peak of the magnetic flux density in the horizontal plane at 15 m below the water line with the degaussing currents as optimisation variables. Figure 6.2 shows the absolute value of the magnetic flux density in this plane. Earth's magnetic field is subtracted in the figure so that only the magnetic signature and the reduced magnetic signature remain.

The plot in figure 6.2a shows the magnetic signature of the steel hull of the ship due to Earth's magnetic field. The plot in figure 6.2b shows the magnetic signature with the optimised degaussing currents through the coils. Although the magnetic signature is reduced, there is still a distortion in the magnetic field. This can be minimised even further by increasing the number of degaussing coils and by optimising the position of the coils.

6.1.2. AC SIGNATURE

In order to find the ripple in the magnetic signature, first the current ripple in the degaussing coils needs to be determined. From the static model, the nominal currents, the inductances and the resistances of the degaussing coils are found. The degaussing coils are then modelled as follows:

$$v_i = R_i i_{L_i} + L_i \frac{\mathrm{d}i_{L_i}}{\mathrm{d}t} + \sum_{\substack{j=1 \\ j \neq i}}^{N} M_{ij} \frac{\mathrm{d}i_{L_j}}{\mathrm{d}t}, \tag{6.2}$$

where v_i is the converter output voltage, i_{L_i} is the current, L_i is the inductance and R_i is the resistance of degaussing coil i. M_{ij} is the mutual inductance between coil i and j. The converter is modelled using the circuit modelling software LTspice [9]. A buck converter is used as the converter topology. The degaussing coils of each converter are magnetically coupled using the mutual inductances M_{ij}. The ripple in the magnetic signature is then determined using eq. (6.1).

The magnetic field produced by the current ripple will experience attenuation due to induced eddy currents in the steel hull of the ship and in the seawater. Other sources of attenuation, like hysteresis losses are not considered here. In order to quantify the amount of attenuation, the COMSOL model presented in section 6.1.1 is used to model the magnetic field in the frequency domain. The magnetic shielding node can not be used for frequency domain analysis. Instead, the transition boundary condition node was used to model the thin metal hull of the ship in the time domain. This node takes the thickness, permeability, permittivity and conductivity of the material into account. This modelling technique was verified by measuring the attenuation of a magnetic field in a steel pipe at several frequencies.

First, the magnetic flux density near an air-cored coil with 34 turns was measured at a distance of 13 cm from the coil with a Stefan Mayer FLC3-70 flux gate sensor. An AC current with a frequency ranging from 0 to 140 Hz was injected by the function generator. The exact same measurements were repeated again, but with a steel pipe with an outer diameter of 20 cm, a thickness of 10 mm and a relative permeability of 320 placed in between the coil and the sensor in order to determine the attenuation of the pipe.

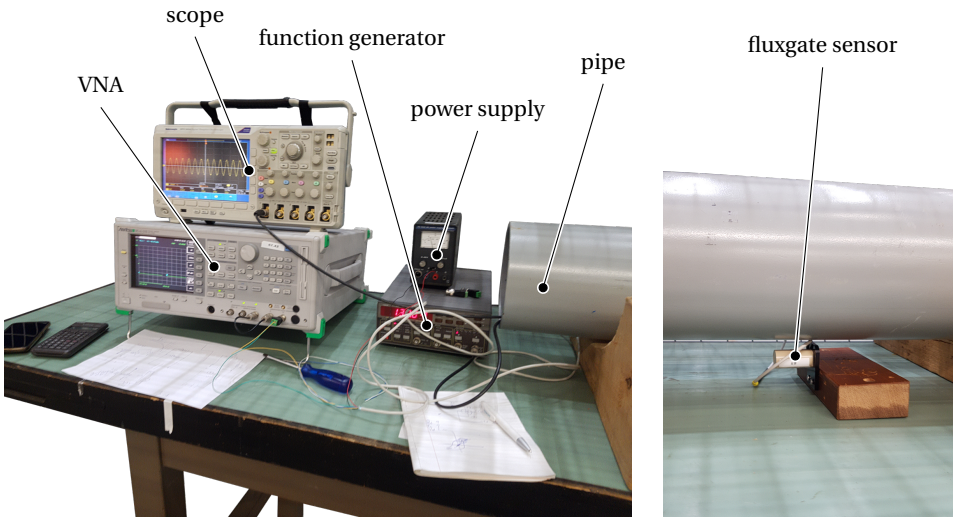

Figure 6.3: Test setup to measure the attenuation of the ripple in the magnetic signature of a steel object as a function of frequency. (a) A coil is placed in a steel pipe where an AC current is induced and measured with a (b) flux gate sensor.

Figure 6.3 shows a photo of this test setup. The results are shown in figure 6.4.

Figure 6.4a shows the measured attenuation of the magnetic field compared to the modelled attenuation in the steel pipe. The measured values match the modelled values. The measurements show a little difference in attenuation with respect to the modelled case. This can be explained by a deviation in the material properties of the pipe. Although the permeability of the material is known, the permittivity and conductivity are an estimation based upon average data for steel. Since the measured results match the simulations, this modelling can also be applied to estimate the attenuation in the full sized ship hull. The ship is assumed to have a hull thickness of 25 mm. For a good comparison, the pipe is also modelled with a thickness of 25 mm. Figure 6.4b shows the attenuation of one of the degaussing coils on the ship as a function of frequency. The ship is also modelled with a hull thickness of 10 mm so it can be compared to the metal pipe.

6.1.3. DISCUSSION

The magnetic signature of a ship is measurable around the ship. It is reduced by applying a magnetic field inside the ship with on-board degaussing coils. The degaussing field translates to the outside of the ship and cancels out the magnetic signature as much as possible. The rate of change of the degaussing field is very low. It only has to change when the ship is moving and it can therefore be considered to be quasi-static. Because of this, it doesn't get attenuated by the hull. The degaussing field also has an alternating component created by the switching of the converter. The attenuation is much higher because of the induced eddy currents in the hull.

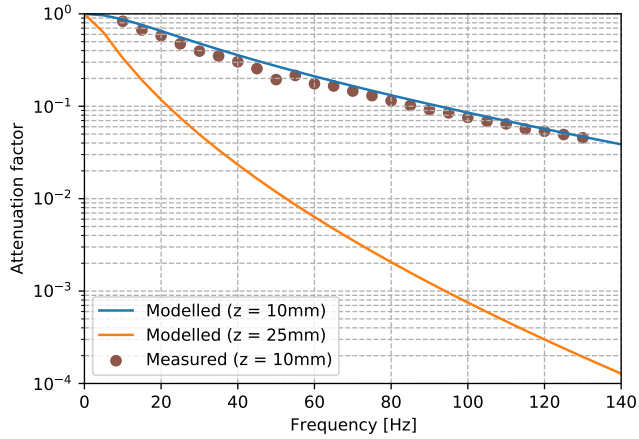

(a)

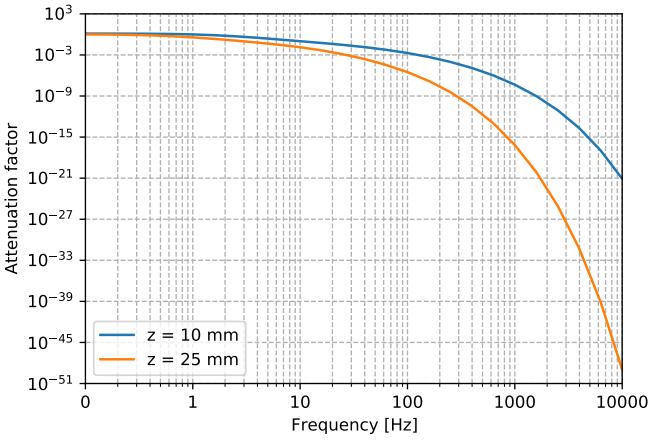

(b)

Figure 6.4: Attenuation of the magnetic field in steel as a function of frequency. (a) Measured in a steel pipe. (b) Simulated for full sized ship.

The magnetic field attenuation increases as the frequency increases. The hull thickness plays an important role in the attenuation of the frequency components of the magnetic signature as well. For a ship with a hull thickness of 10 mm and a converter switching frequency of 10 kHz, the field is already attenuated by a factor 10×10^{-21}. This is so much that it can be considered undetectable. For this reason, it would not be necessary to use a switching frequency modulation scheme in a ship with a conventional degaussing system. However, there are also other potential sources of current ripple in the magnetic signature and there may be ships with a non-magnetisable hull.

High temperature superconductors (HTS) are expected to be a good replacement for copper degaussing coils [10]. When superconductors are used in a degaussing system, the use of a flux pump or a persistent mode current switch may be considered. Flux pumps could improve the efficiency of a degaussing system significantly compared to switched-mode power supplies. However, they operate at a much lower frequency where the attenuation by the hull is also lower [11]. Besides flux pumps and persistent mode current switches, the use of parallel MOSFET's is also a good possibility for an efficient power supply [12]. Due to the large time constant of the HTS degaussing coil, a low switching frequency can be used. This is even necessary when the MOSFET's are placed inside the coolant. The switching losses then need to be reduced in order to minimize dissipated power in the coolant. This can be done by reducing the switching frequency. Flux pumps operate in the range of $1-200\,\text{Hz}$ [11] and a MOSFET based power supply could have a switching frequency as low as 100 mHz [12]. In this frequency range the attenuation by the hull is not sufficient to reduce the peak of the switching frequency in the magnetic signature and the use of switching frequency modulation may be recommendable.

Besides degaussing, there are other sources for a current ripple in the magnetic signature. The impressed cathodic corrosion protection (ICCP) system injects a current directly into the seawater. This current, also provided by a switched-mode converter, is not attenuated by the steel hull of the ship, but only by the sea water [4]. Lastly, non-metal ships don't have any attenuation in the hull. On-board switching equipment might be detected by a magnetic sensor. In these cases the attenuation of the ripple is much lower. For these, it might be useful to use a switching modulation scheme. In section 6.2 various switching modulation schemes are explored.

6.2. RIPPLE REDUCTION BY SWITCHING FREQUENCY MODULATION

Several frequency modulation techniques are explored in this section. The first one, Spread Spectrum Frequency Modulation (SSFM), is a deterministic frequency modulation technique which is used for EMI reduction in high frequency digital systems. SSFM can also be used in power converters [5]. Besides deterministic frequency modulation, also stochastic frequency modulation can be used. Random switching frequency modulation techniques are tested for noise reduction in electrical machines [6]. Four stochastic frequency modulation techniques are discussed and tested in this section, namely,

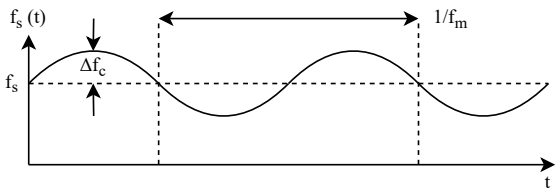

Figure 6.5: Spread spectrum frequency modulation (SSFM)

Random Lead-Lag Modulation (RLL), Random Center Displacement (RCD), Random Duty Cycle (RDC) and Random Switching Frequency (RS).

6.2.1. SPREAD SPECTRUM FREQUENCY MODULATION

When the converter switching frequency is modulated with a constant frequency, each harmonic is spread out over a frequency band. This illustrated in figure 6.5.

The modulated square wave that drives the switch can be expressed as follows:

$$F(t) = \frac{\text{sgn}\{\sin[2\pi f_s t + \Theta(t)]\} + 1}{2} \tag{6.3}$$

where f_s is the non-modulated switching frequency and $\Theta(t)$ is the phase angle so that:

$$\Theta(t) = \int_0^t k_w sin(2\pi f_m t)\, dt \tag{6.4}$$

where k_w is a factor that controls the frequency deviation and f_m is the modulation frequency of, in this case, a sinusoidal modulation profile. In this case the duty cycle, D, is set to be 0.5 as a generalisation. The modulation profile can be any waveform.

To control an SSFM switching scheme, the modulation index, m_f, and the modulation ratio, δ, can be used as follows:

$$m_f = \frac{\Delta f_s}{f_m} \quad \text{and} \quad \delta = \frac{\Delta f_s}{f_s} \tag{6.5}$$

6.2.2. RANDOM FREQUENCY MODULATION

The four random switching methods are shown in figure 6.6. These methods are explained below:

Random lead lag: With RLL modulation the pulse is randomly chosen to be either at the beginning or the end of the switching period. The switching frequency and duty cycle do not vary randomly. This is illustrated in figure 6.6a.

Random switching frequency: In RSF, shown in figure 6.6b, a new switching frequency is chosen for every new switching period at random. This is done within a band where the maximum deviation from the switching frequency f_s can be chosen. The random value α needs to be chosen within the following boundary:

$$\frac{f_s - \Delta f_s}{f_s} < \alpha < \frac{f_s + \Delta f_s}{f_s} \tag{6.6}$$

where, for this research, Δf_s is chosen to be 10 % of f_s.

Random center displacement: With RCD the position of the pulse within the switching period is chosen at random. This is illustrated in figure 6.6c. RCD requires a more extensive control than RLL since the position of the pulse is chosen with more precision. A problem with RCD is that the switching interval between two pulses might become too short when they are placed too close together. The random value α needs to be chosen within the following boundary:

$$-\frac{1}{2}(1-D) < \alpha < \frac{1}{2}(1-D) \tag{6.7}$$

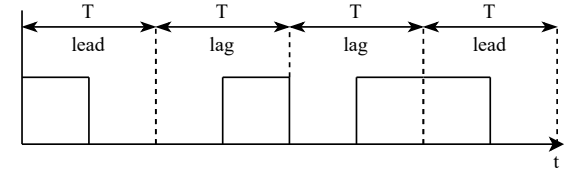

(a)

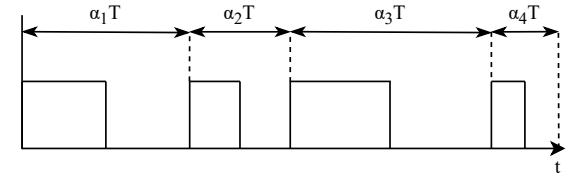

(b)

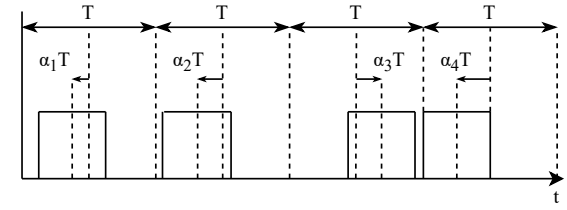

(c)

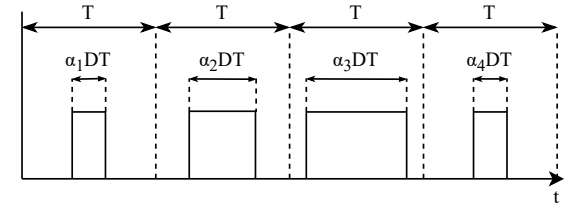

(d)

Figure 6.6: Random switching topologies. (a) Random lead-lag. (b) Random switching frequency. (c) Random center displacement. (d) Random duty cycle.

Random duty cycle: With RDC, the duty cycle is chosen for every switching period at random as shown in figure 6.6d. The random value α needs to be chosen within the following boundary:

$$2 - \frac{1}{D} < \alpha < \frac{1}{D} \tag{6.8}$$

In this research, the values for α are randomly sampled from a uniform distribution between boundaries defined by eqs. (6.6) to (6.8). The value for α is generated every switching cycle.

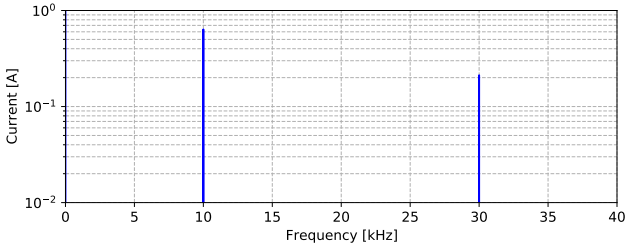

(a) no frequency modulation.

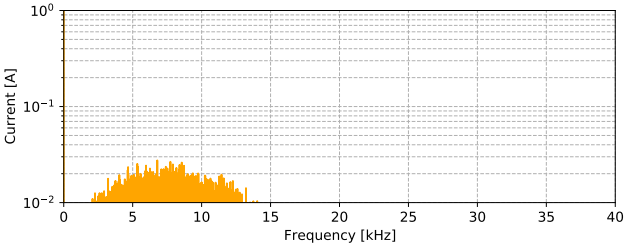

(b) random lead lag.

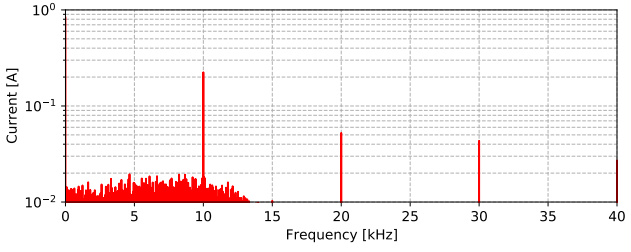

(c) random duty cycle.

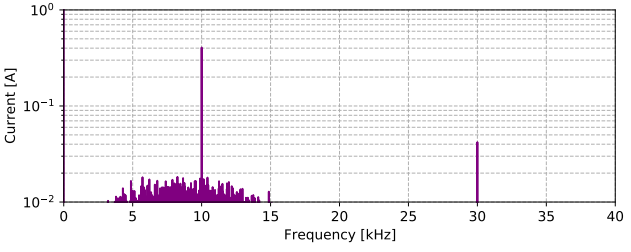

(d) random center displacement.

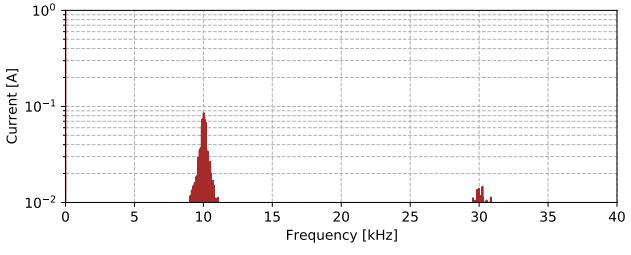

(e) random switching frequency.

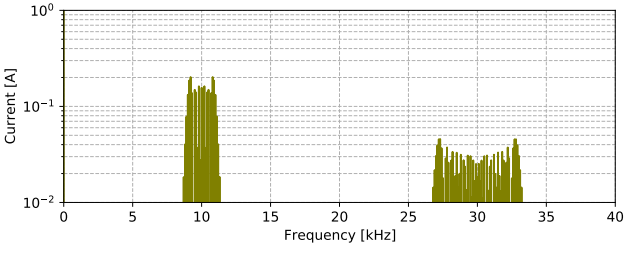

(f) spread spectrum frequency modulation.

Figure 6.7: Frequency components of the ripple with (a) no frequency modulation (blue), (b) random lead lag (orange), (c) random duty cycle (red), (d) random center displacement (purple), (e) random switching frequency (brown) and (f) spread spectrum frequency modulation (green).

6.2.3. RESULTS

The different frequency modulation techniques are tested on the buck converter described in section 6.1.2 with a base switching frequency of 10 kHz and a duty cycle D of 0.5. Figure 6.7 shows the results of the frequency modulation techniques described in this section. They are compared to the case where there is no frequency modulation at all. From the graphs it can be seen that all the modulation schemes reduce the peak at the fundamental switching frequency compared to the use of no modulation scheme with a factor in the range of 2 to 10.

The random frequency modulation techniques introduce some noise around the fundamental frequency. While random center displacement and random pulse width still show a significant peak at the switching frequency, random switching frequency and especially random lead lag show a large reduction of the peak. Spread spectrum frequency modulation spreads the peak into several lower peaks. It seems that random lead lag switching reduces the peak the most and should therefore be the best candidate for switching frequency modulation in our application.

The switching frequency modulation techniques were tested in the lower frequency range where HTS degaussing is expected to operate as described in section 6.1.3. Figure 6.8 shows two plots of the magnetic signature with the use of random lead lag, random switching frequency and no switching frequency at all. In figure 6.8a the base switching frequency is set at 3 Hz and in figure 6.8b the base switching frequency is set at 150 Hz. These plots include the attenuation by the hull of the ship.

At 3 Hz, random lead lag reduces the switching frequency peak significantly and therefore the detectability of the magnetic signature. However, there is some noise produced which is not present without using switching frequency modulation. Especially in the lower frequency band where the attenuation is less. Random switching frequency modulation also slightly reduces the peak, at the expense of spreading the frequency content.

At 150 Hz, the attenuation by the hull also gets higher. The contribution to the magnetic signature of the switching peak is therefore much lower at higher switching frequencies. The switching modulation techniques still reduce the peak by the same percentage as with lower switching frequencies. However, the noise in the lower frequency band is now relatively more visible. Since random switching produces less noise than random lead-lag, in this case, random switching is the best candidate.

6.3. CONCLUSION

The aim of this chapter is to analyze the influence of the current ripple in a degaussing system in the magnetic signature of a ship. A magnetic model of a ship has been made which includes the attenuation of time varying magnetic fields. At high switching frequencies, the metal hull of the ship almost completely absorbs the current ripple from the degaussing currents. The attenuation by the hull strongly depends on the material, the thickness of the hull and the switching frequency. It can be concluded that the current ripple of the degaussing coils will not be detectable from outside the ship with a state-of-the-art magnetic sensor if the switching frequency is around 10 kHz and it has a standard steel hull thickness of 25 mm. However, in a HTS degaussing system the switching frequency is expected to be much lower. The attenuation of the switching frequency peak produced by the metallic hull of the ship is then not enough.

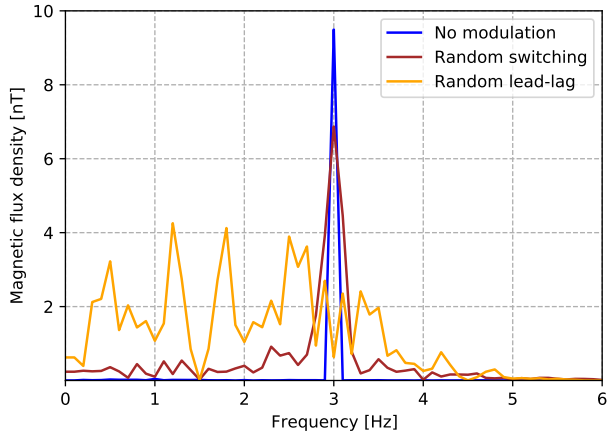

(a)

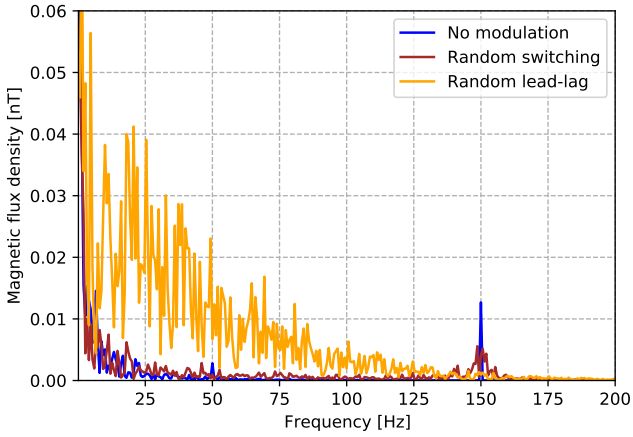

(b)

Figure 6.8: Magnetic signature with switching frequency modulation schemes applied to a degaussing coil with a base switching frequency of (a) 3 Hz and (b) 150 Hz.

There are also other contributors to the AC magnetic signature where the implementation of frequency modulation might be useful. The ICCP system, ships with non-metal hulls and the individual degaussing of on-board equipment are all examples that add a frequency component to the magnetic signature and where its detectability can be reduced by using switching frequency modulation.

An option to reduce the switching ripple in the magnetic signature is to increase the switching frequency. With a higher switching frequency the attenuation by the hull increases and the current ripple in the coil will be smaller. However, the switching losses

will increase, which can be problematic. In a HTS degaussing system with cryo-cooled MOSFETs, the switching losses should be kept to a minimum in order to reduce heat from entering the coolant.

Switching frequency modulation can be used to reduce the peak in the frequency spectrum of the magnetic signature. Several topologies have been tested. All of them reduce the peak at the switching frequency, but random switching frequency and random lead lag show the most promising results. Especially for a system with a low switching frequency it can be useful to implement switching frequency modulation.

BIBLIOGRAPHY

[1] N. B. Michel, "Shipboard Degaussing Installations for Protection Against Magnetic Mines", *Transactions of the American Institute of Electrical Engineers*, vol. 67, no. 2, pp. 1270–1277, Jan. 1948.

[2] M. Hirota, T. Furuse, K. Ebana, *et al.*, "Magnetic detection of a surface ship by an airborne LTS squid mad", *IEEE Transactions on Applied Superconductivity*, vol. 11, no. 1, pp. 884–887, 2001.

[3] J. J. Holmes, "Exploitation of a Ship's Magnetic Field Signatures", *Synthesis Lectures on Computational Electromagnetics*, vol. 1, no. 1, pp. 1–78, Jan. 2006.

[4] H. Nain, M. Isa, M. M. Muhammad, N. Hassanuddin, M. Yati, and I. Nor, "Management of naval vessel's electromagnetic signatures: A review of sources and countermeasures", *Defence S & T Technical Bulletin*, vol. 6, pp. 93–110, Nov. 2013.

[5] A. Santolaria, J. Balcells, D. González, J. Gago, and S. D. Gil, "EMI reduction in switched power converters by means of spread spectrum modulation techniques", *PESC Record - IEEE Annual Power Electronics Specialists Conference*, vol. 1, pp. 292–296, 2004.

[6] M. M. Bech, F. Blaabjerg, and J. K. Pedersen, "Random modulation techniques with fixed switching frequency for three-phase power converters", *IEEE Transactions on Power Electronics*, vol. 15, no. 4, pp. 753–761, 2000.

[7] T. Tanaka, T. Ninomiya, and K. Harada, "Random-switching control in dc-to-dc converters", in *20th Annual IEEE Power Electronics Specialists Conference*, 1989, 500–507 vol.1.

[8] COMSOL AB, *Comsol multiphysics*, version 5.4, Oct. 3, 2018. [Online]. Available: https://www.comsol.com/.

[9] Analog Devices, Inc., *Ltspice*, version 17.1.15, Jan. 9, 2024. [Online]. Available: https://www.analog.com/en/design-center/design-tools-and-calculators/ltspice-simulator.html.

[10] D. Wikkerink, I. Hanse, A. Rodrigo Mor, H. Polinder, and R. Ross, "Demonstration of Degaussing by Copper and HTS Windings", in *Conference Proceedings of iNEC Delft*, IMarEST, Oct. 2020.

[11] T. A. Coombs, J. Geng, L. Fu, and K. Matsuda, "An overview of flux pumps for hts coils", *IEEE Transactions on Applied Superconductivity*, vol. 27, 4 2017.

[12] M. Oomen, M. Leghissa, G. Ries, *et al.*, "HTS Flux Pump for Cryogen-Free HTS Magnets", *IEEE Transactions on Appiled Superconductivity*, vol. 15, no. 2, pp. 1465–1468, Jun. 2005.

7

CONCLUSION

The primary objective of this thesis is to design an adequate power supply for a degaussing system which uses HTS instead of copper degaussing coils. This objective has been broken down into five research objectives. The conclusions for each research objective and recommendations for future work are given in this chapter.

To create a framework in which the magnetic signature and the effect of degaussing can be visualised and quantified.

The magnetic signature consists of many components, but the ones that are relevant for degaussing are the induced and the permanent magnetisation. In order to measure the induced magnetisation properly, one has to remove the permanent magnetisation first by means of deperming. There are several ways to model the magnetic signature of a steel object. The analytical approach is accurate, but is limited to shapes which can be expressed analytically like ellipses and circles. If the shape that needs to be modelled can not be expressed analytically, it can still be approximated by another shape. The model then has a lower accuracy. Another advantage of analytical modelling is that it is fast to compute. This can be an advantage for applications like closed loop degaussing. A more practical and modern approach of modelling is the use of FEM. Any shape can be modelled accurately, but the simulation time is long. A test setup consisting of a cylindrical shipbuilding steel object is used to show that the magnetic signature of the object can be modelled and measured. The permanent magnetisation in the object was removed first by deperming. The measured magnetic signature corresponds to the modelled magnetic signature for both the analytical and the numerical modelling approach. The framework from this chapter is used throughout this thesis to estimate the degaussing parameters of a real ship.

To demonstrate the equivalence of HTS and copper degaussing coils.

The main goal of the demonstrator tests was to demonstrate the equivalent behaviour of HTS degaussing coils compared to copper degaussing coils, and that HTS coils can

thus be qualified as degaussing coils on ships. The magnetic behaviour of both copper and HTS degaussing coils is shown for static and dynamic cases. Overall, both in the static and the dynamic experiments, the copper and HTS coils show a similar behaviour. Although the results were expected from a theoretical point of view, they serve as a convincing proof of concept. The difference in magnetic field between the both sets of coils is small and can be explained by small differences in the positions of the coils and the construction of the pipe. The degaussing performance of both sets of coils is the same. The static test is a good way to visualize and compare the differences between copper and HTS degaussing. These tests gave an insight in the possibilities of using HTS for a degaussing system. The dynamic test is used to test the control system and the dynamics of the degaussing currents. In this test setup, the effect on the dynamics is not notable because the resistance of the degaussing coils is only a small portion of the total resistance in the system. The cables connecting the power supplies to the degaussing coils and the power supplies themselves are also resistive and considerably longer. There was not a notable difference between the time constant of the copper and HTS coils. To further investigate the dynamic effects of HTS coils in a degaussing system, a larger setup is needed so the effect of the time constant of the superconductive coil without damping becomes more present, which would be the case in a full sized ship. In such a setup, the energy efficiencies of both systems are expected to be comparable as well. The power consumption of an optimised cryostat would be relatively low so a fair comparison can be made with the Ohmic losses in a copper degaussing system. On the other hand, the coupling factors of the degaussing coils are so small, that they are negligible. For the experiments conducted, the permeability of the pipe was determined by fitting the measurements of the magnetic signature to simulated magnetic signature. In the future, the permeability of the pipe could be measured directly with an independent measurement. The deperming of the pipe only took place in the longitudinal direction. The magnetising field from the deperming coil might not have affected the end caps of the pipe. A deperming coil in the vertical direction could be employed for this.

To identify a suitable converter topology to reduce converter losses when using HTS coils.

Several converter topologies were investigated for HTS degaussing coils. Some of these topologies have part of the electronics inside the cryostat. The performance of electronic switching components in liquid nitrogen was tested with measurements. It was shown that if a converter with MOSFETs were placed inside the cryostat, the energy efficiency can be increased considerably. By doing this, the rated current for the current leads is drastically decreased and therefore the losses as well. However, by placing the MOSFETs inside the cryostat, the cooler needs to lift more heat. This is an inefficient process which can be counteracted by placing multiple MOSFETs in parallel so that the conduction losses inside the cryostat are limited. As a side effect of cooling and paralleling the MOSFETs, the time constant of the load increases because the on-state resistance decreases. This is beneficial for the energy efficiency of the converter. By adding a smoothing capacitor inside the cryostat, the current leads can be made even smaller. This also limits the need for large peak currents from the current source. It is not useful to use a transformer to completely remove the current leads. The secondary coil and the rectifier inside the cryostat introduce more losses than that the elimination of the current leads

yield. Besides, a transformer makes the circuit more complex.

To design an H-bridge converter type with cryocooled MOSFETs.

When a cryo-cooled MOSFET based H-Bridge converter is used to power an HTS degaussing coil, losses can be decreased significantly. A condition for this converter is that it should operate with a very low duty cycle and switching frequency. A prototype with an HTS load was built successfully. It was found that a load current of 50 A can be achieved with a duty cycle of 0.025 and an input voltage of 3.5 V while still meeting the requirement of a maximum current ripple of 0.5 %. At switching frequencies higher than 100 Hz, the output current decreases. This is a consequence in the inductance in the cables and the lack of damping in the superconductor. This research shows that a cryogenic H-Bridge converter for an HTS degaussing application is a feasible option to improve the performance of an HTS degaussing system. MOSFETs with a low on-state resistance usually have a low blocking voltage. The oscillations in this converter are high because of the lack of resistive damping. The oscillation voltage should be taken into consideration carefully when designing a converter like this. The conducted experiments show that a cryogenic H-Bridge converter for an HTS degaussing application is a viable approach to power energy efficient HTS degaussing systems.

To achieve switching ripple reduction in the magnetic signature by means of switching frequency modulation.

This chapter describes the influence of the ripple in the degaussing current in the magnetic signature of a ship and other pulsed power equipment. A magnetic model of a ship has been made which includes the attenuation of time varying magnetic fields. At high switching frequencies, the metal hull of the ship almost completely absorbs the current ripple from the degaussing currents. The attenuation by the hull strongly depends on the thickness of the hull and the switching frequency. It can be concluded that the current ripple of the degaussing coils will not be detectable from outside the ship with a state-of-the-art magnetic sensor if the switching frequency is around 10 kHz and it has a hull thickness of 25 mm. However, in a HTS degaussing system the switching frequency is expected to be much lower. The attenuation of the switching frequency peak produced by the metallic hull of the ship is then not enough. There are also other contributors to the AC magnetic signature where the implementation of frequency modulation might be useful. The ICCP system, ships with non-metal hulls and the individual degaussing of on-board equipment are all examples that add a frequency component to the magnetic signature and where its detectability can be reduced by using switching frequency modulation. An option to reduce the switching ripple in the magnetic signature is to increase the switching frequency. With a higher switching frequency the attenuation by the hull increases and the current ripple in the coil will be smaller. However, the switching losses will increase, which can be problematic. In a HTS degaussing system with cryo-cooled MOSFETs, the switching losses should be kept to a minimum in order to reduce heat from entering the coolant. Switching frequency modulation can be used to reduce the peak in the frequency spectrum of the magnetic signature. Several topologies have been tested. All of them reduce the peak at the switching frequency, but random switching

frequency and random lead lag show the most promising results. Especially for a system with a low switching frequency it can be useful to implement switching frequency modulation.

All in all, a framework was developed to estimate the magnetic signature and degaussing parameters. It was shown with a demonstrator that HTS can be used to replace copper degaussing coils. Several converter topologies where compared and it was shown that the use of cryo-cooled MOSFETs can increase the performance drastically. A converter was designed which is at least fifteen times more efficient than a conventional solution. A cryo-cooled converter was built and tested successfully. And finally, a solution for the unwanted effects of a small switching frequency in the ripple of the magnetic signature was provided.

FUTURE WORK

The persistent mode seems to be a very efficient mode of operation of HTS degaussing coils. More research is needed into a flux pump topology which can be used for a degaussing system which doesn't introduce extra losses in the cryostat. Besides that, the flux pump needs to be fast enough to control the degaussing current. Alternatively, a transformer can be used to control the degaussing current for ships heading changes and roll, while the flux pumps only compensates for the losses in the HTS joint.

Some flux pumps use rotating magnets as the source of the travelling wave on the superconductor to induce a voltage. Installing a rotating machine inside the cryostat introduces extra cooling losses. However, the cryogenic system needs a nitrogen pump anyway to function. An investigation is needed to see if this pump can be combined with the rotating magnet flux pump principle.

A persistent current switch (PCS) is a device to charge a superconductive coil and bring it into persistent mode. A problem with using HTS tape as a PCS is that the tape has conductive layers like copper and steel. When the PCS is in off state, the conductive parts on the tape still conduct current. This can cause local heat spots and reduce the efficiency of the PCS. Research is needed to make a HTS tape where the HTS is sprayed on a non-conductive material.

HTS degaussing coils need a complicated cryostat to cool the material below the critical temperature. When the temperature is too high, the degaussing system does not work. This introduces more points of failure than for a copper degaussing system. More research is needed on how to design a cryogenic system which is redundant and compartmentalised. A decision should be made if every degaussing has its own cooling system or if all the degaussing coils make use of a centralised cooling system. The same holds for a cryogenic converter. Research should be done to design a converter that is still able to operate when there is no available cooling.

A drawback of using HTS degaussing coils is the need for a cryogenic system. However, when the cryogenic infrastructure is available on the ship, other system could benefit from it as well. Superconductors can be used on board for power cables, bus bars, transformers, electric machines and other applications. Also copper conductors have a lower resistance when cooled with a cryogen which could benefit the overall efficiency. A research should be conducted to see what the benefits of using superconductors for these systems are and to what extend they can share the cryogenic system.

The demonstrator showed that the cooler produces a large amount of acoustic noise. Some ships also have to take care of their acoustic signature, so this can be an unwanted side effect. More research is needed in the availability of silent coolers or dampening the acoustic noise.

Since HTS degaussing coils feature a zero resistance at DC, multiple HTS degaussing coils on the ship could be placed in series. The required magnetic field in these coils can be created by the same current without introducing extra losses. The same sized current source can be used for the coils in series instead of one source per coil. A difference in ampere-turn requirements of the degaussing coils can be compensated for by using a different amount of turns. Besides, a smaller (copper) coil can be placed next to these coils to increase the resolution even further.

It was shown that the use of a cryogenic converter can improve the efficiency of HTS degaussing coils. When using transistors inside the cryogenic environment, the gate signal needs to be transported to the transistors from a room temperature environment. This can be done by copper connections, but that will introduce some heat leak into the cryostat. An alternative should be investigated where the signals are transferred through the magnetic field by means of a transformer. The use of a cryogenic converter can also introduce unwanted voltage oscillations across the transistors. This can be problematic because it introduces extra losses and the transistors can break. Low on-state resistance MOSFETs usually have low blocking voltage capabilities. It is recommended to minimise the parasitic inductance in the design of the PCB and optimise the snubber circuit.

A consequence of the combination of HTS coils and a low resistance converter with long freewheeling time is that there is a lack of damping. Because of this, external electromagnetic noise can cause interference with the HTS degaussing currents and should be investigated further.

This thesis provides all the components and tools to estimate the total power consumption of an HTS degaussing system in a full sized ship and compare it to a copper one. If the requirements of the degaussing coils are known, the total power consumption can be calculated. Finally, it is anticipated that HTS degaussing coils can add a significant value to both merchant and navy ships. It is recommended to explore this field further.

ACKNOWLEDGEMENTS

It was a long but not so-lonesome road towards the end of my PhD. During every step along the way, there was someone to support me. I want to thank everyone involved in the realisation of this thesis and everyone who contributed to the work and supported me during the process. Some people I'd like to thank in particular.

Rob, you took your role as a supervisor very seriously. We rarely missed one of our weekly Friday afternoon progress meetings in which we used to brainstorm and discuss the craziest ideas. You made me understand the importance of having an open mind in science, but also taught me the importance of soft skills like planning, networking and good communication. We had a great time together at the EUCAS conference in Glasgow, where we found our shared interest in good food and playing the guitar. Thanks for being my promotor. Henk, after I finished my master's thesis, you suggested that I could pursue a PhD. I already knew at the time that it was probably a bad idea, but I decided to give it a go anyway. I am now grateful that you placed your trust in me at the time. I've always considered you a mentor, and you managed to steer me in the right direction at the right times. Armando, I will never forget the lunches at the university where we discussed the most random topics. You are indeed an inspiring person. After I finished at the university and already started my job, you insisted on continuing our weekly meetings. I don't remember how many times I missed a deadline or failed to keep an agreement, but you always kept your patience with me. You pushed me till the end, and your persistence definitely caused me to finish the work. Thank you for that. To the rest of the promotion committee, Thiago, Marc, Bart, and Peter, thanks for reviewing my work and taking the time to be part of the promotional ceremony. The consortium partners contributed to this work with support, feedback and funding. I want to thank Ab, Ana-Maria, Cees, Eric, Izak, Marc and Ruud for this.

A big part of my work took place in the lab and I want to thank all the lab staff who helped me with my test setups and measurements. Paul, you created a great work environment in the HV lab and were always ready to share one of your anecdotes. Luis, without you, I only would have measured noise. Wim, you greatly contributed to my test setups by building and advising on all the necessary parts. I much appreciate your help and input. Mladen, you designed an insane PCB that works at $-200\,^{\circ}\mathrm{C}$. I know you spent some time on this, and I'm very thankful for the help. Many thanks to the rest of the staff from the HVT and the DCE&S research groups. A special thanks to Sharmila for guiding me (and every other PhD student) through the whole process with everlasting positivity.

During the PhD, I got to know many new people and made many new friends, which I hope to keep seeing in the future. Jiayang, we used to have very pleasant conversations in our office, and I admire your enthusiastic and caring personality. You made sure that, before drinking, we at least played some badminton. Thanks for teaching me how to make dumplings, a skill that will come in handy for the rest of my life. Fabio, you are a true scientist. Thanks for all the book recommendations and philosophical discus-

sions we have. I will always be ready to watch the music video of We're not gonna take it or Electric eye again. Luis, gracias por enseñarme español. Tuvimos aventuras épicas como recoger el carro desde Bélgica o ir a la zona del fuego (al menos, cerca). Ojalá volvamos al roco pronto y lograr las mentas como don vergas. Y sabes, yo no sabía que iba a terminar el tesis. Tuve fe. Guillermo, thanks for never forgetting la máquina. You never let me down to go for another beer, even if it meant you would miss the last train. It is always a surprise what we will encounter, like El Mago. Alessandro, thanks for all the random Italian curse words in our office. Christian, it's an honour to be a member of your army of Vegetas. Hopefully we will play many games of AoE4 in the future. Thanks, Dhanashree and Guangyao, for making our office the perfect place to work in. To the rest of my DC and HV friends, thanks for all the discussions on climate change and the moon landing, gaming events, birthday parties, defense parties, vrijdagmiddagborrels, sweets from every corner of the world, go-karting, bouldering, and of course drinking beer in Christians favourite bar. Some might think that PhD is done in an office, but the real work is done at bars, cafeterias, coffee machines and food trucks. PhD'ers help each other out by brainstorming and discussing each other's research. The best ideas are created during these moments. I want to thank all my colleagues for inspiring me and making my time at the university unforgettable.

Many thanks to my brother and sister for your support and interest in my work (although I never really like to talk about it). Rinske, thanks for designing the cover of this thesis and for wanting to be the paranymph at the defense ceremony. To my parents, now that I am about to receive my final degree, I realise that the most important education is the one you receive at home. Where normal families would go to the beach to go swimming, you would explain how to prove Pythagoras' theorem by drawing triangles in the sand. You'd send critical e-mails to my electronics teacher pointing out how an exam question was mathematically incorrect, and we used to make impossible objects from wood. I've learned so much, and for that, I am forever grateful. Juul, you helped me a lot by motivating me to finish this thesis and I couldn't have done this without you. The last couple of years were stressful, with me finishing my PhD and you finishing your second master's next to our jobs. I'm glad we both managed to complete it. I believe that now more relaxed times will come. I love you.

CURRICULUM VITÆ

Djurre Pier WIKKERINK

19-03-1990	Born in Drachten, The Netherlands.

EDUCATION

2013–2017	**Master Electrical Power Engineering** Delft University of Technology, Delft
2007–2012	**Bachelor Electrical Engineering** Hanze University of Applied Sciences, Groningen

EXPERIENCE

2022–current	**Consultant Electric Power Systems** RH Marine, Schiedam
2018–2022	**PhD Researcher** Delft University of Technology, Delft
2017–2018	**Electrical Engineer** Teamwork Technology, Alkmaar
2016–2017	**Graduate** Teamwork Technology, Alkmaar
2012–2013	**Junior Plant Technician** Total E&P, Offshore (North Sea)
2012–2013	**Graduate** KEMA – DNV GL, Groningen
2010–2010	**Intern** Koninklijke Grolsch NV, Enschede
2008–2009	**Intern** University Medical Center Groningen, Groningen

LIST OF PUBLICATIONS

JOURNAL

4. **D. Wikkerink**, M. Gagić, A. Rodrigo Mor, H. Polinder, and R. Ross, *Cryogenic H-Bridge Converter for HTS Degaussing Application*, IEEE Transactions on Applied Superconductivity, vol. 34, no. 1, pp. 1-7, Jan. 2024.

3. **D. Wikkerink**, A. Rodrigo Mor, H. Polinder, and R. Ross, *Converter Design for High Temperature Superconductive Degaussing Coils*, IEEE Access, vol. 10, pp. 128656-128663, Dec. 2022.

2. **D. Wikkerink**, A. Rodrigo Mor, H. Polinder, and R. Ross, *Magnetic Signature Reduction by Converter Switching Frequency Modulation in Degaussing Systems*, IEEE Access, vol. 10, pp. 74103–74110, July 2022.

1. I. Hanse, **D. Wikkerink**, R. Keijzer, M. Dhallé, H. H. J. ten Kate and H. J. M. ter Brake, *Modeling and Characterization of a ReBCO HTS Degaussing Demonstrator*, IEEE Transactions on Applied Superconductivity, vol. 32, no. 6, pp. 1-5, June 2022.

CONFERENCE

3. **D. Wikkerink**, I. Hanse, A. Rodrigo Mor, H. Polinder and R. Ross. *Demonstration of Degaussing by Copper and HTS Windings*, International Naval Engineering Conference and Exhibition (iNEC), 5-9 October, Delft, The Netherlands, 2020.

2. I. Hanse, **D. Wikkerink**, C. Vermeer, H. Holland. M. Dhallé and H.J.M. ter Brake. *Cryogenics for an HTS Degaussing System Demonstrator*, International Naval Engineering Conference and Exhibition (iNEC), 5-9 October, Delft, The Netherlands, 2020.

1. **D. Wikkerink**, A. Rodrigo Mor, H. Polinder and R. Ross. *Design of a Test Setup to Measure Magnetic Signature Reduction*, International Conference on Marine Engineering and Technology (ICMET), 6-8 November, Muscat, Oman, 2019.